

# Analysis and modelling of settlements of a road embankment

## A case study of the E45 highway in Marieholm

Master's Thesis in the Master's Programme Infrastructure and Environmental Engineering

FILIP BERGSTRÖM  
JOHANNA MEDIN



MASTER'S THESIS 2015:34

# Analysis and modelling of settlements of a road embankment

A case study of the E45 highway in Marieholm

*Master's Thesis in the Master's Programme Infrastructure and Environmental Engineering*

FILIP BERGSTRÖM

JOHANNA MEDIN

Department of Civil and Environmental Engineering

*Division of GeoEngineering*

*Geotechnical Engineering Research Group*

CHALMERS UNIVERSITY OF TECHNOLOGY

Göteborg, Sweden 2015



Analysis and modelling of settlements of a road embankment  
A case study of the E45 highway in Marieholm

*Master's Thesis in the Master's Programme Infrastructure and Environmental Engineering*

FILIP BERGSTRÖM

JOHANNA MEDIN

© FILIP BERGSTRÖM & JOHANNA MEDIN, 2015

Examensarbete 2015:34/ Institutionen för bygg- och miljöteknik,  
Chalmers tekniska högskola 2015

Department of Civil and Environmental Engineering  
Division of GeoEngineering  
Geotechnical Engineering Research Group  
Chalmers University of Technology  
SE-412 96 Göteborg  
Sweden  
Telephone: + 46 (0)31-772 1000

Cover:

Schematic picture of the studied embankment, results from settlement calculations in section 1/000 and distribution of additional stresses in section 1/085.

Department of Civil and Environmental Engineering. Göteborg, Sweden, 2015



Analysis and modelling of settlements of a road embankment

A case study of the E45 highway in Marieholm

*Master's thesis in the Master's Programme Infrastructure and Environmental Engineering*

FILIP BERGSTRÖM

JOHANNA MEDIN

Department of Civil and Environmental Engineering

Division of GeoEngineering

Geotechnical Engineering Research Group

Chalmers University of Technology

## ABSTRACT

The aim of the project was to analyse measured settlements of a road embankment constructed in year 1967 in the Marieholm area in Gothenburg. The studied embankment is constructed on thick layers of clay, and partly founded on embankment piles. A literature study was carried out on theory behind settlements and embankment piling. Three sections of the embankment were modelled in the computer software GeoSuite Settlement and settlement calculations were performed with Chalmers creep soil model. Two of the sections are founded on embankment piles. Construction drawings, earlier performed soil tests and investigations have been used as input data for the calculations. The results from GeoSuite Settlement were compared with measured settlements and it was found that the calculations gave a smaller total settlement. However, the rate and magnitude of settlements between year 1980 and 2014 is captured rather good in the section that is not founded on piles. There are many uncertainties regarding the modelling of embankment piles. Therefore, the model of the section not founded on piles is considered to be a more realistic model. According to the calculations, the additional stresses in the soil are close to or have exceeded the preconsolidation pressure in all studied sections. This is considered to be one of the main reasons for the measured settlements. The calculations also indicate that the consolidation process is slow due to the thick layers of clay under the embankment and not completed in year 2014. A sensitivity analysis was carried out where it was found that the permeability of the clay and the geotechnical bearing capacity of the piles have a large impact on the calculated results. The results are not sensitive to changes of the creep parameters. The measured settlements are probably not only caused by the consolidation of the clay. It is likely that other factors such as compression of embankment material or construction defects have contributed to the measured settlements.

Key words: Settlements, Embankment piles, GS Settlement, Chalmers creep soil model, Consolidation, Creep, Marieholm

Analys och modellering av sättningar av en vägbank  
- En fallstudie av väg E45 i Mariefholm

Examensarbete inom masterprogrammet Infrastructure and Environmental Engineering

FILIP BERGSTRÖM

JOHANNA MEDIN

Institutionen för bygg- och miljöteknik

Avdelningen för geologi och geoteknik

Forskargrupp för geoteknik

Chalmers tekniska högskola

## SAMMANFATTNING

Syftet med rapporten var att analysera uppmätta sättningar av en vägbank byggd år 1967 i Mariefholm i Göteborg. Den studerade vägbanken är byggd på mäktiga lerlager och är delvis grundlagd på bankpålar. En litteraturstudie genomfördes om teorier kring sättningar och bankpålning. Tre av vägbankens sektioner modellerades i datorprogrammet GeoSuite Settlement och sättningsberäkningar genomfördes med jordmodellen Chalmers kryp. Två av sektionerna är grundlagda på bankpålar. Konstruktionsritningar, tidigare genomförda fältundersökningar och studier ligger till grund för indata till beräkningarna. Resultaten från GeoSuite Settlement jämfördes med uppmätta sättningar och det konstaterades att beräkningarna gav en mindre totalsättning. Sättningshastigheten och sättningens storlek mellan år 1980 och 2014 stämmer dock väl överens med uppmätta sättningar i den sektion som inte är grundlagd på pålar. Osäkerheter finns kring modellering av bankpålar, därför anses modellen av sektionen utan pålar vara mer verklighetstrogen. Enligt beräkningarna har tillskottsspänningarna i jorden överstigit eller nästan överstigit förkonsolideringstrycket i alla studerade sektioner. Detta anses vara en av de största anledningarna till de uppmätta sättningarna. Beräkningarna visar också att konsolideringsprocessen är långsam på grund av de mäktiga lerlagren under vägbanken och ej avslutad vid år 2014. En känslighetsanalys genomfördes där det konstaterades att lerans permeabilitet och pålarnas geotekniska bärförmåga har en stor inverkan på beräkningsresultaten. Resultaten påverkas inte nämnvärt av ändringar av krypparametrarna. De uppmätta sättningarna har troligtvis inte enbart orsakas av konsolidering av leran. Det är troligt att andra faktorer så som kompression av materialet i vägbanken eller byggfel kan ha bidragit till de uppmätta sättningarna.

Nyckelord: Sättningar, Bankpålning, GS Settlement, Chalmers kryp, Konsolidering, Kryp, Mariefholm

# Contents

ABSTRACT	I
SAMMANFATTNING	II
CONTENTS	III
PREFACE	VII
NOTATIONS	VIII
1 INTRODUCTION	1
1.1 Background	1
1.2 Aim and objectives	1
1.3 Methodology	2
1.4 Limitations	2
2 LITERATURE STUDY	3
2.1 Settlements and consolidation theory	3
2.1.1 Consolidation settlements	3
2.1.2 Mathematical model of consolidation	4
2.1.3 Creep effects	6
2.2 Important soil parameters for evaluation of long-term settlements	7
2.2.1 Stress history and preconsolidation pressure	7
2.2.2 Compression modulus	9
2.2.3 Permeability	10
2.2.4 Coefficient of secondary compression	11
2.2.5 Time resistance and time resistance number	12
2.3 Piled foundations	13
2.3.1 Different types of piles	13
2.3.2 Negative skin friction and the neutral plane	14
2.3.3 Piled embankments	15
2.4 Geotechnical bearing capacity of piled foundations	17
2.5 Settlements of piled foundations	18
3 DESCRIPTION OF GEOSUITE SETTLEMENT	20
3.1 Description of the Chalmers creep soil model	20
3.1.1 The improved compression modulus	21
3.1.2 The creep equation	22
4 CASE STUDY OF ROAD EMBANKMENT	24
4.1 History of the area	24
4.2 Geotechnical description	25
4.2.1 Soil profile	26
4.2.2 Soil parameters	27

4.3	Embankment and foundation design	32
4.4	Earlier settlement investigations	33
5	SETTLEMENT CALCULATIONS	35
5.1	Soil model	36
5.2	Modelling of additional stresses	37
5.2.1	Section 1/000	37
5.2.2	Section 1/045 and 1/085	38
5.3	Stress charts	41
6	RESULTS FROM SETTLEMENT CALCULATIONS	44
6.1	Section 1/000	44
6.2	Section 1/045	47
6.3	Section 1/085	50
6.4	Discussion of the results	52
7	SENSITIVITY ANALYSIS	55
7.1	Initial permeability	55
7.2	Time resistance numbers – $r_0$ and $r_1$	57
7.3	Preconsolidation pressure	61
7.4	Geotechnical bearing capacity of piles	64
7.5	An alternative approach of modelling including ongoing settlements	66
7.6	Discussion of results from sensitivity analysis	68
7.6.1	Initial permeability	68
7.6.2	Time resistance numbers	68
7.6.3	Preconsolidation pressure	69
7.6.4	Geotechnical bearing capacity	69
7.6.5	Alternative approach of modelling including ongoing settlements	70
8	OTHER FACTORS CAUSING EMBANKMENT SETTLEMENT	71
8.1	Properties of the embankment material	71
8.2	Pile and pile cap design	71
8.3	Lateral displacement	72
8.4	Construction defects	73
9	CONCLUSIONS	74
10	RECOMMENDATION FOR FURTHER INVESTIGATIONS	76
11	REFERENCES	77





## **Preface**

This Master of Science thesis was conducted at the geotechnical department at ÅF Infrastructure AB in Gothenburg between January and June in 2015.

We would like to thank our supervisor at ÅF Infrastructure AB, Roger Oscarsson for his valuable guidance and for providing us with background material during the work with this project. We are also grateful to the employees at the geotechnical department at ÅF for their useful help and for creating a pleasant working environment.

Furthermore, we would like to thank our supervisor at Chalmers, Mats Karlsson for always taking time to answer our questions. Without the instructive guidance and constructive feedback, the work with the project would have been far more difficult.

Göteborg June 2015

Filip Bergström and Johanna Medin

# Notations

## Roman upper case letters

$A_s$	Area of the pile section at the pile toe
$E$	Action effect
$M$	Compression modulus, oedometer modulus
$M_0$	Compression modulus when $\sigma' < \sigma'_c$
$M_L$	Compression modulus when $\sigma'_L > \sigma' > \sigma'_c$
$M'$	Modulus number
$N_{cp}$	Bearing capacity factor for pile toe
$R$	Time resistance
$R$	Resistance
$R$	Geotechnical bearing capacity
$R_d$	Geotechnical bearing capacity (design value)
$R_{toe}$	Resistance at pile toe
$T_v$	Time factor
$U_v$	Degree of consolidation
$Q$	Load
$Q_m$	Load distributed from pile shaft
$Q_s$	Load distributed from pile toe

## Roman lower case letters

$a_0$	Factor at which the improved modulus curve start to decrease linearly
$a_1$	Factor at which the improved modulus curve stops to decrease linearly
$b_0$	Factor for time resistance number $r_0$
$b_1$	Factor for time resistance number $r_1$
$c$	Pile spacing
$c_u$	Undrained shear strength
$c_{uk}$	Undrained shear strength (unreduced)
$c_v$	Coefficient of consolidation
$d$	Drainage distance
$f_m$	Shaft resistance
$k$	Permeability
$k_{init}$	Initial permeability
$k_z$	Vertical permeability
$q_t$	Traffic load
$r_0$	Initial time resistance number for $\sigma' \leq b_0 \sigma'_c$
$r_1$	Time resistance number for $\sigma' \geq b_1 \sigma'_c$
$r_s$	Time resistance number
$r$	Time resistance number
$s_c$	Consolidation settlements
$s_i$	Immediate settlements
$s_s$	Secondary consolidation or creep settlements
$s_t$	Total settlements
$t_r$	Reference time
$t_0$	Time when the R-t curve start to be linear
$u$	Pore pressure
$\Delta u$	Excess pore water pressure

$w_L$	Liquid limit
$w_N$	Water content

### Greek letters

$\alpha$	Adhesion factor
$\alpha_{okorr}$	Uncorrected adhesion factor
$\alpha_s$	Coefficient of secondary compression
$\beta_k$	Permeability reduction coefficient
$\gamma$	Unit weight
$\gamma_{mAs}$	Partial factor for variation of circumference at the pile toe
$\gamma_{mcs}$	Partial factor for variation of shear strength at the pile toe
$\gamma_{mNcp}$	Partial factor for $N_{cp}$
$\gamma_{mcm}$	Partial factor for variation of shear strength along the pile
$\gamma_{m\alpha}$	Partial factor for variation of adhesion factor
$\gamma_{m\theta}$	Partial factor for variation of circumference
$\gamma_n$	Partial factor for safety class
$\gamma_w$	Unit weight of water
$\varepsilon$	Strain
$\varepsilon_{cr}$	Creep strain
$\varepsilon_v$	Vertical strain
$\varepsilon_{vol}$	Volumetric strain
$\varepsilon_z$	Vertical strain
$\varepsilon_z^{cr}$	Vertical creep strain
$\varepsilon_z^{ep}$	Vertical elastic and plastic strain
$\dot{\varepsilon}$	Strain rate
$\dot{\varepsilon}_{cr}$	Creep strain rate
$\theta$	Circumference of the pile
$K_{OCR}$	Correction factor with respect to the OCR
$K_T$	Correction factor with respect to time after installation
$K_f$	Correction factor with respect to the pile shape
$K_t$	Correction factor for undrained shear strength
$K_\emptyset$	Correction factor with respect to the diameter of the pile
$\sigma'$	Effective stress
$\sigma'_0$	In-situ stress
$\sigma'_c$	Preconsolidation pressure
$\sigma'_L$	Effective stress where the compression modulus start to increase
$\sigma'_v$	Effective vertical stress

### Abbreviations

CRS	Constant rate of strain
GS	GeoSuite
IL	Incremental loading
OCR	Overconsolidation ratio



# 1 Introduction

Settlements are a major concern in all construction projects carried out on soft soil. When roads are constructed on embankments, different measures can be taken in order to prevent settlements. However, it can be seen on old road embankments that these measures have sometimes been insufficient. This project is a case study of an old road embankment where large settlements have been measured. The background, aim and the methodology of the project is presented in the following chapter. Furthermore, the limitations of the study are described.

## 1.1 Background

The E45 highway is one of the main roads in Gothenburg. A traffic interchange of the road is called Slakthusmotet and is located in an industrial area, Marieholm, close to the Göta Älv River (Trafikverket, 2013). Slakthusmotet is planned to be reconstructed in the near future and it has been noted that two road embankments adjacent to the Slakthusbron Bridge has been exposed to large settlements. Slakthusbron Bridge is an old concrete bridge built in the late 1960's. The road embankments connected to the bridge are founded on deep clay layers with a large number of piles. In the beginning and in the middle of the 1980's, a few measurements of the road embankment settlements were performed. In year 2014 ÅF Infrastructure AB started to monitor the settlements as a part of the investigation for the new traffic interchange. The location of Slakthusmotet and the studied embankment can be seen in Figure 1.1.



Figure 1.1. Location of Slakthusmotet and the studied embankment, modified (Lantmäteriet, 2013).

## 1.2 Aim and objectives

The purpose of this project is to analyse measured settlements of the E45 highway road embankments adjacent to the Slakthusbron Bridge. The analysis should include calculations that comply with measured settlements and also lead to an understanding

of how and why the existing settlements have developed. The aim is also to find out how well settlements can be predicted with a model in GeoSuite Settlements software. Specified objectives are as follows:

- Describe local geology, geological history, soil parameters, geometry and foundation design of the studied embankment
- Set up a model of the embankment and perform settlement calculations in GeoSuite Settlements
- Compare the calculated and measured settlements
- Carry out a sensitivity analysis on input data and analyse the results
- Suggest recommendations for further studies

### **1.3 Methodology**

The project will contain a literature study on settlements and embankment piling, and a case study of the road embankment in Marieholm including settlement calculations.

The literature study will be carried out in order to provide information regarding settlement theories including creep settlements. It will also include a description of embankment piles, their function and how piles can be accounted for in settlement calculations.

The case study of the road embankment will include a survey of old documents such as construction drawings, existing soil tests and settlement measurements. This survey will provide input data to settlement calculations.

Settlement calculations will be performed with the software GeoSuite Settlement.

### **1.4 Limitations**

Field investigations have been performed at the location of the studied embankment; however, these investigations cannot provide all needed soil parameters. The soil model will therefore be based on data collected in a larger area.

The model has been based on original construction drawings, possible deviation between the planned and built construction are therefore not accounted for.

Only the southern embankment connected to Slakthusbron Bridge has been studied and no effects of surrounding buildings and roads have been taken into account in the analysis.

The settlements of the embankment have only been measured at six different occasions; therefore, it is only possible to compare the calculated results with the developed settlements at these specific times.

Only one-dimensional vertical displacements are taken into account in the calculations. Possible lateral displacements are neglected.

## 2 Literature study

This chapter include a literature study of theory behind settlements; such as consolidation settlement and creep settlement. The chapter also include basic theory of embankment piling.

### 2.1 Settlements and consolidation theory

The settlements that may occur when a load is applied on a soft soil consist of three components according to the equation (2.1) (Holtz & Kovacs, 1981):

$$s_t = s_i + s_c + s_s \quad (2.1)$$

Where  $s_t$  = total settlements [m]

$s_i$  = immediate settlements [m]

$s_c$  = consolidation settlements [m]

$s_s$  = secondary consolidation or creep settlements [m]

The immediate settlements are the deformation that occurs at once when the load is applied. The consolidation settlement is a time dependent deformation that occurs in soils with low permeability due to pore water drainage that causes increased effective stresses in the soil. Creep settlements that are also time dependent, take place with constant effective stress. Consolidation and creep settlements will be described more in detail in the following sections.

#### 2.1.1 Consolidation settlements

The classic consolidation theory first published by Terzaghi in 1923 is the foundation of the consolidation theories used today (Claesson, 2003).

The consolidation process can be described by the spring analogy, where saturated soil is modelled as a water-filled cylinder containing a spring that is connected to a piston (Holtz & Kovacs, 1981), see Figure 2.1.

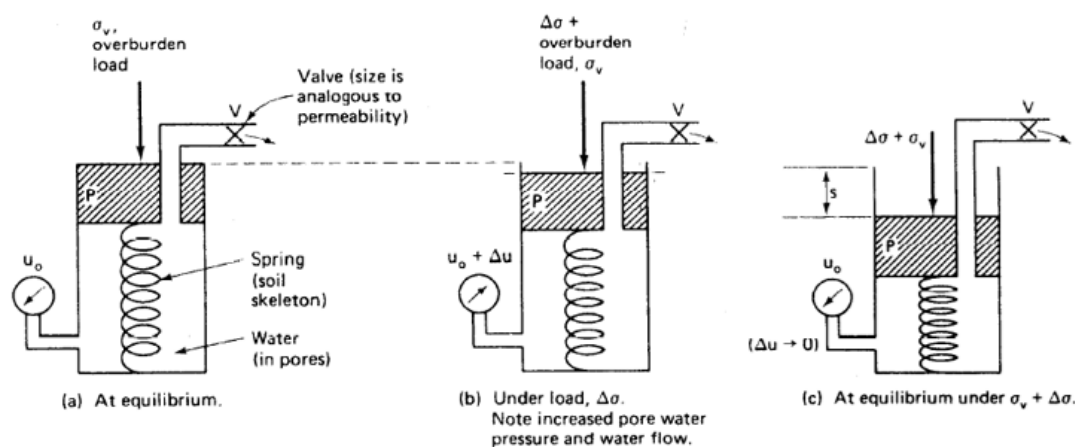


Figure 2.1. The spring analogy applied to the consolidation process (Holtz & Kovacs, 1981).

The spring in the model represents the soil mineral skeleton and the stress in the spring is equivalent to the effective stress,  $\sigma'$ . The pressure in the water corresponds to the pore water pressure in the soil,  $u$ , and an open valve at the top of the piston represents the pore sizes in the soil. When the system is in equilibrium there is no flow of water through the valve, see Figure 2.1a. When an additional load,  $\Delta\sigma$ , is applied there is an increase in water pressure,  $\Delta u$ , that is equivalent to the additional load, Figure 2.1b. As the water flows out through the valve, more load is transferred from the water to the spring and a vertical deformation takes place. The rate of the deformation is governed by the flow of the water which depends on the pore sizes in the soil. After some time, the spring will again be in equilibrium with the overburden pressure and no further water will be squeezed out of the cylinder, Figure 2.1c. The transition of the load from increased pore water pressure to increased effective stress is shown in Figure 2.2.

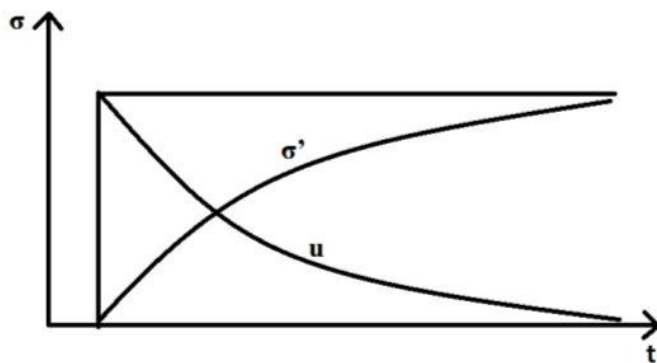


Figure 2.2. Transition of load from pore water pressure to effective stress during consolidation.

### 2.1.2 Mathematical model of consolidation

Terzaghi (1943) developed a mathematical model for determination of the degree of consolidation at a certain time. The model is based on a number of assumptions:

1. The soil is homogenous.
2. The soil is fully saturated.
3. The solid particles and water are incompressible.
4. Compression and flow are one-dimensional.
5. Strains are small.
6. Darcy's law is valid at all hydraulic gradients.
7. The coefficient of permeability and the coefficient of volume compressibility remain constant throughout the process.
8. There is a unique relationship, independent of time between void ratio and effective stress.

The consolidation process can be described with equation (2.2)

$$\frac{\partial u}{\partial t} = \frac{M}{\gamma_w} \cdot \frac{\partial}{\partial z} \left( k \cdot \frac{\partial u}{\partial z} \right) \quad (2.2)$$

Where;  $u$  = pore pressure [kPa]

$t$  = time [s]

$M$  = oedometer modulus [kPa]

$\gamma_w$  = unit weight of water [kN/m<sup>3</sup>]

$k$  = permeability [m/s]

$z$  = depth [m]

Since the permeability is assumed to be constant with depth equation (2.2) can be rewritten as

$$\frac{\partial u}{\partial t} = c_v \frac{\partial^2 u}{\partial z^2} \quad (2.3)$$

Where  $c_v = \frac{M \cdot k}{\gamma_w}$  [m<sup>2</sup>/s]

$c_v$  is defined as the coefficient of consolidation, which determines the speed of the consolidation process.  $k$ ,  $M$  and  $\gamma_w$  are assumed to be constant,  $c_v$  is therefore constant during consolidation (Knappett & Craig, 2012).

Since the solution to the differential equation is complicated the so called time factor  $T_v$  is normally used when calculating consolidation settlements.

$$T_v = \frac{c_v \cdot t}{d^2} [-] \quad (2.4)$$

Where  $t$  = time [s]

$d$  = drainage distance [m]

When  $T_v$  is known it is possible to find the average degree of consolidation  $U_v$  by using graphs as shown in Figure 2.3. The different curves represent the relationships between  $U_v$  and  $T_v$  for different initial variations of excess pore water pressures due to loading.

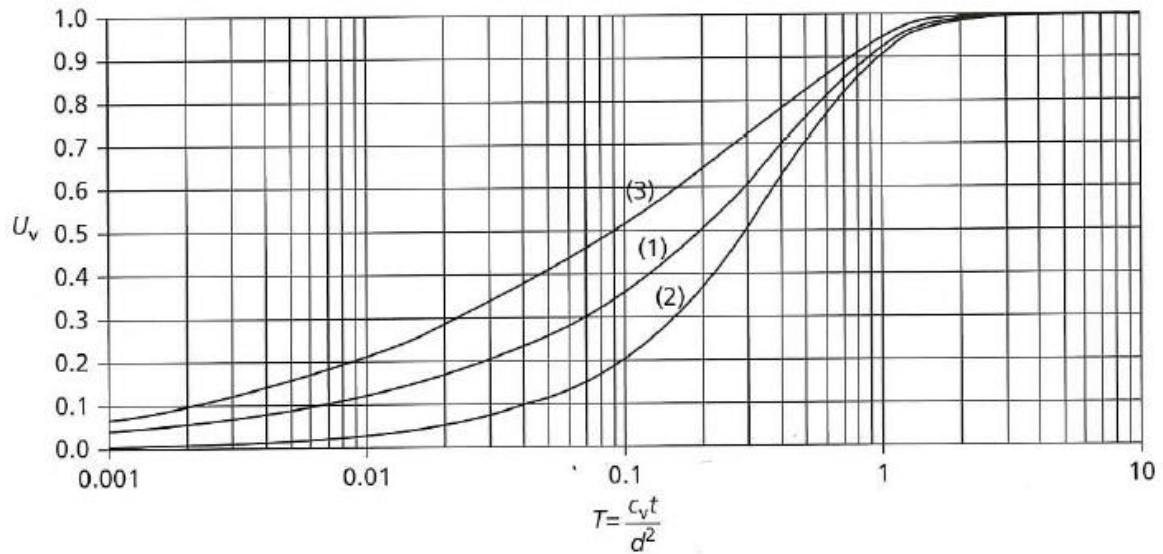


Figure 2.3. Relationships between average degree of consolidation  $U_v$  and time factor  $T_v$  for different initial variations of excess pore water pressures (Knappett & Craig, 2012).

### 2.1.3 Creep effects

The consolidation process is often divided into two phases; primary and secondary consolidation (Olsson, 2010). In the primary consolidation phase, which is described in section 2.1.1, the dissipation of excess pore water pressure is the dominating compression factor. When most of the excess pore water pressure has dissipated, the secondary consolidation takes place. In the secondary consolidation, the dominating compression factor is creep strains. The two different phases can be plotted in a graph with log-time plotted against the strain,  $\varepsilon$ , or void ratio,  $e$ , see Figure 2.4.

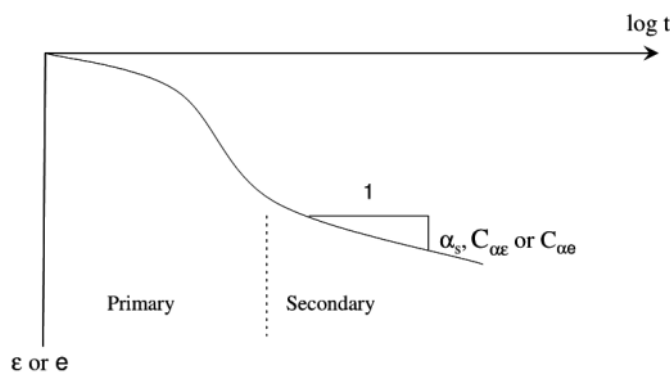


Figure 2.4. Consolidation curve, describing the primary and secondary consolidation phases (Olsson, 2010).

In literature, there are several different names regarding the secondary consolidation phase, such as; secondary compression and creep. Creep is defined as the decrease in volume during a constant effective stress (Holtz & Kovacs, 1981). During creep, the bonds between the particles within the soil are compressed and the soil becomes more compacted. Compression due to creep occurs at a lower rate than compression due to consolidation. It is hard to distinguish the creep effect from the primary consolidation phase. Older consolidation models have often assumed that creep only occur during

the secondary consolidation phase. However, today there are several models including the creep effect in both primary and secondary consolidation.

One of the models was developed by Bjerrum in year 1967, who presented that creep and primary consolidation occurs simultaneously (Claesson, 2003). The graph in Figure 2.5 defines two different situations; when the effective stress and compression increases over time due to dissipation of excess pore water pressure, and when the excess pore water pressure is disregarded effective stress are transferred to the clay structure. The dashed line in the graph, represent the latter situation while the solid line represent the case where excess pore water pressure dissipates. It can be seen that even if no excess pore water pressure dissipates in the soil, there will still be settlements, in this case called creep settlements.

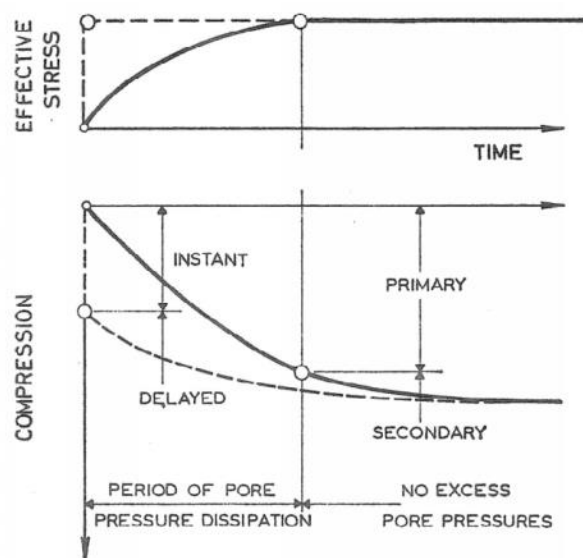


Figure 2.5. Settlement or compression illustrated by the Bjerrum model describing instant and delayed compression. The dashed line represents compression and effective stress if the pore water pressure could be disregarded. The solid line represents the effective stress and compression when excess pore water pressure dissipates over time (Claesson, 2003).

## 2.2 Important soil parameters for evaluation of long-term settlements

There are several soil parameters that are important and affect the settlement and consolidation process. This section will describe these parameters.

### 2.2.1 Stress history and preconsolidation pressure

Soils can be described as either overconsolidated or normally consolidated (Larsson, 2008). Depending on the stress history of the soil, the in-situ stress,  $\sigma'_0$ , can be greater or less compared to the stresses it has been exposed to in the history. If the soil has been subjected to a greater stress than the in-situ stress, it is overconsolidated and if the in-situ stress is the maximum stress it has ever been exposed to, it is normally consolidated. The ratio between the maximum value of stress in the past (also called preconsolidation pressure,  $\sigma'_c$ ) and in-situ stress is defined as the overconsolidated

ratio (OCR) and can be written as in the following equation (Knappett & Craig, 2012):

$$OCR = \frac{\sigma'_0}{\sigma'_c} \quad (2.5)$$

Where  $\sigma'_0$  = in-situ stress [kPa]  
 $\sigma'_c$  = preconsolidation pressure [kPa]

In Figure 2.6, the stress-strain relationship for clay is illustrated (Sällfors, 2001). The line A-C can be seen as a loading process of the clay, where the in-situ stresses is increasing to the point C and the soil becomes more compacted and the deformation is mostly plastic. At this stage, the stresses in point C can be seen as the preconsolidation pressure. When the clay is unloaded e.g. by excavation or erosion, only a small part of the deformation will regress (C-D). In-situ stresses that are lower than the preconsolidation pressure will only result in small elastic deformations when reloading (D-E). When the in-situ stress becomes larger than the preconsolidation pressure, plastic deformations will occur (E-F).

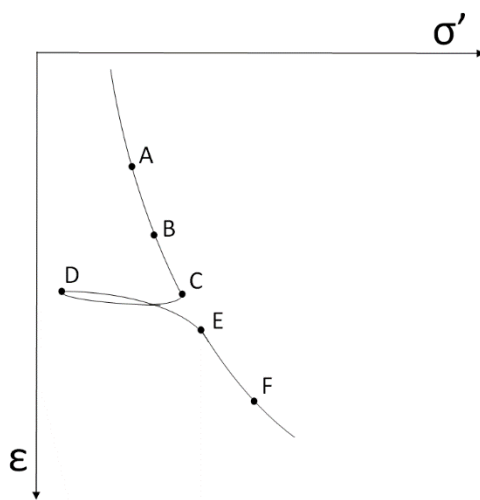


Figure 2.6. Stress-strain relationship for clay.

Clays that are normally consolidated can sometimes behave as slightly overconsolidated clays (Olsson, 2010). This is due to the ageing effect which Bjerrum (1967) illustrated by plotting vertical pressure against void ratio, see Figure 2.7. The diagram describes how clay compresses over a period of years with constant vertical stress due to creep effects (point A to B). When the vertical stresses increases after a period of years, small strains will occur until the clay is reaching the pre-consolidation pressure (point C). The preconsolidation pressure which cannot be related to any previous in-situ stresses applied to the clay is often called the quasi-preconsolidation pressure.

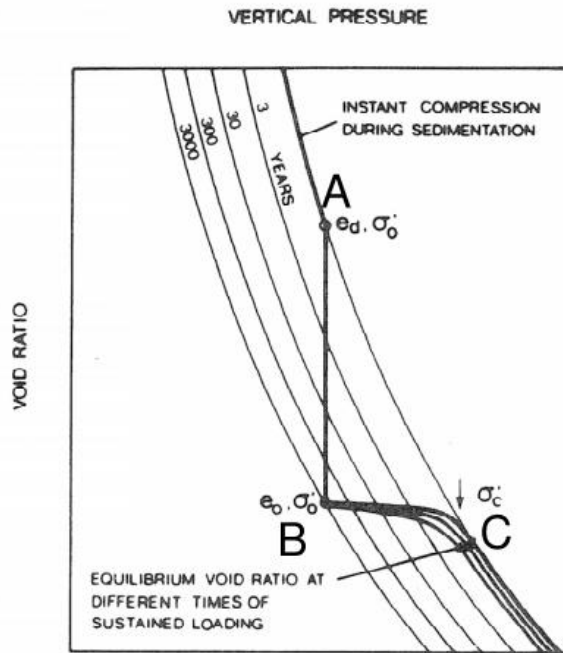


Figure 2.7. Vertical pressure plotted against void ratio illustrating the ageing effect, from Bjerrum (1967) (Olsson, 2010).

### 2.2.2 Compression modulus

The compression modulus describes the deformation in the soil when the effective vertical stresses increases. Compression modulus is given from the following equation (Sällfors, 2001):

$$M = \frac{d\sigma'_v}{d\varepsilon_v} \quad (2.6)$$

$M$  can be evaluated from a test where the vertical effective stress is increased while no horizontal displacement is allowed. Figure 2.8 shows the typical stress-strain relationship for clay and the compression modulus is the derivative of the curve. As can be seen, the modulus is changing depending on the stress level (Larsson, 2008).

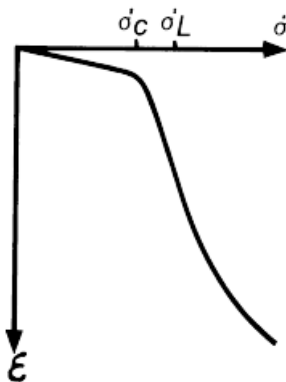


Figure 2.8. Typical stress-strain relationship for clay, where  $M$  is the derivative of the curve (Larsson, 2008).

When the effective stresses are below the preconsolidation pressure, the modulus is constant and is written as  $M_0$ . The modulus between the preconsolidation pressure and  $\sigma'_L$  (which is the stress level where the compression modulus starts to increase) is also constant. In this interval, the modulus is written as  $M_L$ . When the effective stresses are greater than  $\sigma'_L$ , the modulus is increasing and can be calculated with equation (2.7).

$$M = M_L + M'(\sigma' - \sigma'_L) \quad (2.7)$$

Where  $M'$  is the modulus number and defined in Figure 2.9.

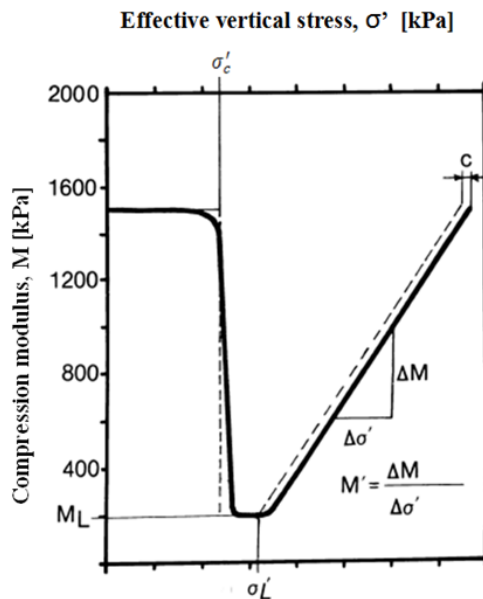


Figure 2.9. Illustration of the compression modulus at different stress levels, modified, (Larsson, 2008).

The compression modulus can be graphically evaluated when it is plotted at different stress levels, see Figure 2.9 (Larsson, 2008). It should be noted that  $M_0$  is in general low from CRS tests why empirical values can be used from equation (2.8):

$$M_0 = 250 \cdot c_u \quad (2.8)$$

Where  $c_u$  is the undrained shear strength.

### 2.2.3 Permeability

The permeability,  $k$ , describes how easily water can flow through a soil and is of great importance when evaluating time-dependent settlements. The permeability is decreasing when the soil is compressed since it is dependent on the pore-size and total pore-volume (Larsson, 2008). For most soils there is a linear relation between the compression (change in void ratio) and the logarithm of the permeability, see Figure 2.10.

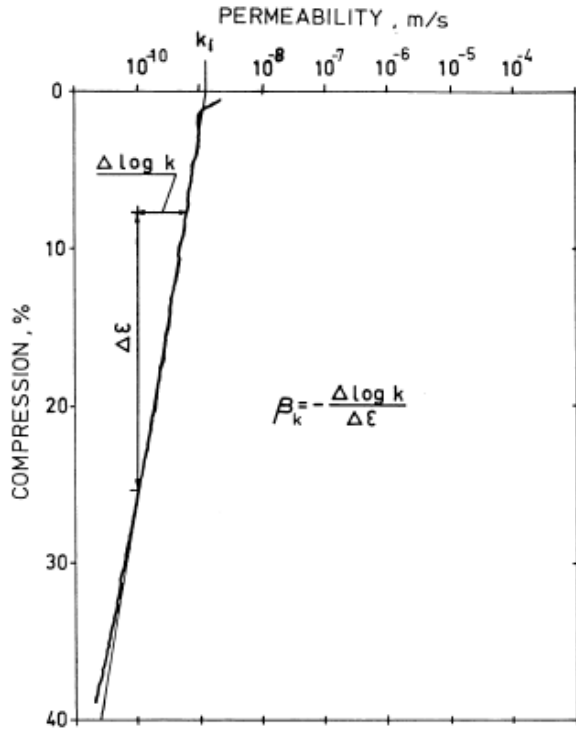


Figure 2.10. Relation between compression and the logarithm of the permeability for clay (Larsson, et al., 1997).

The permeability for a certain compression can be calculated according to equation (2.9).

$$\log_{10} k = \log_{10} k_{init} - \beta_k \epsilon_{vol} \quad (2.9)$$

Where  $k_{init}$ =permeability at initial conditions prior to loading [m/s]

$\beta_k$ =permeability reduction coefficient [-]

$\epsilon_{vol}$ = volumetric strain (compression) [-]

## 2.2.4 Coefficient of secondary compression

A parameter describing the soils creep characteristic is the coefficient of secondary compression (Larsson, et al., 1997). This parameter have normally been used in Sweden and is defined by equation (2.10).

$$\alpha_s = \frac{\Delta \epsilon_{cr}}{\Delta \log(t)} \quad (2.10)$$

Where  $\alpha_s$ =coefficient of secondary compression [ $s^{-1}$ ]

$\epsilon_{cr}$ =creep strain [-]

$t$ = time [s]

Laboratory investigations shows that the coefficient of secondary compression in clay is very low until it reaches the effective stress at a level of  $0,8 \cdot \sigma'_c$ . The coefficient then reaches its maximum when the effective stress is equal to the preconsolidation pressure. When the preconsolidation pressure is exceeded, the coefficient start to

decline. Figure 2.11 shows the relationship between the coefficient of secondary compression and strain.

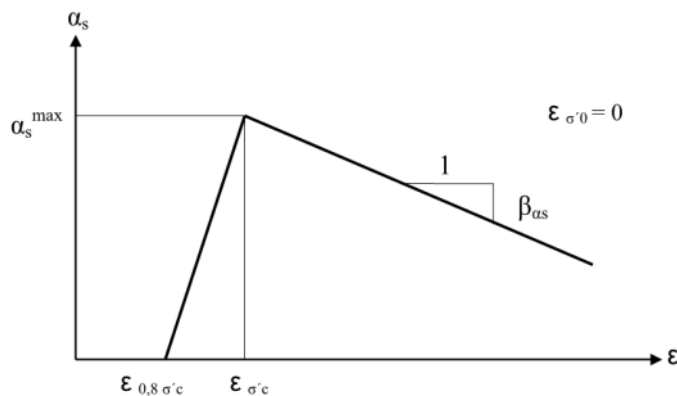


Figure 2.11. Relationship between coefficient of secondary compression and strain (Claesson, 2003).

### 2.2.5 Time resistance and time resistance number

A different way to describe the creep characteristic of the soil is by the time resistance (Claesson, 2003). The time resistance was introduced by Janbu in 1969 and can be explained by equation (2.11).

$$R = \frac{dt}{d\varepsilon} \quad (2.11)$$

Where  $R$  =time resistance [s]

$t$ =time [s]

$\varepsilon$ =strain [-]

It has been shown that the time resistance of clay is increasing linearly with time, and can therefore be written as:

$$r_s = \frac{dR}{dt} \quad (2.12)$$

Where  $r_s$  is the time resistance number. Figure 2.12 illustrates that the time resistance is increasing linearly after a certain time, thus, the time resistance can also be written as:

$$R = r_s \times (t - t_r) \quad (2.13)$$

Where  $t_r$  is the reference time for the idealised curve shown in Figure 2.12. It should be noted that equation (2.13) is only valid after time  $t_0$  where the time resistance starts to increase linearly.

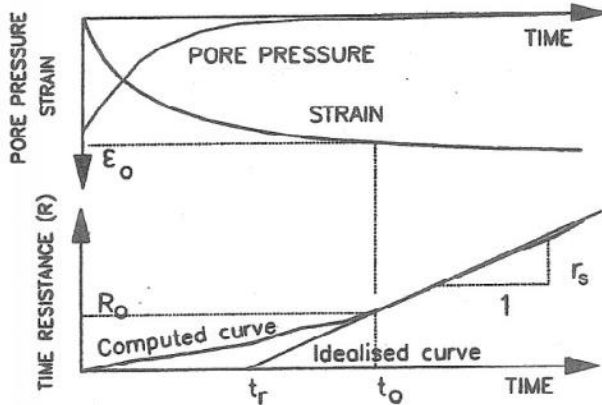


Figure 2.12. Relationship between time resistance and time, from Svanö et al., 1991 (Claesson, 2003).

In order to estimate the creep strain rate at a certain time, equation (2.14) can be used:

$$\dot{\epsilon}_{cr} = \frac{d\epsilon_{cr}}{dt} = \frac{1}{R} = \frac{1}{r_s \cdot (t - t_r)} \quad (2.14)$$

If equation (2.14) is integrated from  $t_0$  to  $t$ , the creep strain can be calculated according to equation (2.15):

$$\Delta\epsilon_{cr} = \frac{1}{r_s} \int_{t_0}^t \frac{dt}{(t - t_r)} = \frac{1}{r_s} \ln \frac{t - t_r}{t_0 - t_r} \quad (2.15)$$

From equation (2.15), the time resistance number can be written as:

$$\frac{1}{r_s} = \frac{d\epsilon_{cr}}{d\ln(t)} \quad (2.16)$$

Based on equation (2.10) and (2.16), the coefficient of secondary compression can be expressed with time resistance number, see equation (2.17).

$$\alpha_s = \frac{\ln 10}{r_s} \quad (2.17)$$

## 2.3 Piled foundations

The main purpose of a foundation is to transfer the loads from a construction into the subsoil in an optimal way. When using piles the loads are transferred to deeper soil layers that normally have higher strength and stiffness than shallow layers (Olsson & Holm, 1993). The purpose of installing piles can be to achieve sufficient geotechnical bearing capacity, reduce settlements or a combination of the two.

### 2.3.1 Different types of piles

Piles can be divided into different types based on a number of classifications such as material, way of function or way of installation (Olsson & Holm, 1993). When classifying piles based on the way they function, piles are often divided into end-

bearing piles and shaft-bearing piles. End-bearing piles transfer the load mainly by the pile toe to bedrock or a stiff soil layer, while shaft-bearing piles transfer the load to the surrounding soil by shear forces mobilized at the interface between the shaft and the surrounding soil. Some part of the load may be transferred by the pile toe of a shaft-bearing pile, this part is however often negligible in cohesive soils such as clay. Figure 2.13 shows the function of an end-bearing pile and a shaft-bearing pile.

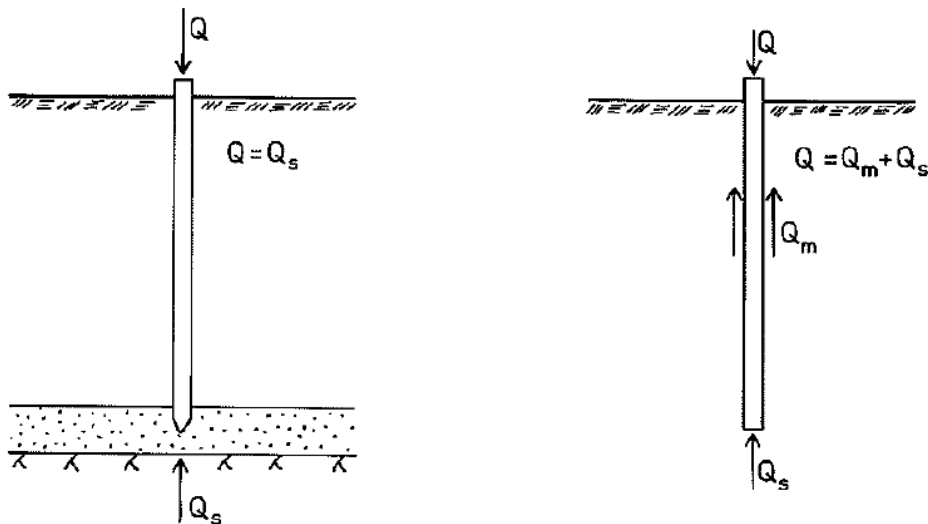


Figure 2.13. Function of an end-bearing pile (left) and a shaft-bearing pile (right) (Olsson & Holm, 1993).

### 2.3.2 Negative skin friction and the neutral plane

If settlements occur in a soil layer where piles are installed a phenomena called negative skin friction or down drag may occur (Eriksson, et al., 2004). If the soil settles faster than the piles the downward movement of the soil relative the piles will mobilize shear stresses along the pile shaft. The effect of eventual negative skin friction must be considered when performing settlement calculations for piled foundations. According to Swedish practice the effect is taken into account for the parts of the pile where the soil settles 5 mm more than the pile. The Swedish Commission on Pile Research suggests that the negative skin friction should be considered along the part of the pile where the effective stresses in the soil due to all loads except the pile loads are larger than  $0,8 \cdot \sigma'_c$ . The basis to this suggestion is that long term settlements due to creep is more likely to occur at theses effective stresses. The negative skin friction and the loading at the pile head are added to achieve the total action effect in the pile.

The action effect  $E$  in a pile at depth  $z$  can be obtained as (Alén, 2012):

$$E = Q + \int_0^z f_m dA \quad (2.18)$$

Where  $Q$  = the loading of the pile [kN]

$f_m$  = the shaft resistance per shaft unit area [kPa]

$A$  = the shaft area [m<sup>2</sup>]

Similarly the resistance  $R$  at depth  $z$  can be obtained as:

$$R = R_{toe} + \int_z^{L_p} f_m dA \quad (2.19)$$

Where  $R_{toe}$  = the resistance at the pile toe [kN]

$L_p$  = the length of the pile [m]

For a pile to be in equilibrium the action effect and the resistance must be equal. At a certain depth the negative skin friction must therefore change into friction resistance, also called skin friction. This depth is defined as the neutral plane (Olsson & Holm, 1993). At the neutral plane the settlement of the pile is equal to the settlement of the soil. Finding the neutral plane is therefore important when calculating settlements of piles. The neutral plane can be found by drawing the load distribution curves for the resistance and for the action effect, the neutral plane is located at the intersection of the two curves, see Figure 2.14.

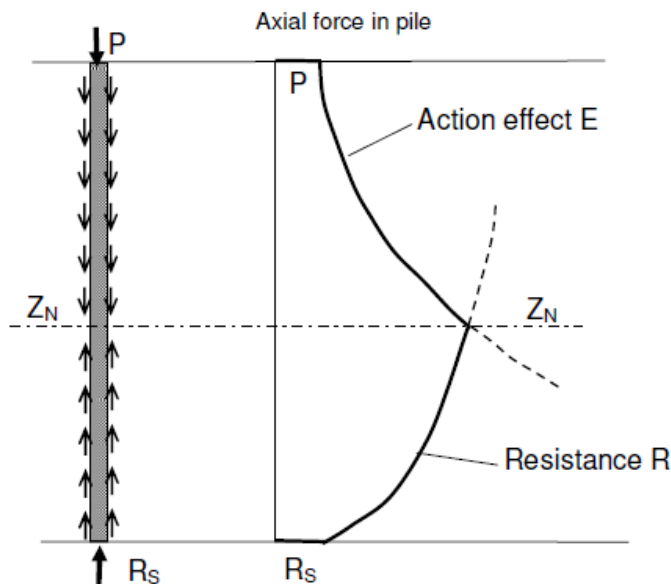


Figure 2.14. Determination of location of the neutral plane (Alén, 2012).

### 2.3.3 Piled embankments

Road embankments built on soft soils are often supported by piles. In order to improve the load transfer from the embankment to the piles, pile caps are placed on the pile heads (Satibi, et al., 2007). It is also common to use geotextile to reinforce the soil in the bottom of the embankment. The design of the pile caps and of the geosynthetics is governing how well the loads are transferred to the piles. Figure 2.15 shows a schematic picture of a piled embankment with pile caps and geosynthetic reinforcement.

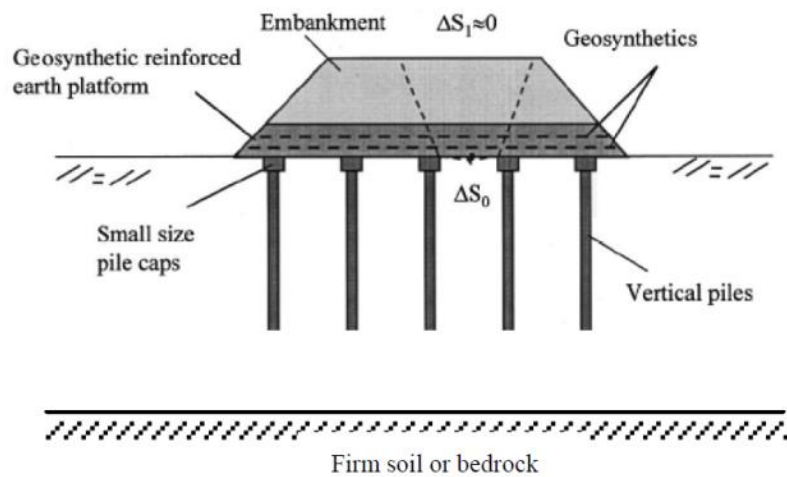


Figure 2.15. Schematic picture of a piled embankment (Satibi, et al., 2007).

The loads from the embankment as well as the external loads acting on the embankment are transferred down to the piles by a soil arching mechanism as shown in Figure 2.16. The embankment load below the soil arch will be transported to the piles via the geosynthetic layer. If no geosynthetic layer is used, this load will be transferred directly to the soft soil.

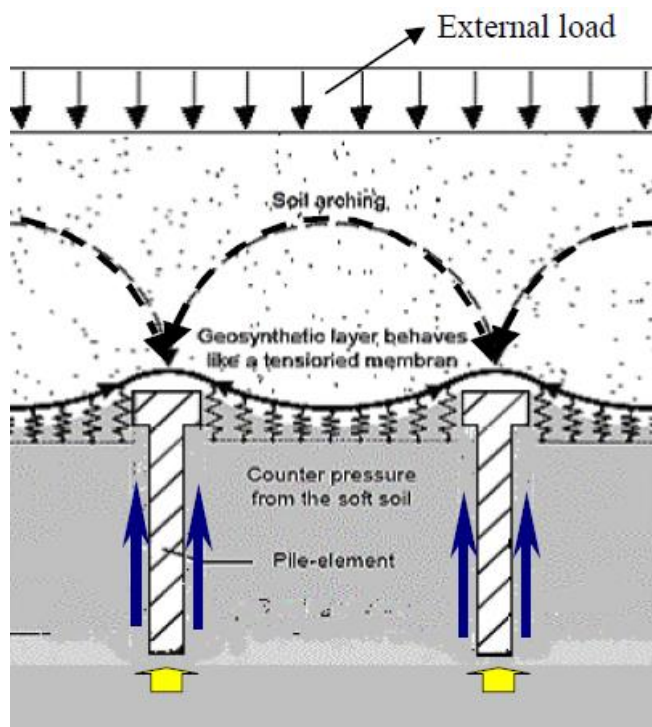


Figure 2.16. Function of a piled embankment with a geosynthetic layer (Satibi, et al., 2007).

When designing a piled embankment it is important that the embankment is high enough, so that there is room for the arching effect to develop. The pile spacing and the size of the pile caps are other important design considerations. Swedish practice for determination of pile spacing and embankment height can be found in (Trafikverket, 2011). The required pile spacing can be calculated according to:

$$c = \sqrt{R_d / (h \cdot \gamma + q_t)} \quad (2.20)$$

Where:  $R_d$  = the bearing capacity of the pile (design value) [kN]  
 $h$  = the height of the embankment above the pile cap [m]  
 $\gamma$  = the unit weight of the embankment material [kN/m<sup>3</sup>]  
 $q_t$  = the traffic load (design value) [kPa]

The size of the pile caps is determined as an area-covering ratio, which should be larger than 40 % for an embankment without geosynthetic reinforcement.

## 2.4 Geotechnical bearing capacity of piled foundations

The geotechnical bearing capacity of a shaft-bearing pile is governed by the shaft area together with the shear forces mobilized between the pile and the soil (Eriksson, et al., 2004). According to Swedish practice the bearing capacity of a shaft-bearing pile is determined based on the undrained shear strength of the soil. This method is often referred to as the  $\alpha$ -method since the adhesion factor for the shear strength mobilized between the pile and the soil is denoted  $\alpha$ . It is recommended by the Swedish Commission on Pile Research to calculate the bearing capacity of a shaft-bearing pile according to equation (2.21).

$$R_d = \frac{1}{\gamma_n} \int_{L_p} \frac{\alpha}{\gamma_{ma}} \cdot \frac{\theta}{\gamma_{m\theta}} \cdot \frac{c_{uk}}{\gamma_{mcm}} dz + \frac{N_{cp}}{\gamma_{mNcp}} \cdot \frac{A_s}{\gamma_{mAs}} \cdot \frac{c_{uk}}{\gamma_{mcs}} \quad (2.21)$$

Where:  $R_d$  = the bearing capacity of the pile (design value) [kN]  
 $L_p$  = the length of the pile [m]  
 $\alpha$  = adhesion factor [-]  
 $\theta$  = circumference of the pile [m]  
 $c_{uk}$  = undrained shear strength of the soil (unreduced) [kPa]  
 $N_{cp}$  = bearing capacity factor for pile toe [-]  
 $A_s$  = area of the pile section at the toe [m<sup>2</sup>]  
 $\gamma_{[-]}$  = partial factors [-]

It should be noted that the end-bearing capacity is small in relation to the shaft-bearing capacity and therefore often ignored.

The undrained shear strength of clay is dependent on the speed of the loading (Eriksson, et al., 2004). It is therefore recommended by the Swedish Commission on Pile Research to reduce the undrained shear strength with a factor  $K_t$  that is depending on the duration of the loading. For long term loading  $K_t = 0,7$  should be used. It is recommended to use the undrained shear strength evaluated from field vane tests.

The adhesion factor,  $\alpha$ , is dependent on the diameter and shape of the pile and of the OCR of the soil.  $\alpha$  can be calculated according to equation (2.22) where a number of correction factors are multiplied with an uncorrected adhesion factor.

$$\alpha = \alpha_{okorr} \cdot K_{\phi} \cdot K_f \cdot K_{OCR} \cdot K_T \quad (2.22)$$

Where:  $\alpha_{okorr}$  = uncorrected adhesion factor (1,0) [-]

$K_{\phi}$  = Correction factor with respect to the diameter of the pile [-]

$K_f$  = Correction factor with respect to the pile shape [-]

$K_{OCR}$  = Correction factor with respect to the OCR of the soil [-]

$K_T$  = Correction factor with respect to time after installation [-]

It has been shown that the adhesion factor is decreasing with an increasing pile diameter. According to the Swedish Commission on Pile Research the value of  $K_{\phi}$  can however be chosen to 0,9 for piles with a diameter between 0,2 and 0,35. The  $K_f$ -factor can be chosen as 1,0 for piles with a constant cross-section. For piles with a cross-section that is decreasing with depth, such as timber piles installed with the root up, the factor can be chosen to 1,2. The adhesion factor is generally lower in soils with a high OCR than in normally consolidated soils. The  $K_{OCR}$  can however for Swedish normally consolidated or slightly overconsolidated clays ( $OCR < 1,25$ ) be chosen to 1,0. When a pile is installed the adhesion between the pile and the soil is low due to the disturbance of the soil. After installation the adhesion is developing over time. The time it takes to achieve full adhesion varies depending on the pile material. Figure 2.17 can be used to achieve the  $K_T$  factor.

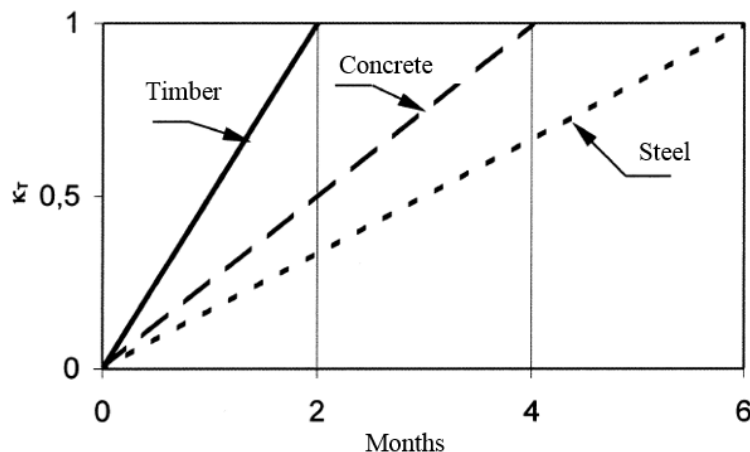


Figure 2.17. Adhesion after installation (Eriksson, et al., 2004).

## 2.5 Settlements of piled foundations

Estimation of settlements of a piled foundation requires knowledge of where the neutral plane is located and of the settlements of the soil below the neutral plane (Fellenius, 2004). The settlement of the pile head is equal to the settlements at the neutral plane plus the shortening of the piles above the neutral plane. The shortening of the piles can however often be neglected due to the high stiffness of the piles (Alén, 2012).

In all settlement calculations it is essential to calculate the additional stresses in the soil. When calculating settlements for a pile group some different principles can be used in order to obtain the additional stresses (Eriksson, et al., 2004). The pile loads can be modelled as point loads acting along the pile or along a part of the pile. They can also be modelled as surface loads (equivalent footings) acting on different levels below the neutral plane. The simplest way to model the pile loads is as an equivalent footing on the level of the neutral plane, this method is however only recommended for rough hand-calculations. Figure 2.18 shows three different ways of modelling pile loads.

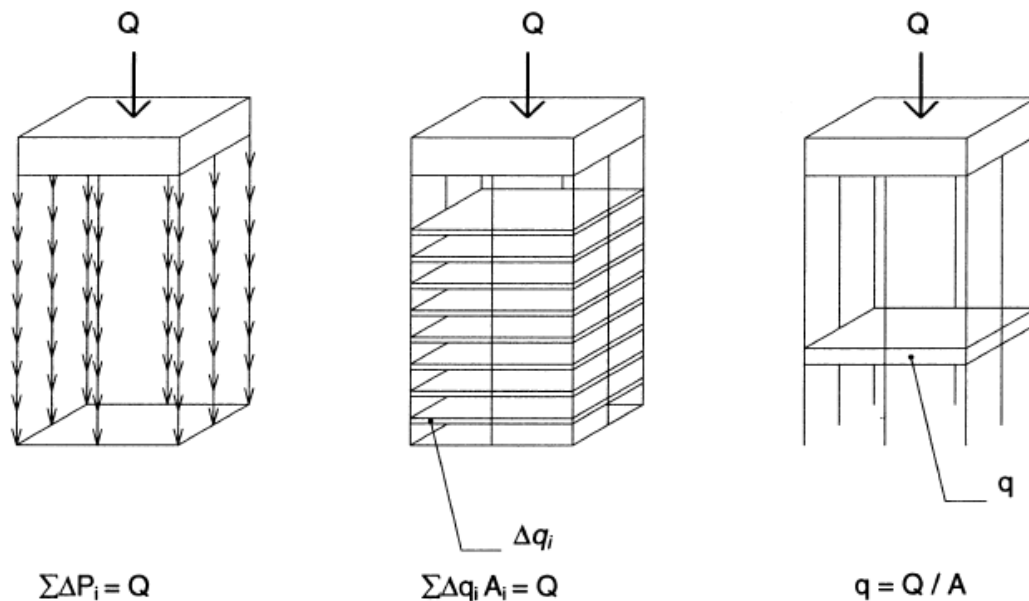


Figure 2.18. Different ways to model pile loads, as point loads acting along the piles (left), as equivalent footings on many planes (middle) and as an equivalent footing acting on the neutral plane (right) (Eriksson, et al., 2004).

In a case where load from the structure is larger than the geotechnical bearing capacity of the piles, the neutral plane will be located close to or at the level of the pile caps (Fellenius, 2004). The foundation will then work according to the creep pile principle, which means that the capacity of the piles is fully utilized and the load on the piles is equal to the pile's failure load (Jendeby, 1986). The load from the structure will in this case be carried both by the piles and by the soil at the level of the pile caps.

### 3 Description of GeoSuite Settlement

GeoSuite Settlement (GS Settlement) is a program included in the GeoSuite Toolbox for calculation of time dependent settlements due to loads and boundary conditions that varies over time (Vianova GeoSuite AB, 2013). The program is based on the general finite element program GEOnac (Geotechnical nonlinear analysis code). Settlement calculations are one-dimensional and uniaxial deformations and vertical pore water flow is assumed. (Vianova Systems AS, u.d.). To calculate settlements of a cross-section or over a 3D-area a number of 1D-calculations at different points are used and the settlements between the points can be achieved by interpolation. GS Settlement is a rather simple program that makes it possible to take creep effects into account and it is commonly used in engineering practice.

A number of soil models can be used in the program including Janbu's model, Krykon and Chalmers model. When using Krykon or Chalmers model, creep effects are taken into account. There are also a number of permeability models included in the program, such as the  $C_v$  based, the exponential and the log-based (strain) models. In this case study, the Chalmers model and the log-based (strain) permeability model is used. The log-based (strain) permeability model uses the parameters  $k_i$  and  $\beta_k$  to calculate the permeability with regard to the volumetric strain according to equation (2.9).

#### 3.1 Description of the Chalmers creep soil model

The Chalmers creep model is based on a model presented by (Claesson, 2003) and is a suitable model for calculating settlements including creep in fine grained soils such as clay (Olsson, 2010).

The deformation model in the Chalmers creep model was developed by Alén in 1998 and is based on Terzaghi's one-dimensional consolidation theory and that time dependent strain can be divided into three components; consolidation, elastic-plastic deformation and creep deformations (Claesson, 2003). Figure 3.1 shows the deformation model used in the Chalmers creep model.

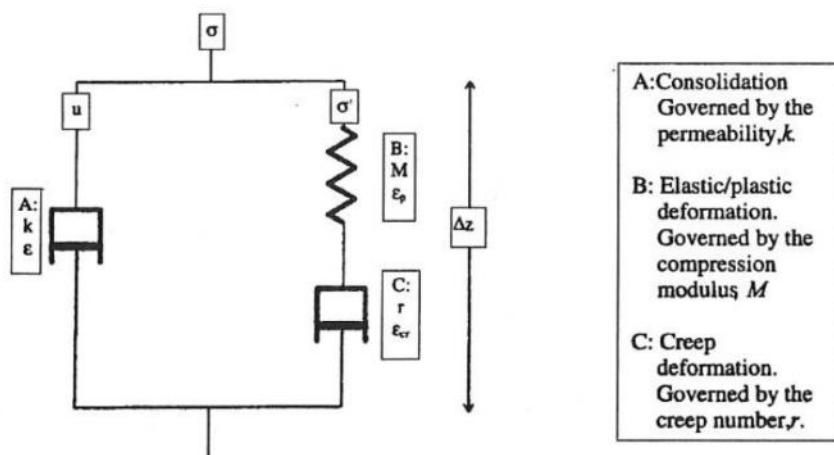


Figure 3.1. Deformation model in the Chalmers creep soil model developed by Alén 1998 (Claesson, 2003).

The strain rate in the consolidation phase in the model is described with the equation for one-dimensional consolidation as follows:

$$\frac{\partial \varepsilon_z}{\partial t} = - \frac{\partial}{\partial z} \left[ \frac{k_z}{\gamma_w} \cdot \left( \frac{\partial u}{\partial z} \right) \right] \quad (3.1)$$

Where  $\varepsilon_z$ = total vertical strains [-]  
 $k_z$ = vertical permeability [m/s]

During the elastic-plastic phase, the total stress is considered to be constant; therefore, the change in effective stress is depending on the change in pore water pressure. Equation (3.2) shows how the elastic-plastic strain is dependent on the vertical effective stress.

$$\Delta \varepsilon_z^{ep} = \frac{\Delta \sigma'_z}{M(\sigma'_z)} \quad (3.2)$$

Where  $\varepsilon_z^{ep}$  is the vertical elastic and plastic strain. The creep behaviour in the model is expressed by the time resistance:

$$R = \frac{\partial t}{\partial \varepsilon_z^{cr}} \quad (3.3)$$

Where  $\varepsilon_z^{cr}$  is the vertical creep strain.

### 3.1.1 The improved compression modulus

The definition of the compression modulus was earlier described in section 2.2.2. It was there stated that the compression modulus was constant for both  $M_0$  and  $M_L$ . However, the compression modulus in the Chalmers creep model is improved in order to illustrate the behaviour of clay better (Claesson, 2003). As can be seen in Figure 3.2, the compression modulus is depending on the effective stress-strain curve. Close to the preconsolidation pressure, the stress-strain curve is changing in a parabolic shape.

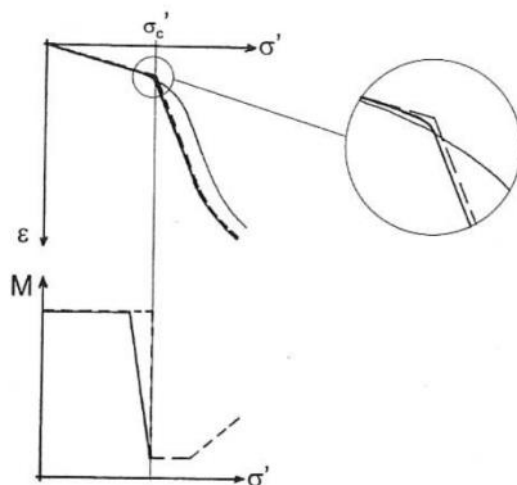


Figure 3.2. The relationship between compression modulus and effective stress (Claesson, 2003).

In order to describe the change of the compression modulus close to the preconsolidation pressure, the modulus is assumed to decrease linearly between  $M_0$  and  $M_L$ . Figure 3.3 shows how the improved modulus curve in the model is changing, the two factors  $a_0$  and  $a_1$  is describing at which stress-state the modulus is decreasing linearly.

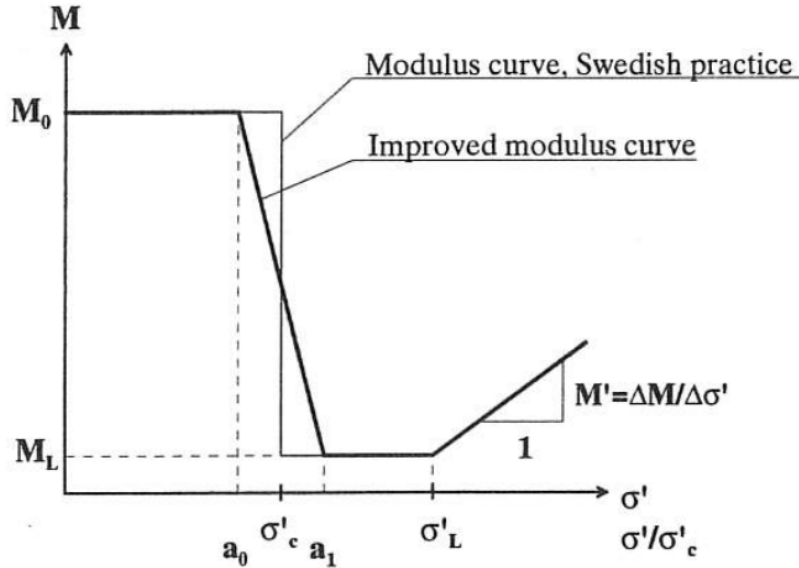


Figure 3.3. Illustration of the improved compression modulus curve in the Chalmers creep model (Claesson, 2003).

The different compression modulus are calculated by the following relationship in the program (Vianova GeoSuite AB, 2013):

$$M = \begin{cases} M_0, & \sigma'_v < a_0 \sigma'_c \\ M_0 + (M_L - M_0) \frac{\sigma'_v - a_0 \sigma'_c}{a_1 \sigma'_c - a_0 \sigma'_c}, & a_0 \sigma'_c \leq \sigma'_v < a_1 \sigma'_c \\ M_L, & a_1 \sigma'_c \leq \sigma'_v < \sigma'_L \\ M_L + M'(\sigma'_v - \sigma'_L), & \sigma'_v \geq \sigma'_L \end{cases} \quad (3.4)$$

### 3.1.2 The creep equation

The creep strain rate in the model is a function of the creep strain and the time resistance number at the current effective stress, see equation (3.5) (Vianova GeoSuite AB, 2013).

$$\dot{\epsilon} = \frac{1}{-r \cdot t_r} e^{-r \cdot \epsilon_{cr}} \quad (3.5)$$

Where  $t_r$  is the reference time where the program starts to take the creep effects into account, for further description of how the reference time is defined, see section 2.2.5 (Claesson, 2003).

According to (Claesson, 2003), the time resistance number is a more accurate way to describe the creep behaviour of clay than the coefficient of secondary compression, especially in the stress range around  $0,7$  and  $1,0 \cdot \sigma' / \sigma'_c$ .

Figure 3.4 illustrates laboratory tests where the coefficient of secondary compression and the time resistance number is plotted against normalised effective stress.

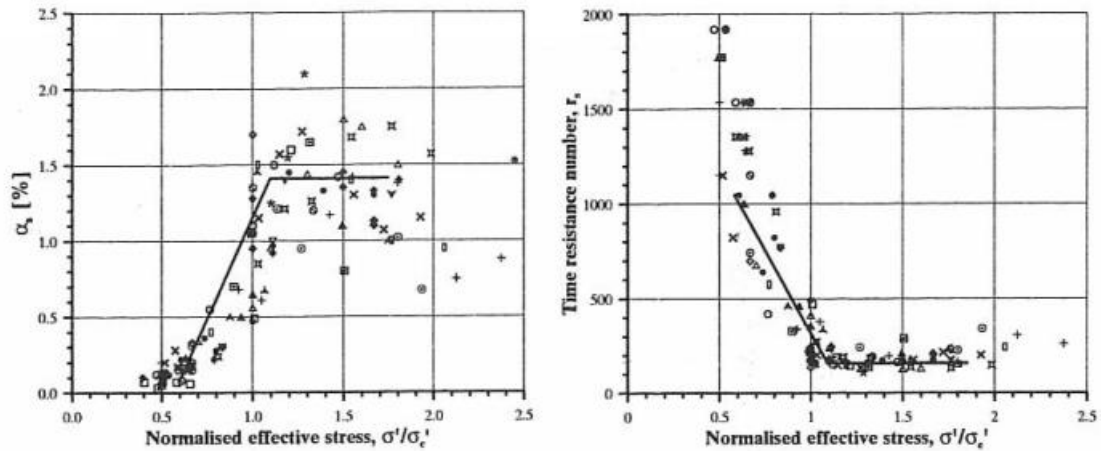


Figure 3.4. Results from laboratory tests where the coefficient of secondary compression and the time resistance number is plotted against normalised effective stress. The solid lines represent a linearization of the results (Claesson, 2003).

In the Chalmers creep model, the time resistance number is defined by  $r_0$  and  $r_1$  and the two normalized stress factors  $b_0$  and  $b_1$ , to fit the corresponding linearization seen in Figure 3.4. Figure 3.5 shows the time resistance curve plotted against normalized effective stress implemented in GS Settlement.

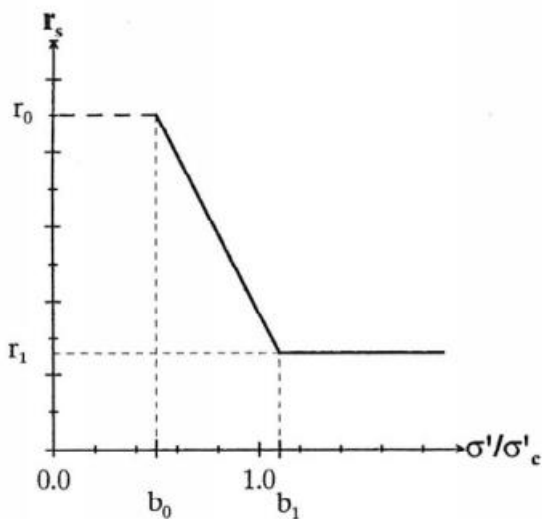


Figure 3.5. Time resistance number as a function of normalized effective stress (Claesson, 2003).

The time resistance number is calculated in the program by the following expression (Vianova GeoSuite AB, 2013):

$$r_s = \begin{cases} r_0, & \sigma'_v \leq b_0 \sigma'_c \\ r_0 + (r_1 - r_0) \frac{\sigma'_v - b_0 \sigma'_c}{b_1 \sigma'_c - b_0 \sigma'_c}, & b_0 \sigma'_v < \sigma'_v < b_1 \sigma'_c \\ r_1, & \sigma'_v \geq b_1 \sigma'_c \end{cases} \quad (3.6)$$

## 4 Case study of road embankment

The Slakthusbron Bridge is a part of the E45 highway at a traffic interchange called Slakthusmotet. The interchange is located about 3 km north-east of central Gothenburg in the Marieholm industrial area. A local street, Marieholmsgatan is running parallel to the highway at the western side. The highway bridge is crossing a local street called Slakthusgatan that is connected to Marieholmsgatan. At both sides of the bridge the highway runs on embankments. An overview of the highway bridge and the embankments can be seen in Figure 4.1.

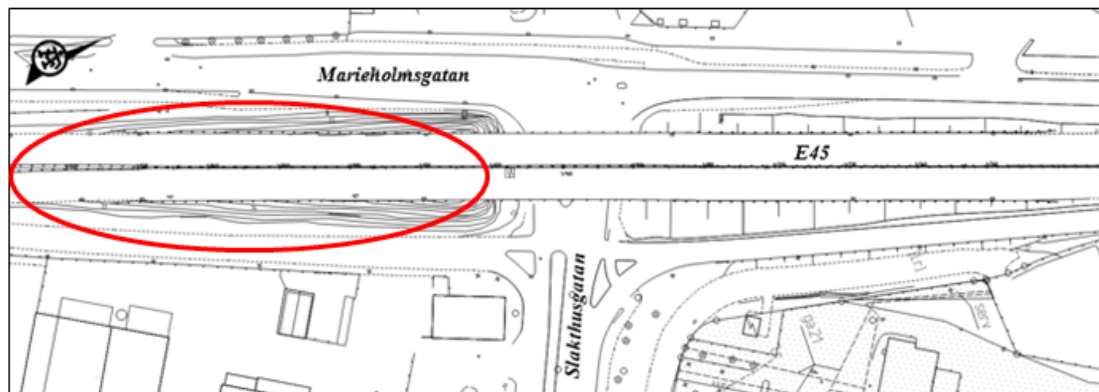


Figure 4.1. Overview of the highway bridge and the embankments at Slakthusmotet modified from (ÅF Infrastructure AB, 2015). The studied embankment is marked with the ellipse.

The following chapter will describe the history of the area, the local geology and the geotechnical conditions. The design of the embankments and their foundations will also be described as well as earlier investigations performed in the area, including settlement measurements of the embankments.

### 4.1 History of the area

It can be seen in old maps over the area that Marieholm was an island in the Göta Älv River until the second half of the 19<sup>th</sup> century. Figure 4.2 shows two maps over the area around Marieholm from year 1809 and year 1855. The Göta Älv River was in the beginning of the 19<sup>th</sup> century divided into two river beds, one on each side of Marieholm. At the middle of the eastern river bed large amounts of water entered the Göta Älv River from the Sävån River. The inflow of water caused calm conditions that allowed sedimentation of sand and silt, which eventually stopped the flow in the eastern riverbed. It can be seen in the map from year 1855 that the eastern riverbed has turned into a wetland north of the Sävån River. Marieholm started to develop as an industrial area around year 1900 when a number of larger industries were established, among them Slakthuset in year 1903 (Lönnroth, 2000). Since then Marieholm has continued to be an industrial area and a number of large infrastructural projects have been carried out there. A railway bridge was built in the southern part of the area in year 1909 (Hallingberg, et al., 1996) and the E45 highway crossing the area from north to south was built in the late 1960's.

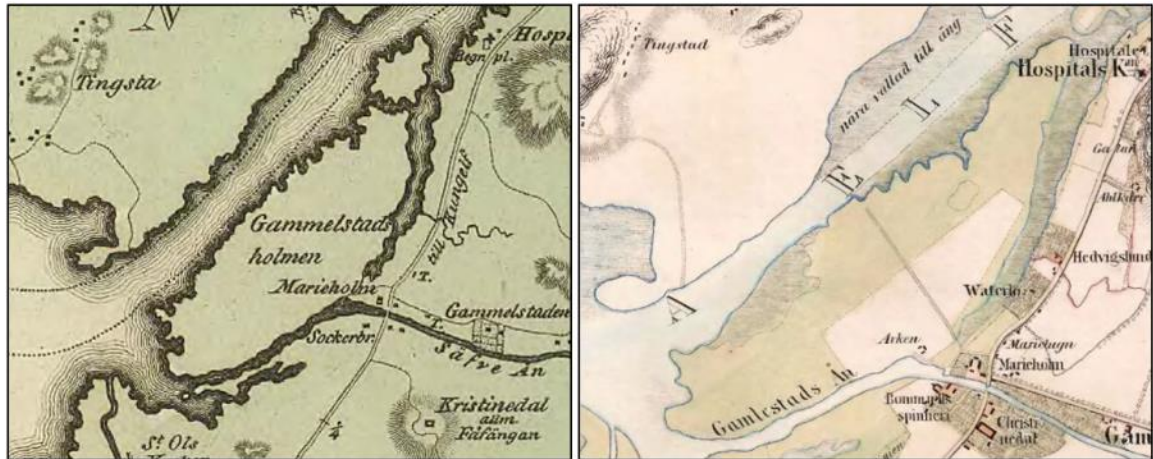


Figure 4.2. Marieholm in year 1809 (left) and in year 1855 (right) (Göteborgs Stadsbyggnadskontors Arkiv, 2015).

## 4.2 Geotechnical description

The geotechnical conditions in the Marieholm area is described by (Hallingberg, et al., 1996). The soil consists of deep layers of clay with a varying depth from 70 m to 100 m. The ground surface is generally horizontal covered with approximately 0,5 m to 2,5 m of filling material.

According to (Hallingberg, et al., 1996), the behaviour of the clay in Marieholm is the typical behaviour of Gothenburg-clay with a water content around 65 % to 85 % and an undrained shear strength of 15 to 20 kPa in the upper layers and increasing to 65 to 70 kPa in a depth of 50 m.

From oedometer test it has been shown that the OCR is above 1,0 in the whole area and that it is varying depending on the age of the soil layer (Hallingberg, et al., 1996). This OCR can be explained by a quasi-preconsolidation pressure as described in section 2.2.1. The in-situ stresses have been measured close to the Slakthusbron Bridge and from the results it has been stated that the in-situ stress is around  $0,8 \cdot \sigma'_c$  or greater and settlements have been classified as creep settlement with a rate of 0,5-2 mm/year.

The soil profile and soil parameters at the location of the Slakthusbron Bridge will be presented in following sections. Data is collected from previously performed geotechnical investigations in the area (Trafikverket, 2013b), (Trafikverket, 2014) and (ÅF Infrastructure AB, 2013). All the boreholes are located within the area illustrated in Figure 4.3. A detailed plan of the boreholes used for this case study can be seen in Appendix 1.1-1.6.

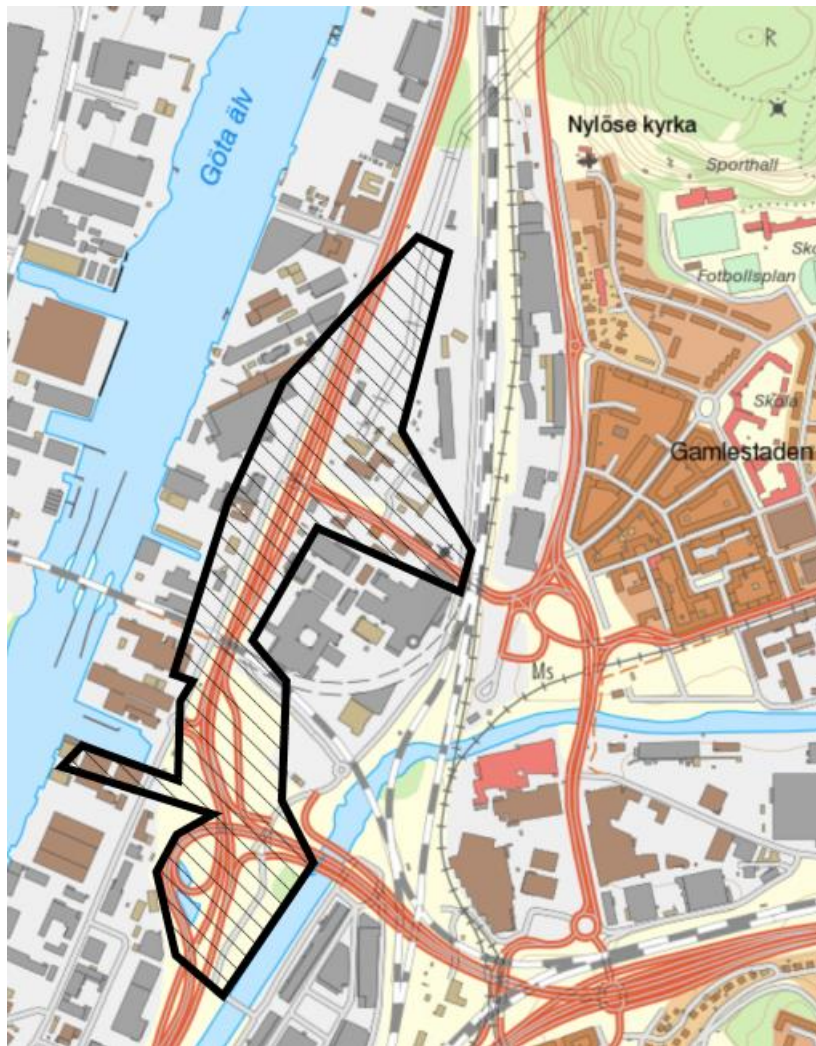


Figure 4.3. Overview of the area where the selected boreholes are located, modified from (Lantmäteriet, 2013)

#### 4.2.1 Soil profile

Geotechnical investigations were performed by Kjessler & Mannerstråle AB in 1966 before the construction of Slakthusmotet. Undisturbed samplings from borehole 81-16 shows that the soil profile consisted of deep layers of clay overlaid by a dry crust with a thickness of 2,5 m. Samplings performed in 1975 at the western side of the southern embankment by Göteborgs Gatukontor (boreholes 547-1 – 547-4) shows that the upper 2-2,5 m of the soil profile consists of filling material containing sand, gravel, clay and silt.

Soundings at the location of the bridge and its embankments have been performed down to a depth of 50 m without reaching refusal. About 300 m south-east of the studied embankment, the rock is located about 100 m below the ground surface (Hallingberg, et al., 1996).

It is therefore assumed that the clay layer under the studied embankment has a thickness of at least 70 m.

## 4.2.2 Soil parameters

In the following section, data is collected in order to evaluate important soil parameters. The data that is used is gathered from selected boreholes in the area around the Slakthusmotet. The quality of most of the undisturbed samples has been evaluated from the volume change at reconsolidation as described in (Larsson, et al., 2007). All samples were of good or fairly good quality. The location of the boreholes can be seen in Appendix 1.1 – 1.6.

### Unit weight - $\gamma_{soil}$

The unit weight of the clay is rather constant with depth. In the upper part of the soil profile, the unit weight is approximately  $16 \text{ kN/m}^3$ , where in the deeper layers, the unit weight becomes around  $17 \text{ kN/m}^3$ . The data is achieved from investigations performed by Kjessler & Mannerstråle in 1966 (borehole 81-16) and SGI in 1973 (borehole S84-SGI1).

### Water content $w_N$ and liquid limit $w_L$

The water content and the liquid limit are gathered from undisturbed samples from the boreholes S84-SGI, 81-16 and 81-21. The evaluated values plotted against depth are shown in Appendix 2.1. The water content is varying between 70% and 90% in the first 15 m, below 15 m; the water content becomes lower and has a value around 60% to 80%. The liquid limit in the area is varying less with depth compared to the water content and has a value throughout the whole profile around 65% to 80%. By comparing the water content and the liquid limit it can be seen that the water content in the soil is above or very close to the liquid limit at all depths in the profile.

### Pore water pressure – $u$

The groundwater table is varying in the area from 0,5 to 1,5 m below the ground surface (ÅF Infrastructure AB, 2013). The measured pore water pressure distribution and the hydrostatic pore pressure are plotted against depth in Appendix 2.2. When calculating the hydrostatic pore pressure, the groundwater level is assumed to be located 1 meter below ground surface. The pore water pressure is generally around 10 kPa higher than the hydrostatic pore pressure below a depth of 20 m.

### Undrained shear strength - $c_{uk}$

The undrained shear strength is evaluated from field-vane tests performed by Kjessler & Mannerstråle in 1966 at the location of the bridge. Figure 4.4 shows the undrained shear strength plotted against depth to a depth of 16 m. A linearization of the plotted values gives the following equation:

$$c_{uk} = \begin{cases} 12,6 \text{ kPa} & z < 4 \\ 12,6 + 1,8(z - 4) \text{ kPa} & z \geq 4 \end{cases} \quad (4.1)$$

In Figure 4.5 shear strength values at greater depths evaluated from other boreholes in the Marieholm area are added to the plot in Figure 4.4. All values are evaluated from field-vane tests. It can be seen that the linear increase continues also at greater depths. The presented values of the undrained shear strength are not corrected with respect to the liquid limit  $w_L$ , since it is recommended by the Swedish Commission on Pile Research to use uncorrected values when calculating bearing capacity of shaft-bearing piles.

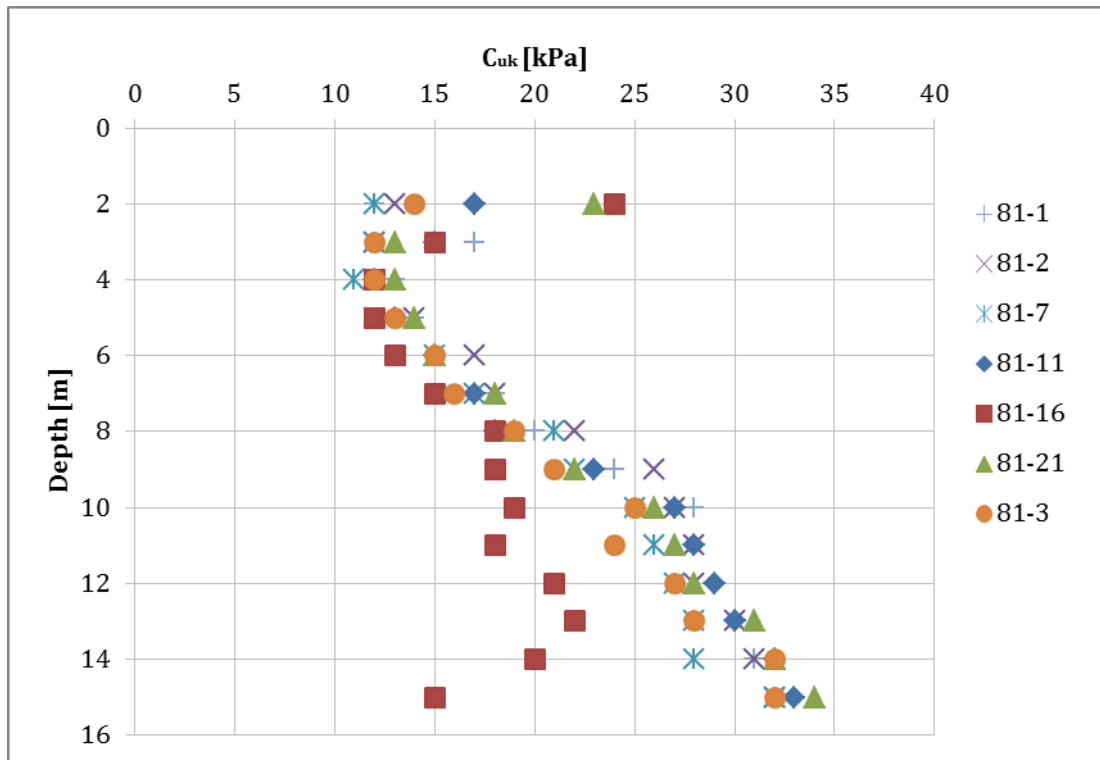


Figure 4.4. Undrained shear strength plotted against depth. The location of the boreholes can be seen in Appendix 1.1 – 1.6. The undrained shear strength is evaluated from field vane tests.

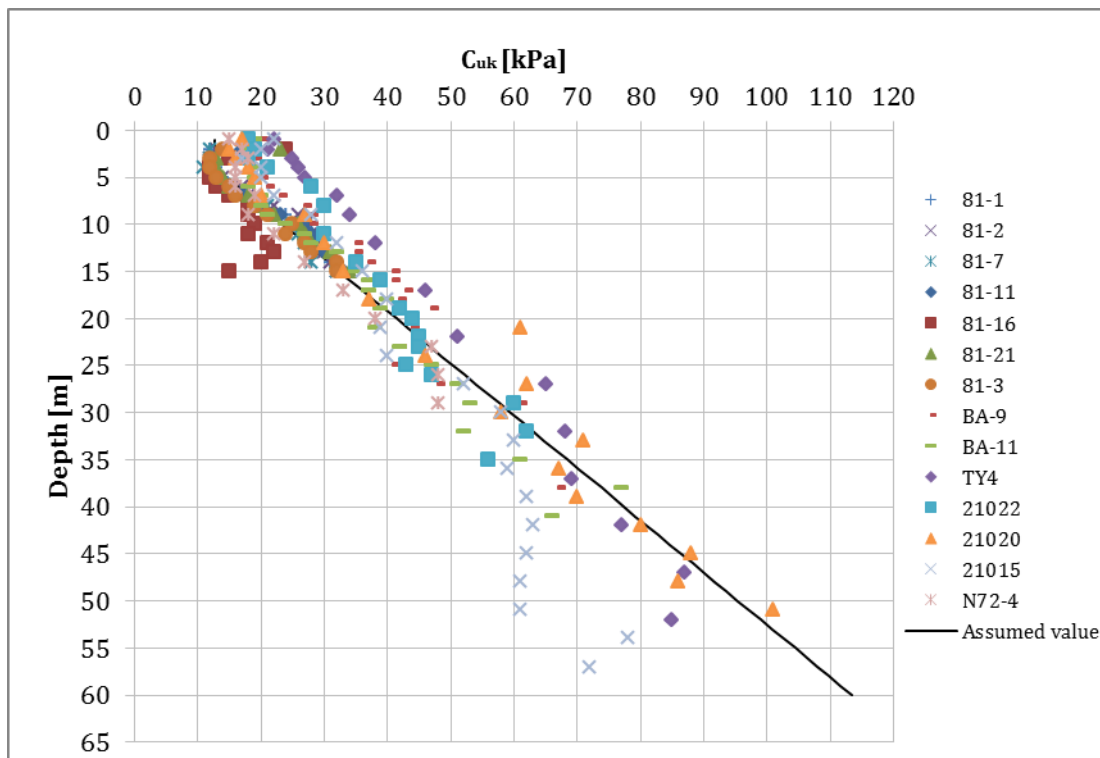


Figure 4.5. Undrained shear strength plotted against depth. The location of the boreholes can be seen in Appendix 1.1 – 1.6. The undrained shear strength is evaluated from field vane tests. The solid line shows the assumed shear strength used in the calculations.

### **Initial permeability, $k_{init}$ , and permeability reduction coefficient, $\beta_k$**

The initial permeability and permeability reduction coefficient was estimated from CRS tests. The initial permeability is decreasing almost linearly from approximately  $9,5 \cdot 10^{-10}$  to  $4,8 \cdot 10^{-10}$  m/s in the first 30 m, below 30 m it becomes rather constant around  $4,8 \cdot 10^{-10}$  m/s. The permeability reduction coefficient is almost constant around 3,75 throughout the depth. Evaluated values for  $k_{init}$  and  $\beta_k$  plotted against depth can be seen in Appendix 2.3.

### **Preconsolidation pressure – $\sigma'_c$**

The preconsolidation pressure in the area is evaluated from oedometer test, both CRS and increment loading. CRS-tests have been used for all boreholes except 81-16 and 844-2, where increment loading tests have been used. In Figure 4.6 both the preconsolidation pressure and the effective in-situ stress is plotted against depth. It should be noted that the effective in-situ stress in this plot is calculated based on only the weight of the soil without additional loads on the ground surface. It can be seen that the preconsolidation pressure is increasing linearly by depth. A linearization of the preconsolidation pressure gives following equation:

$$\sigma'_c = \begin{cases} 31,6 \text{ kPa} & z < 4 \\ 1,87 + 7,44z \text{ kPa} & z \geq 4 \end{cases} \quad (4.2)$$

Borehole BA-9 and 21022 are not taken into account in the linearization since the results from these boreholes are not following the general trend.

By comparing the effective in-situ stress and the preconsolidation pressure, the OCR is estimated. According to Figure 4.6, the clay seems to be normally consolidated or underconsolidated to a depth of 7 m, below this depth, OCR is between 1,1 to 1,2.

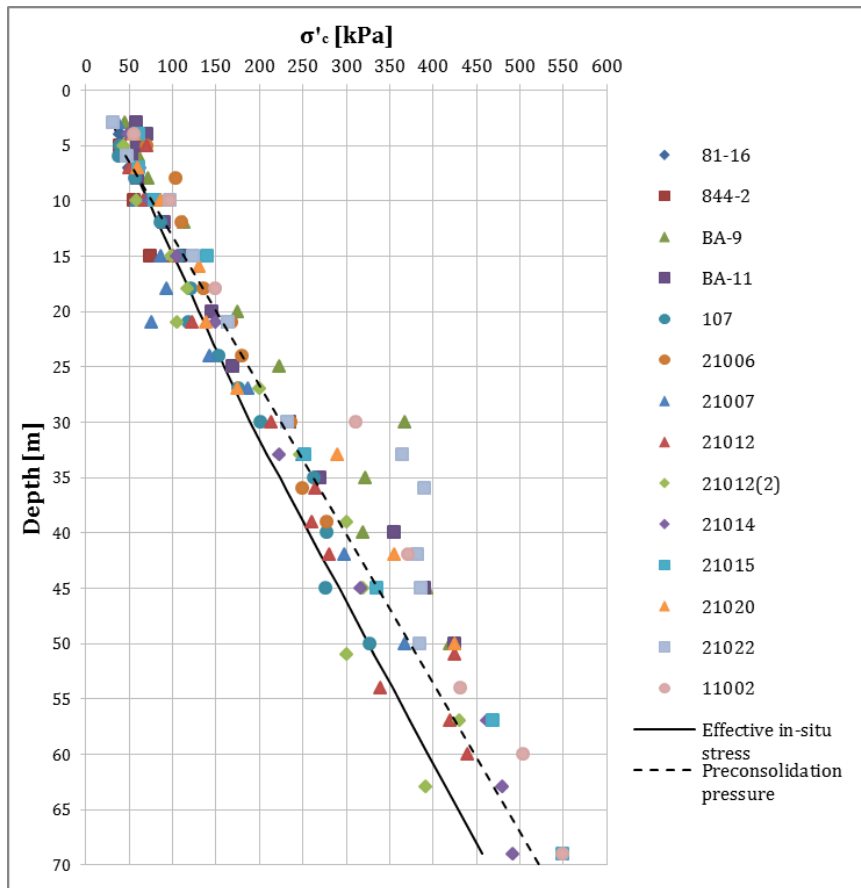


Figure 4.6. Preconsolidation pressure and effective in-situ stress plotted against depth. The preconsolidation pressure is evaluated from CRS-tests at all boreholes except 81-16 and 844-2, where IL-oedometer tests have been used. The dashed line represents the assumed preconsolidation pressure used in the calculations.

$\sigma'_L$  is increasing linearly by depth according to equation (4.3). The equation is given by linearization of evaluated values. The evaluated values plotted against depth are shown in Appendix 2.4.

$$\sigma'_L = 40,1 + 9,9z \quad (4.3)$$

### Compression modulus - $M_L$ , $M_0$ , $M'$

The compression modulus  $M_L$  and  $M'$  are evaluated from CRS tests performed on undisturbed samples from a number of boreholes in the Marieholm area. The evaluated values for  $M_L$  are plotted against depth in Figure 4.7. The evaluated values for  $M'$  plotted against depth are shown in Appendix 2.5. The location of the boreholes can be seen in Appendix 1.1 – 1.6.

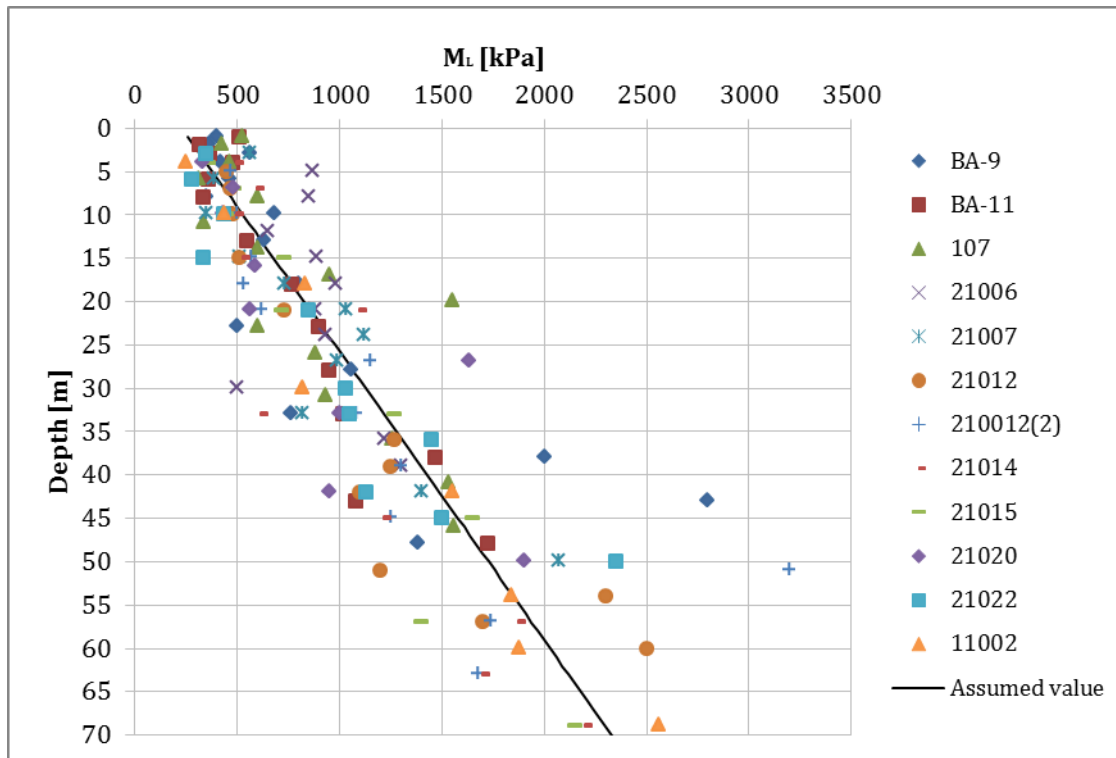


Figure 4.7. Compression modulus  $M_L$  evaluated from CRS tests from different boreholes in the Marieholm area plotted against depth. The solid line shows the assumed values used for the calculations.

As can be seen in Figure 4.7, the compression modulus is increasing linearly with depth. A linearization of the compression modulus gives following equation:

$$M_L = 229 + 30z \quad (4.4)$$

It should be noted that boreholes BA-9, 107, 2120 and 21012(2) are omitted since they are not following the general trend. The compression modulus  $M_0$  is evaluated from the empirical correlation with the undrained shear strength according to equation (2.8). The equation is recommended by the Swedish Geotechnical Institute and gives an approximate value of  $M_0$ . Equation (4.5) gives the assumed values for  $M_0$  in the studied area.

$$M_0 = \begin{cases} 3150, & z < 4 \\ 3150 + 450(z - 4), & z \geq 4 \end{cases} \quad (4.5)$$

#### Factors for improved modulus model - $a_0$ , $a_1$

The factors  $a_0$  and  $a_1$  were estimated from CRS test from two different boreholes (21015 and 21020) and the factors were evaluated as described in (Olsson, 2010). The factors are almost constant with depth. The average value of  $a_0$  is 0,8 while the average value of  $a_1$  is 1,1. The evaluated values for  $a_0$  and  $a_1$  is shown in Appendix 2.6.

#### Time resistance numbers - $r_0$ , $r_1$

The time resistance number  $r_1$  is estimated empirically from the natural water content according to equation (4.6) (Olsson, 2010).

$$r_1 = \frac{75}{w_N^{1.5}} \quad (4.6)$$

The natural water content is evaluated from undisturbed samples from three different boreholes. The value of  $r_1$  is increasing almost linearly from 90 at a depth of 4 m to around 130 at a depth of 30 m. Below 30 m the value is constant around 130. The evaluated  $r_1$  values plotted against depth are shown in Appendix 2.7.

The initial time resistance  $r_0$  is difficult to evaluate from the available field investigations performed in the Marieholm area. (Claesson, 2003) evaluated  $r_0$  from IL-oedometer tests for a number of test sites including one at Lundby strand in Gothenburg with a geology and geological history similar to Marieholm. The  $r_0$  value for this site was found to be around 1500. This value is assumed to be adequate also for Marieholm.

#### Factors for time resistance number model - $b_0, b_1$

The value of the factor  $b_0$  is set to  $\sigma'_0/\sigma'_c$  and the value of  $b_1$  is set to 1,1. These values are relevant for describing the creep behaviour for full-scale conditions according to (Claesson, 2003).

### 4.3 Embankment and foundation design

All the information about the embankment and foundation design is gathered from construction drawings and blueprints made by Kjessler & Mannerstråle AB in the late 1960's. Drawings of the pile design and pile installation plan can be seen in Appendix 3.1 and 3.2. In Figure 4.8, a schematic picture of the studied road embankment and sections is shown.

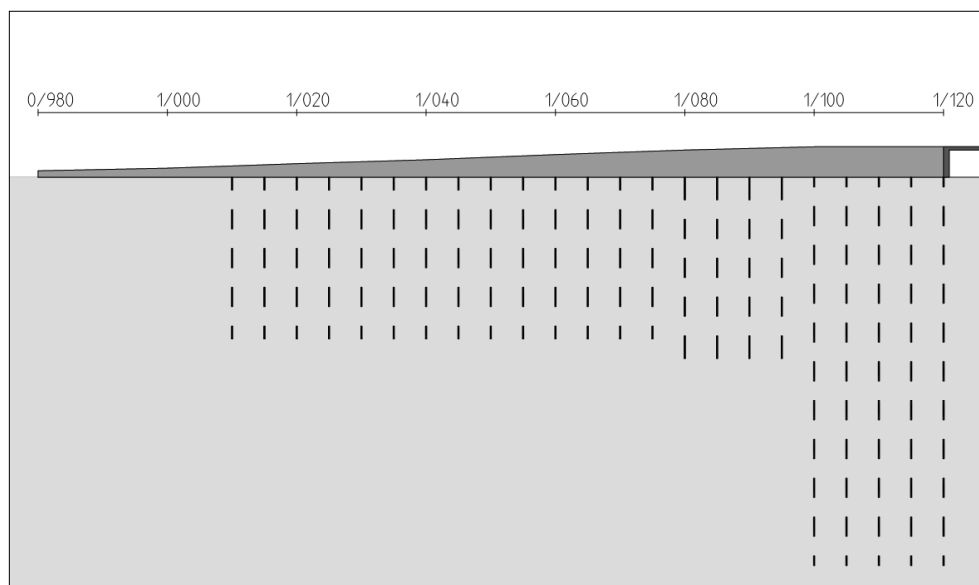


Figure 4.8. Schematic picture over the studied embankment where the location of the sections can be seen. The height and length of the embankment and the length of the piles are drawn to scale. It should be noted that the spacing of the piles is not drawn to scale.

The embankment is approximately 130 meters long and the height is approximately 5 m close to the bridge and 1 m in the lowest part close to section 1/000. The embankment material mainly consists of sand and gravel and also some filling material. In order to stabilize the steep slopes of the embankment, the western side of the embankment is filled with larger stone material.

The embankment is founded on a large number of piles. There are several different types of piles used in the foundation; either there are plain timber piles or timber piles jointed with a concrete pile. All piles are constructed with pile caps of concrete with varying dimensions. Under the centre line of the road, the piles are driven in vertical direction, while the rest of the piles under the embankment are driven with an inclination of 4:1. Closest to the bridge, the embankment is founded with jointed timber and concrete piles with a length of 60 meters followed by timber and concrete piles of 34 meters. Further away from the bridge, the embankment is founded on plain timber piles with a total length of 28 meters followed by shorter timber piles of 25 meters. The spacing between the piles are varying, generally there are less space between the piles close to the bridge. The intensity of piles is decreasing further away from the bridge. Detailed drawing of the pile design and pile installation plan can be seen in Appendix 3.1 and 3.2.

#### **4.4 Earlier settlement investigations**

Several settlement measurements performed in the Marieholm area shows on-going settlements. A hose-settlement gauge installed in year 2003 close to borehole 21015 indicates that settlements occur down to a depth of about 25 m, with the largest settlements in the top 10 m (Trafikverket, 2014). Between year 2003 and 2008 the soil settled about 30 mm at 2 m depth and about 10 mm at 10 m depth. This gives a rate of settlement of 6 mm/year at 2 m depth and 2 mm/year at 10 m depth. The variation of the natural water content indicates that settlements should occur mostly in the top 20 m since the water content below this level is rather low and constant with depth.

The settlements of the studied road embankment have been investigated in the 1980's and in 2014 (ÅF Infrastructure AB, 2015). Both investigations included measurements of the road surface level at a number of points along the embankments and also geophysical measurements of the asphalt thickness. The investigations showed that the asphalt thickness varied along the embankment between approximately 50 cm to around 150 cm. The measured asphalt thickness and the variations along the embankment did not vary significantly between the 1980's and 2014. Profiles of the eastern and western side of the road embankment showing the measured road surface level and the asphalt thickness in year 2014 together with the designed road surface level in year 1967 can be seen in Appendix 4.

Based on the measured levels of the road surface and the asphalt thickness, an analysis of the ground settlement has been performed for the south embankment. Three sections of the embankment were chosen to the analysis; 1/000, 1/045 and 1/085. Section 1/000 and 1/085 were chosen to be analysed since the earlier investigations indicates large settlements. Section 1/045 was chosen because of the relatively small settlements compared to the other two sections.

The level of the road surface of the embankment was measured in year 1980,-81,-85 and 2014. The settlement of the ground was calculated by adding the measured settlement of the road surface and the difference in the asphalt thickness. The calculated settlements from year 1967 to 2014 can be seen in Figure 4.9. A mean level between the east side and the west side has been used when evaluating the settlements.

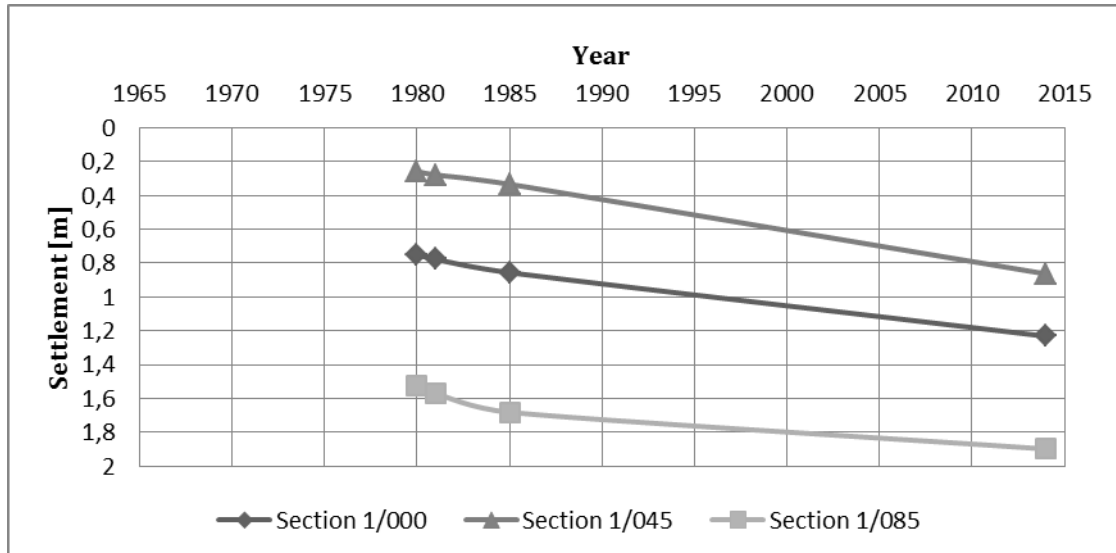


Figure 4.9. Measured settlements from year 1967 to 2014 of the south embankment at different points. The settlements are calculated based on data measured in year 1980,-81,-85 and 2014.

As can be seen in Figure 4.9, large initial settlements take place in section 1/000 and 1/085. Section 1/085 has the largest total settlement of approximately 2 m. Section 1/000 has a total settlement of around 1,2 m. The third section, 1/045, have the smallest settlements of approximately 0,8 m.

## 5 Settlement calculations

In order to model the development of settlements in GS Settlement, the calculation is performed over a long period of time. The calculation starts at the year 1950 and continues over a period of 100 years, until year 2050. The calculations have been performed at three sections along the studied embankment. The three sections are section 1/000, 1/045 and 1/085. The geometry of the embankment at the three sections can be seen in Figure 5.1 and is based on construction drawings performed by Kjessler & Mannerstråle AB in the 1960's.

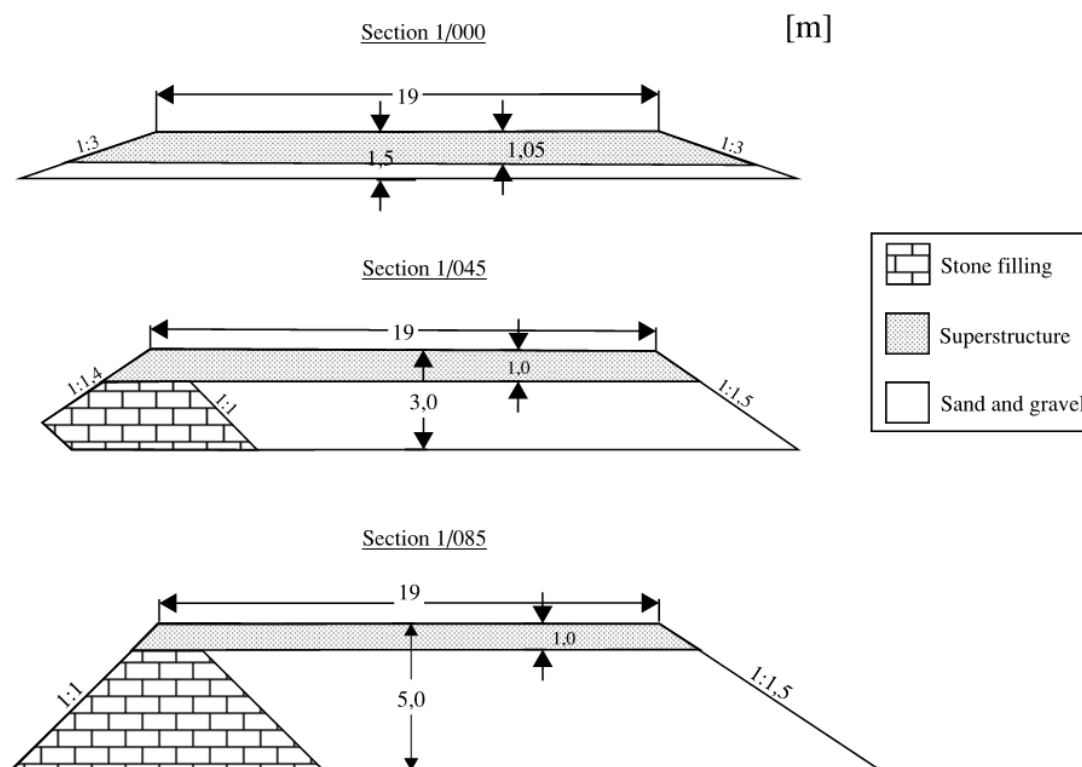


Figure 5.1. Geometry of section 1/000, 1/045 and 1/085 based on construction drawings.

The dominating material in the embankment is sand and gravel. In section 1/045 and 1/085, the western slope is supported by stone filling. The assumed unit weight of the materials in the embankment can be seen in Table 5.1.

Table 5.1. Assumed unit weight of the embankment material (Trafikverket, 2011).

Material	Unit weight [kN/m <sup>3</sup> ]
Superstructure	22
Stone filling	19
Gravel and sand	19

Hand calculations have been performed for section 1/000 in order to verify the results from GS Settlements. The hand calculations have been carried out according to methods described in (Sällfors, 2001). A simplified soil model have been used, where the soil is divided into nine homogenous layers. The additional stresses caused by the

embankment are calculated with the 2:1 method. In the hand calculations, the additional asphalt added after construction of the embankment is not taken into account. The performed hand calculations can be seen in Appendix 5.

## 5.1 Soil model

The soil model implemented in GS Settlement is based on the soil parameters described in section 4.2.2. It is assumed that the soil profile consist of clay to a depth of 70 m with a 1,5 m thick layer of dry crust and filling material on top. The groundwater level is assumed to be located one meter below ground surface. The pore water pressure in the clay is set to be linearly increasing from 0 kPa at a depth of 1 m to 10 kPa higher than the hydrostatic pore water pressure at a depth of 70 m. The profile is considered to be drained in both directions. The compression modulus and preconsolidation pressure is set to high values in the crust in order to avoid settlement in this layer. Since the soil seems to be normally consolidated in the first 7 m, the preconsolidation pressure is assumed to be equal to the in-situ stress down to a depth of 7 m. The reference time,  $t_r$ , is set to - 0,00274 years (- 1 day). The soil parameters that are implemented in the GS Settlement model are listed in Table 5.2.

Table 5.2. Soil parameters implemented in the GS Settlement model.

Layer	Depth	$\gamma_{soil}$ [kN/m <sup>3</sup> ]	$M_0$ [kN/m <sup>2</sup> ]	$M_L$ [kN/m <sup>2</sup> ]	$M'$ [-]	$a_0$ [-]	$a_1$ [-]	$\sigma'_c$ [kN/m <sup>2</sup> ]
Crust	0,0	18	15000	1000	12	0,8	1,1	500
	1,5	18	15000	1000	12	0,8	1,1	500
Clay 1	1,5	16	3150	274	12	0,8	1,1	25
	4	16	3150	349	12	0,8	1,1	38
Clay 2	4	16	3150	349	12	0,8	1,1	38
	7	16	4500	439	12	0,8	1,1	55
Clay 3	7	16	4500	439	12	0,8	1,1	55
	30	16	14850	1129	12	0,8	1,1	225
Clay 4	30	17	14850	1129	12	0,8	1,1	225
	70	17	32850	2329	12	0,8	1,1	522

Layer	Depth	$\sigma'_L$ [kN/m <sup>2</sup> ]	$b_0$ [-]	$b_1$ [-]	$r_0$ [-]	$r_1$ [-]	$k_{init}$ [m/years]	$\beta_k$ [-]
Crust	0,0	550	-	-	-	-	0,03	3,75
	1,5	550	-	-	-	-	0,03	3,75
Clay 1	1,5	79,7	1	1,1	1500	90	0,03	3,75
	4	79,7	1	1,1	1500	95	0,028	3,75
Clay 2	4	79,7	1	1,1	1500	95	0,028	3,75
	7	109,4	1	1,1	1500	99	0,0265	3,75
Clay 3	7	109,4	0,87	1,1	1500	99	0,0265	3,75
	30	337,1	0,87	1,1	1500	130	0,015	3,75
Clay 4	30	337,1	0,87	1,1	1500	130	0,015	3,75
	70	733,1	0,87	1,1	1500	130	0,015	3,75

## 5.2 Modelling of additional stresses

In year 1950, a load of 2 kPa is applied on the ground surface in order to try to start the calculations in the program before the embankment is constructed in year 1967. Since the geometry and the foundation of the embankment are varying along the road stretch, the additional stresses caused by the embankment have to be modelled differently in the sections. In the following subchapters, the modelling of the additional stresses is explained. The assumed load distribution areas in the different sections are shown in Appendix 6.

### 5.2.1 Section 1/000

Since the embankment in section 1/000 is not founded on piles, the additional stresses caused by the embankment are modelled as a surface load in GS Settlement. The additional stresses in the soil profile are then calculated in the program according to the finite Boussinesq model. The surface load is chosen to be stretching from section 0/950 to 1/010 as can be seen in Appendix 6. The height of the embankment is increasing closer to the Slakthusbron Bridge while the embankment is assumed to be quite similar to section 1/000 southward the section. Therefore, an infinite elongated surface load governed by the size of the embankment would not be appropriate to illustrate the real situation. Furthermore, the embankment is founded on piles from section 1/010 (see Figure 4.8) which will lead to a different stress situation in the ground due to the stress distribution caused by the piles. Closer to the piled foundation the stresses will probably be higher in the deeper soil layers and lower in the upper layers since the piles are transferring the load to deeper soil layers. However, since the settlement is most likely to appear in the upper part of the soil, the impact of increasing stresses in the lower part of the profile is assumed to be negligible. Therefore, a 50 meter long load south of section 1/000 and 10 meter long load north of the section is assumed to be an adequate way to describe the stress situation in section 1/000.

According to earlier investigations, asphalt has been added on the road surface between year 1967 and 2014. The amount of asphalt added between year 1967 and 1981 is approximately 0,66 m, and between year 1981 and 2014, 0,14 m. In the calculations, asphalt is assumed to be added three times between year 1967 and 1981, 0,22 m each time. Between year 1981 and 2014, 0,07 m of asphalt is assumed to be added twice. Applied loads from the embankment and asphalt can be seen in Figure 5.2.

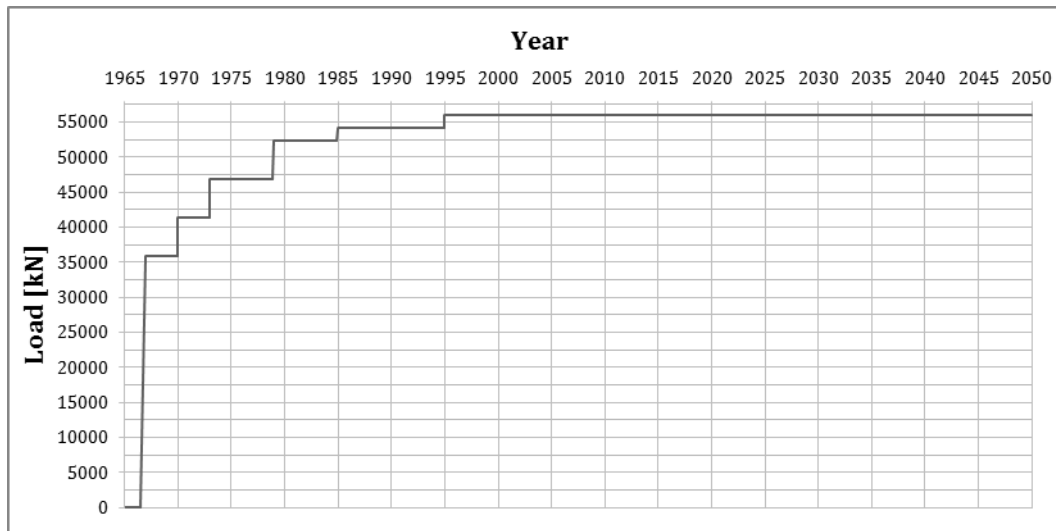


Figure 5.2. Applied loads in section 1/000. The embankment is built in year 1966, asphalt is assumed to be added at five times after the construction of the embankment.

### 5.2.2 Section 1/045 and 1/085

Section 1/045 and 1/085 are founded on piles; the distribution of the additional stresses is therefore hand calculated separately before implementation in GS Settlement. The calculation is based on the neutral plane principle where the resistance of a pile is compared to the action effects as described in section 2.3.2. Since both sections are founded on two different types of piles (TT1 and TT2 in section 1/045 and TT4 and TT5 in section 1/085), a mean value of the resistance and geotechnical bearing capacity is used in each section. The calculations of resistance and geotechnical bearing capacity are taking into account the varying shaft area, adhesion and shear strength of the soil along the piles (see Appendix 7.1 and 7.2). The resistance is calculated for each meter and by comparing the resistance of each meter with the geotechnical bearing capacity of the piles, a percentage of the geotechnical bearing capacity is calculated for each meter below the neutral plane. It is thereafter assumed that the load distributed at each level of the foundation is equal to the percentage of the geotechnical bearing capacity. In order to calculate the stresses at each level, load is distributed over the piled area at the certain level. The piled area is increasing by depth due to the tilted piles. The stress distribution under each level is calculated according to the 2:1-method (as described in (Sällfors, 2001)).

In cases where the geotechnical bearing capacity of the foundation is exceeded, the remaining load from the embankment that cannot be distributed by the foundation is assumed to be distributed with the 2:1-method from ground surface.

When calculating the stresses in section 1/045 it is assumed that the embankment is horizontal with a length of 60 m and a width of 19 m. The dimensions of the embankment are chosen in order to try to illustrate the stress situation in the section. By studying the pile installation plan and the dimensions of the surrounding embankment, the inclination and design of the embankment within these 60 m seems to be quite similar.

According to the earlier investigation, 0,2 m of asphalt have been added to the road between year 1967 and 1981 and an additional 0,1 m between year 1981 and 2014. In

the calculations, 0,1 m of asphalt was added three times between year 1967 and 2014. The applied loads at the different time steps can be seen in Figure 5.3. Since the geotechnical bearing capacity of the piles are not exceeded, all loads are assumed to be distributed to the piles.

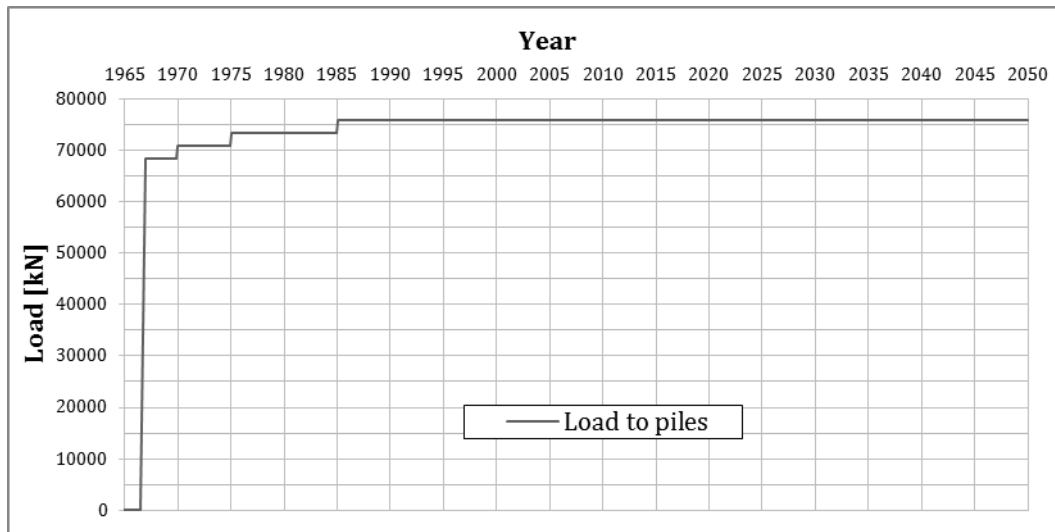


Figure 5.3. Applied loads at different time steps in section 1/045. Asphalt is assumed to be added at three occasions after the construction of the embankment.

The additional stresses in the soil profile at section 1/045 for different time steps are shown in Figure 5.4.

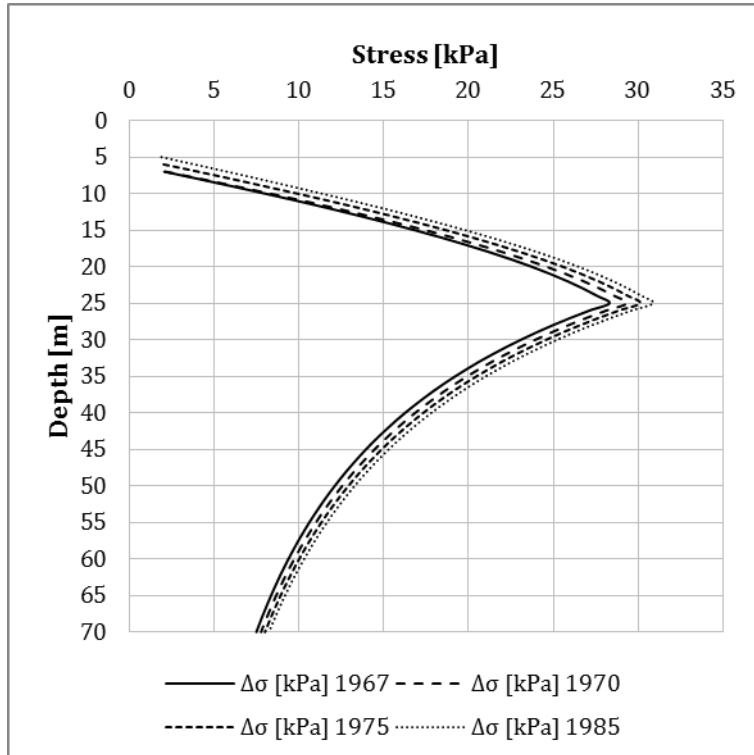


Figure 5.4. Calculated additional stresses implemented in GS Settlement in section 1/045.

The additional stresses in section 1/085 are calculated assuming a horizontal embankment with the dimensions of 40 times 19 m. Since the bridge is located at section 1/120 and there are 60 m long concrete piles close to the support of the bridge, it is likely that the stresses in the upper soil layers will be decreasing close to the bridge. Therefore, the load from the embankment is chosen to be covering a smaller area than in section 1/045.

Earlier investigations shows that between year 1967 and 1981, 1,3 m of asphalt have been added to the road, and 0,1 m between year 1981 and 2014. In the modelling of the embankment, 0,3 m of asphalt were chosen to be added at four times between year 1967 and 1981 followed by 0,1 m once after year 1981. Figure 5.5 shows the applied loads at different time steps in section 1/085. The geotechnical bearing capacity of the piles is exceeded in year 1973; the loads applied thereafter are therefore applied as surface loads.

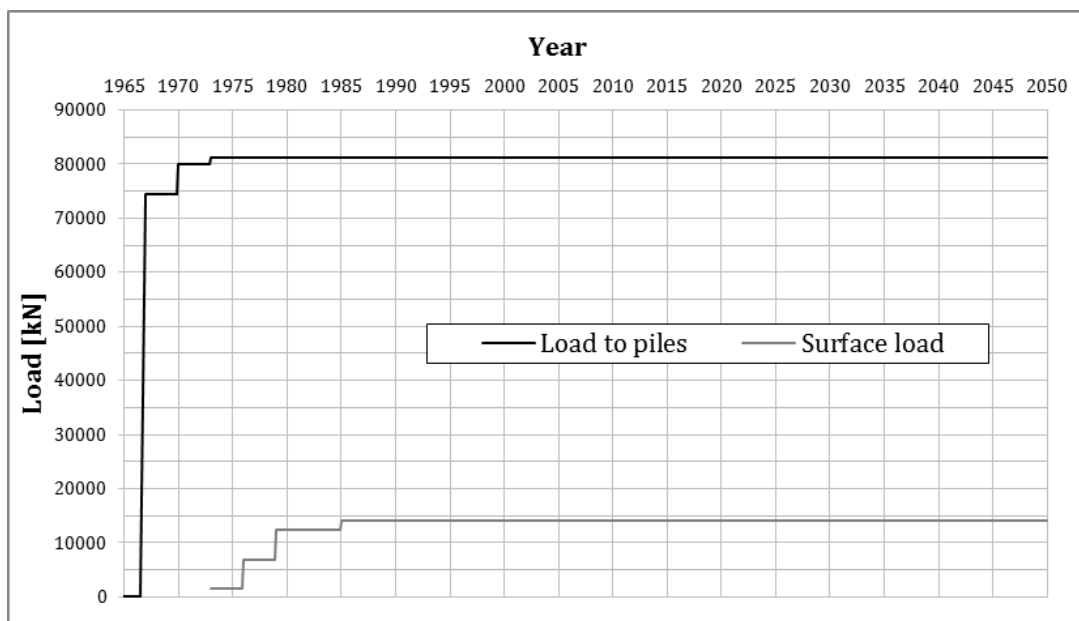


Figure 5.5. Applied loads at different time steps in section 1/085. Asphalt is assumed to be added at five occasions after the construction of the embankment. After year 1973 the geotechnical bearing capacity of the piles is exceeded and loads are applied as surface loads.

The additional stresses in the soil profile at different time steps are shown in Figure 5.6.

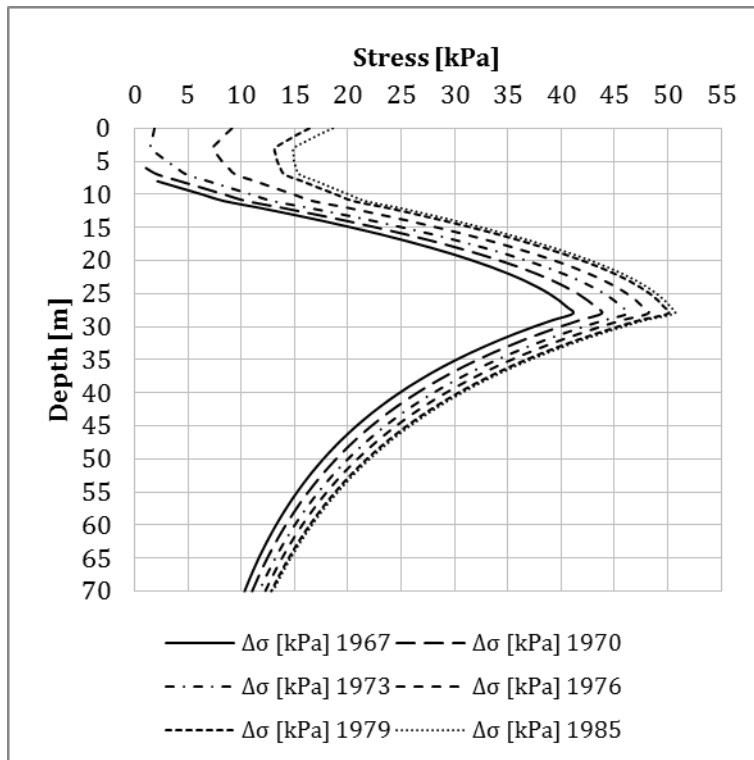


Figure 5.6. Calculated additional stresses implemented in GS Settlement in section 1/085.

### 5.3 Stress charts

When plotting the additional stresses calculated in section 5.2 against depth together with the effective in-situ stresses and the preconsolidation pressure the following stress charts are obtained. Figure 5.7 shows the stresses in section 1/000 in the upper 35 m of the soil profile, the stresses at all depths can be seen in Appendix 8.1. Since asphalt is added after the construction of the embankment the additional stresses are increasing over time. It is assumed that all asphalt has been added between year 1967 and 1995. It can be seen that the sum of the effective in-situ stress and the additional stresses is exceeding the preconsolidation pressure from a depth of 1 m down to a depth between 15 m and 20 m.

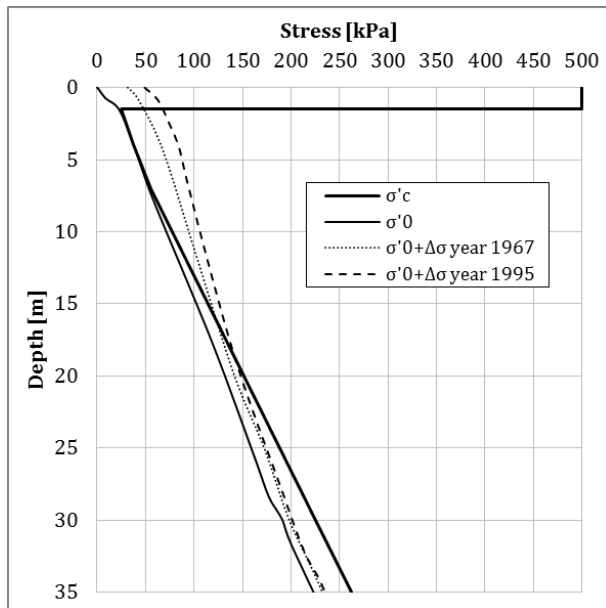


Figure 5.7 Stress chart for section 1/000 in the upper 35 m of the soil profile. The stresses at all depths can be seen in Appendix 8.1.

The stresses to a depth of 45 m in section 1/045 are shown in Figure 5.8, Appendix 8.2 shows the stresses at all depths. Due to the piles in this section the additional stresses are smaller and also applied at a larger depth than in section 1/000. Since the amount of asphalt that is added after the construction of the embankment is rather small, the additional stresses are not increasing significantly over time. It is assumed that all asphalt has been added between year 1967 and 1985. The sum of the effective in-situ stress and the additional stresses is slightly exceeding the preconsolidation pressure from a depth of approximately 7 m to 27 m.

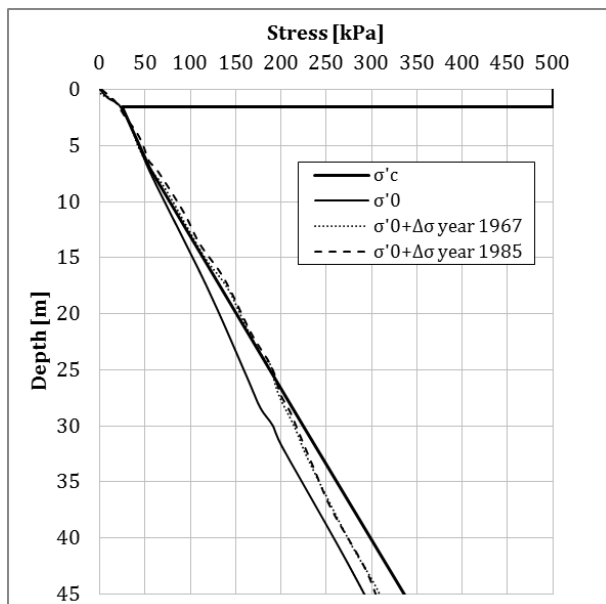


Figure 5.8. Stress chart for section 1/045 in the upper 45 m of the soil profile. The stresses at all depths can be seen in Appendix 8.2.

Figure 5.9 shows the stresses in section 1/085 for the upper 45 m of the soil profile, to see the stresses at all depths, see Appendix 8.3. In this section it is assumed that all

asphalt has been added between year 1967 and 1985. Due to the large amount of added asphalt and the exceeded geotechnical bearing capacity of the piles, there is a rather big difference between the additional stresses in year 1967 and in 1985. In year 1967 the preconsolidation pressure is exceeded at the depths between 10 to 30 m. In year 1985 the preconsolidation pressure is exceeded from the ground surface to a depth of about 35 m.

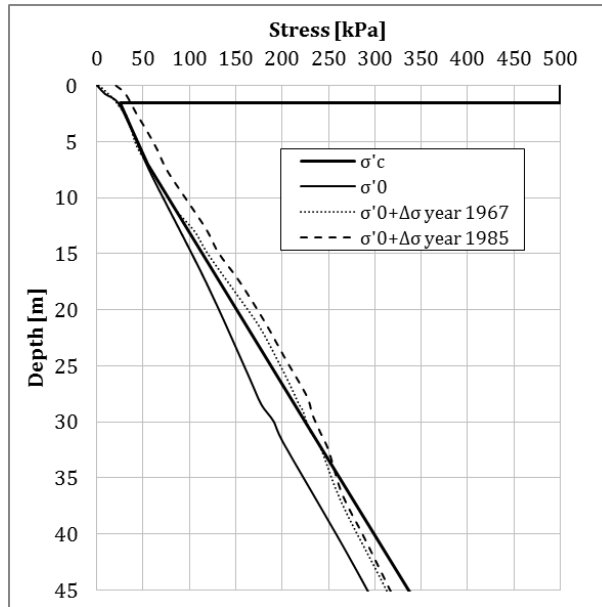


Figure 5.9. Stress chart for section 1/085 in the upper 45 m of the soil profile. In Appendix 8.3, the stresses at all depths are shown.

## 6 Results from settlement calculations

The results from the calculations performed in GS Settlement are presented in the following chapter.

### 6.1 Section 1/000

The resulting settlement from the calculations with and without creep for section 1/000, together with the measured settlements and applied loads are shown in Figure 6.1. The loads in section 1/000 are applied as surface loads since embankment is founded without piles. The settlement have been measured in year 1980, -81, -85 and 2014, the line representing the measured settlement is an interpolation between these measurements.

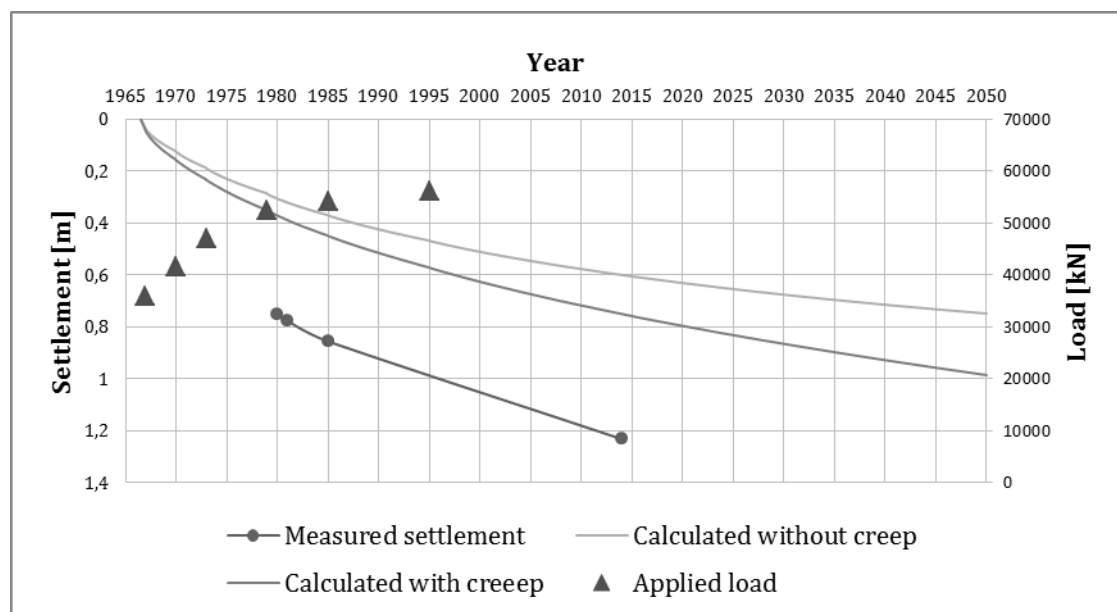


Figure 6.1. Resulting settlement in section 1/000 from calculations in GS Settlement, with and without creep. Measured settlement and applied loads are also shown in the figure. The applied loads are applied as surface loads since the section is founded without piles. Note the different scales on the y-axes.

As can be seen in Figure 6.1, calculated settlements with creep is about 0,5 m less than the measured settlement in year 2014. In year 1980 and 1985 the difference between measured settlement and calculated settlement with creep is approximately 0,4 m. The measured rate of settlement between year 1985 and 2014 is around 13 mm/year while the calculated rate of settlement is approximately 10 mm/year when calculating with creep and 8 mm/year when calculating without creep.

Figure 6.2 shows a comparison between the development of the settlements over time according to the hand calculations and calculations in GS Settlement. Both the hand calculations and calculations performed in GS Settlement are in this case calculated without creep and without additional surface loads after the construction of the embankment. It can be seen that between year 1967 and 1990 the hand calculations and the calculations in GS Settlement is showing almost the same results. However, in year 2050 the difference between the two calculations is approximately 0,1 m.

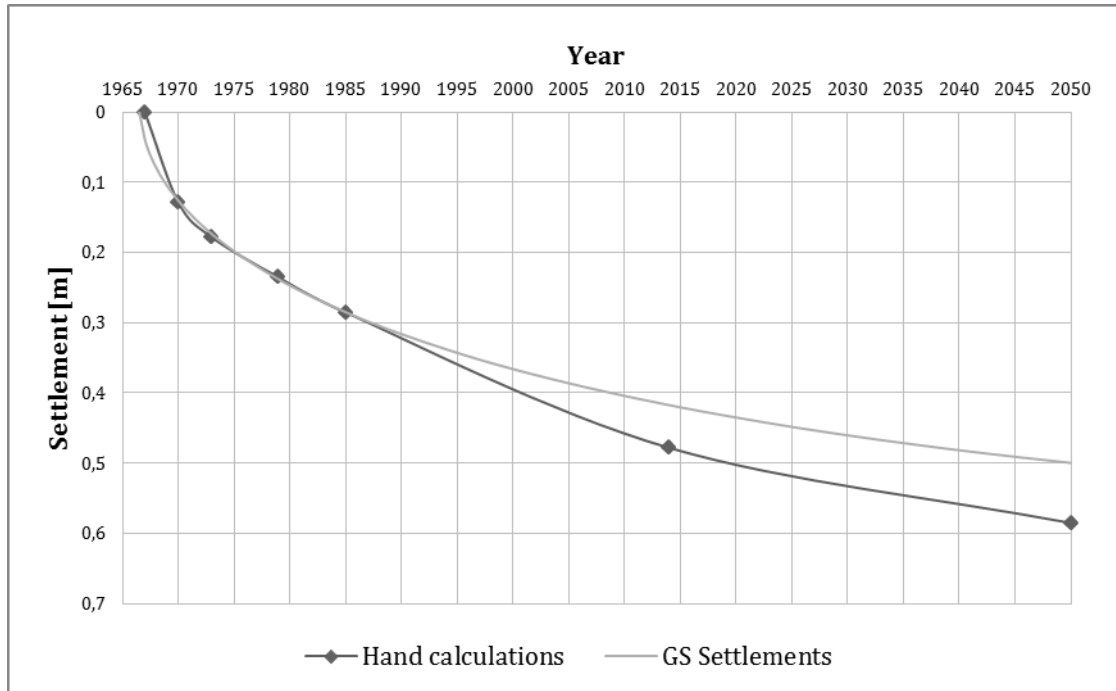


Figure 6.2. Settlements at section 1/000 according to hand calculations and calculations with GS Settlement where additional asphalt and creep effects are omitted.

Figure 6.3 shows the excess pore water pressure in section 1/000 at the years 1967, 2014 and 2050, when no asphalt has been added after construction of the embankment. As can be seen, the excess pore water pressure is higher in the upper part of the soil profile and lower at the deeper soil layers in year 1967 compared to 2050. It can also be seen that the excess pore water pressure between year 1967 and 2014 have started to dissipate and even out over the profile, however, there are still excess pore water pressure in year 2050.

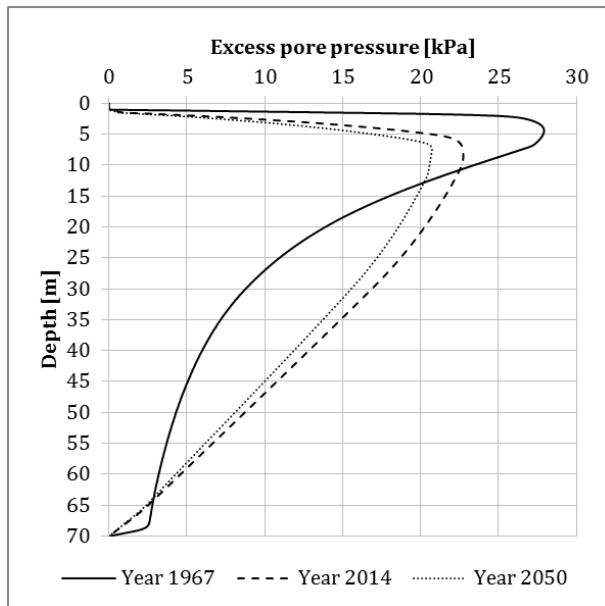


Figure 6.3. Excess pore water pressure plotted against depth at the year 1967, 2014 and 2050 in section 1/000 from a calculation where no additional asphalt have been added to the embankment.

Figure 6.4 shows the excess pore water pressure in section 1/000 from a calculation where additional asphalt has been added to the embankment. The excess pore water pressure has increased at the year 2014 and 2050 compared to 1967.

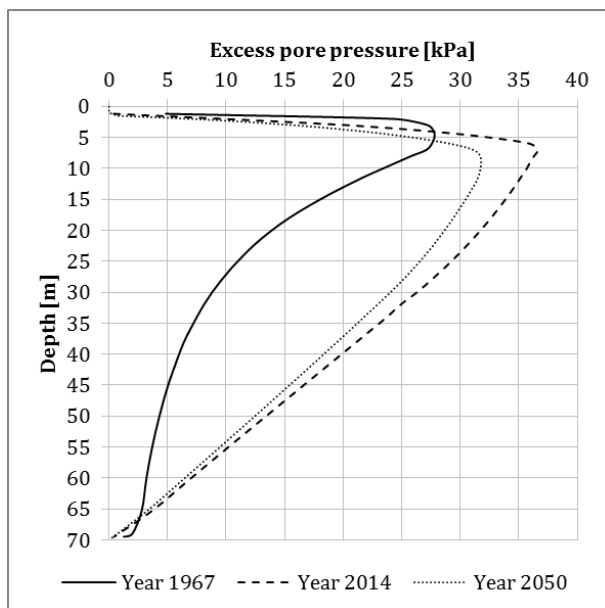


Figure 6.4. Excess pore water pressure plotted against depth at the year 1967, 2014 and 2050 in section 1/000. In this model, asphalt has been added to the embankment.

Figure 6.5 shows the calculated effective stresses and the preconsolidation pressure in section 1/000 to a depth of 60 m. It can be seen that in year 2014 the effective stresses have exceeded the preconsolidation pressure down to a depth of about 7 m.

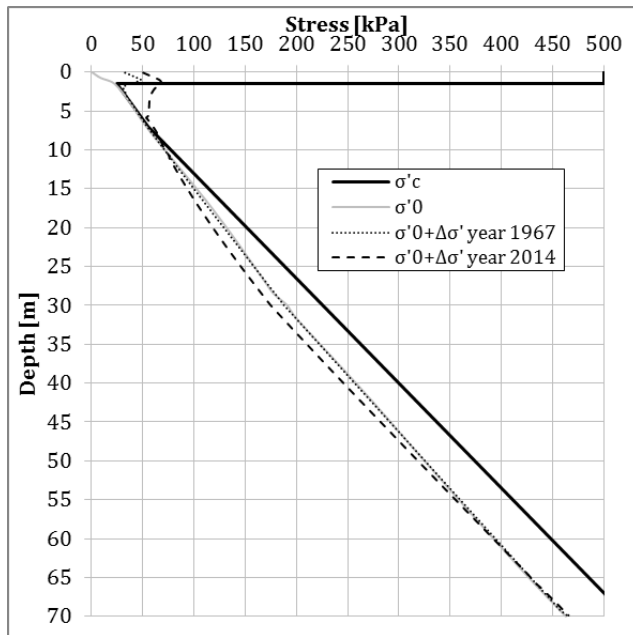


Figure 6.5. Preconsolidation pressure and calculated effective stresses in year 1967 and 2014 in section 1/000.

Figure 6.6 shows the calculated strains in the soil profile in section 1/000. The largest strain occurs in the upper part of the profile, while small strains can be seen in the bottom of the profile.

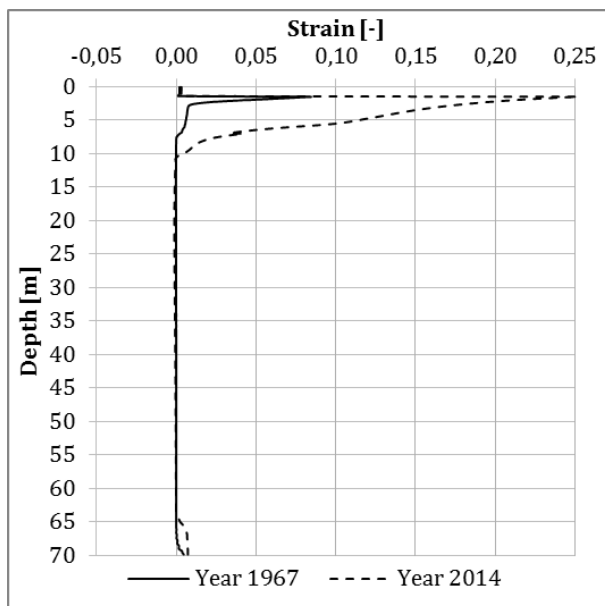


Figure 6.6. Calculated strain plotted against depth in the year 1967 and 2014 in section 1/000.

## 6.2 Section 1/045

The results from the settlement calculations in GS Settlement for section 1/045, and the measured settlements together with the applied loads are shown in Figure 6.7. Section 1/045 is founded on piles and the load is distributed as explained in section 5.2.2. The settlement have been measured in year 1980, -81, -85 and 2014, the line representing the measured settlement is an interpolation between these measurements.

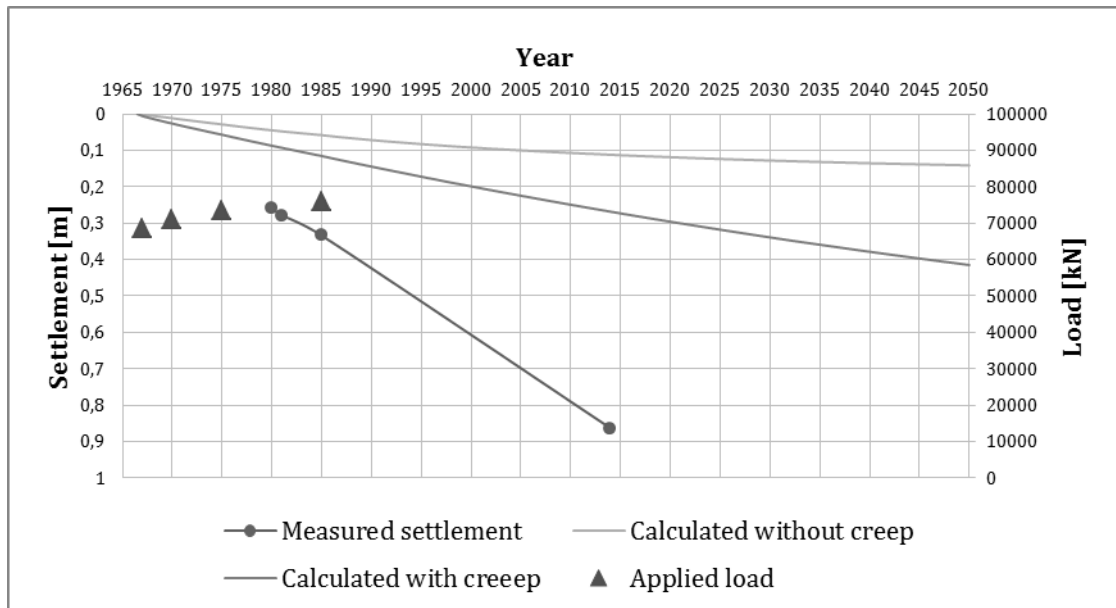


Figure 6.7. Resulting settlement in the piled section 1/045 from calculations in GS Settlement, with and without creep. Measured settlement and applied loads are also shown in the figure. Note the different scales on the y-axes.

By studying Figure 6.7, it can be seen that calculated settlements with creep is about 0,6 m less than the measured settlement in year 2014. The measured rate of settlement between 1985 and 2014 is approximately 18 mm/year while the calculated rate of settlement is around 5 mm/year when calculating with creep and 2 mm/year when calculating without creep.

In Figure 6.8 the development of calculated excess pore water pressure in section 1/045 is shown. It can be seen that the highest excess pore water pressure can be found at a depth of approximately 25 m in 1967 which is at the same depth as the pile toes. In 2014, the excess pore water pressure has started to dissipate and event out over the profile. However, there is still excess pore water pressure in year 2050.

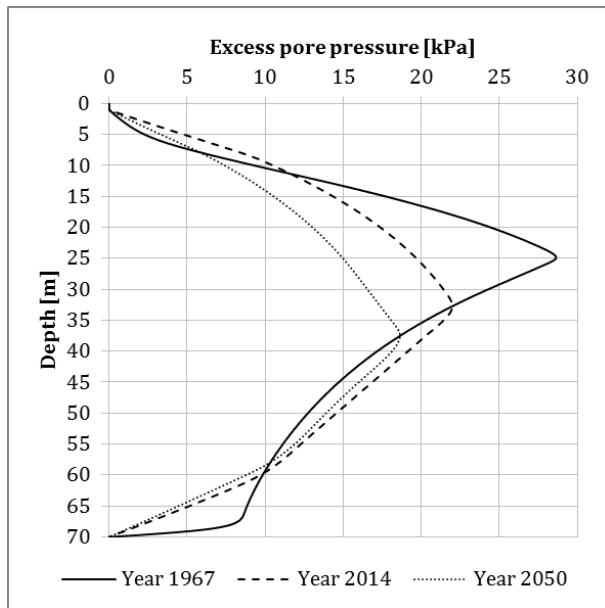


Figure 6.8. Calculated excess pore water pressure plotted against depth in year 1967 and 2014 in section 1/045.

The calculated effective stresses in section 1/045 are shown in Figure 6.9. The preconsolidation pressure is slightly exceeded in the top five meters. Below this depth the effective stresses are close to the preconsolidation pressure without exceeding it.

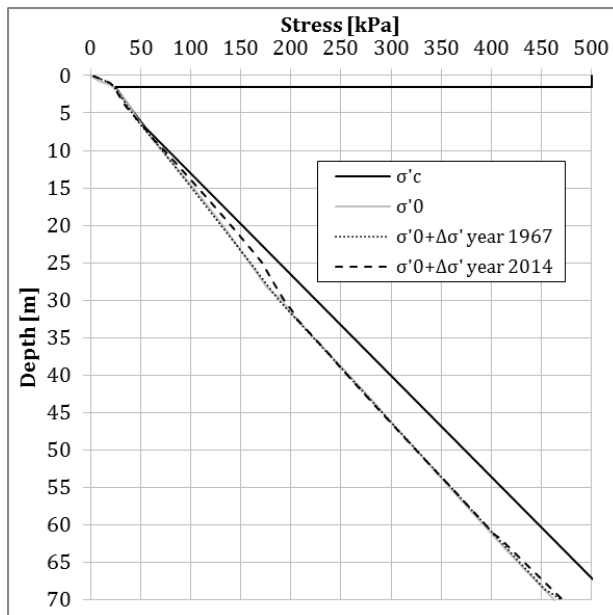


Figure 6.9. Preconsolidation pressure and calculated effective stresses in year 1967 and 2014 in section 1/045 plotted against depth.

Figure 6.10 illustrates the calculated strain in the soil profile in section 1/045. As can be seen, the largest strains occur between 10 m and 25 m, where also the largest effective stresses arise (see Figure 6.9).

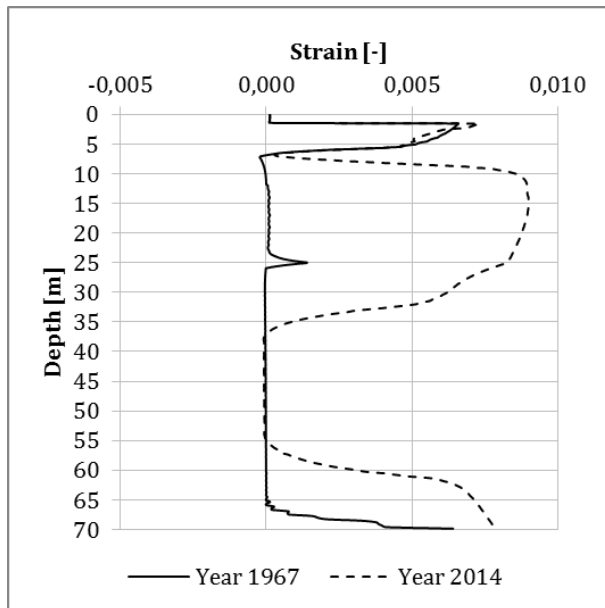


Figure 6.10. Calculated strain plotted against depth in section 1/045 in year 1967 and 2014.

### 6.3 Section 1/085

The results from the settlement calculations in GS Settlement together with the measured settlements and applied loads in section 1/085 are shown in Figure 6.11. Section 1/085 is founded on piles and the load is distributed as described in 5.2.2. The settlement have been measured in 1980, -81, -85 and 2014, the line representing the measured settlement is an interpolation between these measurements.

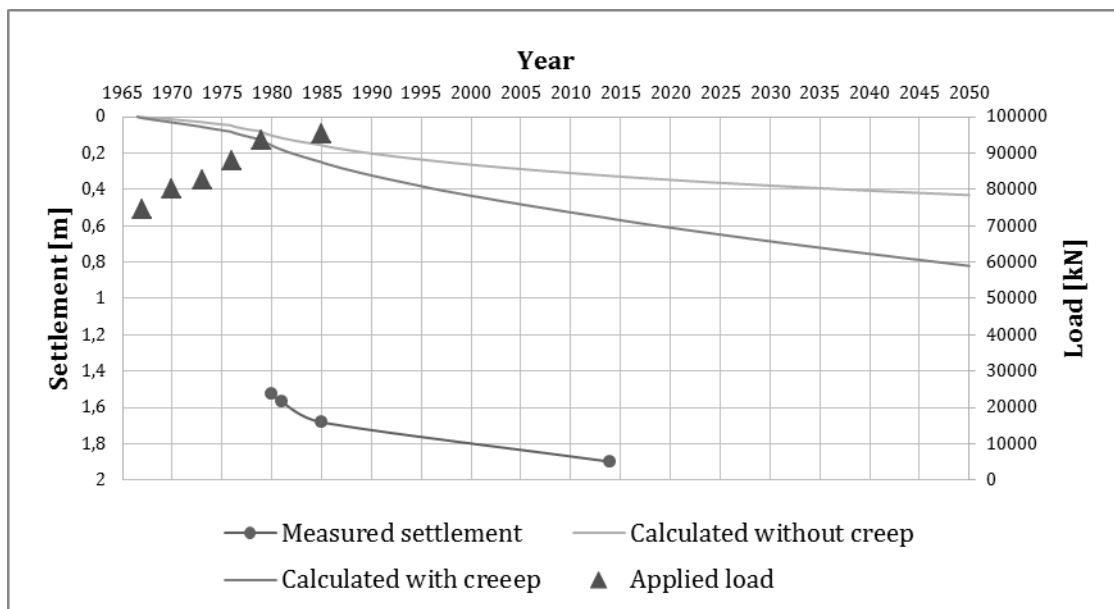


Figure 6.11. Resulting settlement in the piled section 1/085 from calculations in GS Settlement, with and without creep. Measured settlement and applied loads are also shown in the figure. Note the different scales on the y-axes.

In Figure 6.11, it can be seen that calculated settlements with creep is approximately 1,3 m less than the measured settlement in year 2014. The measured rate of settlement

between year 1985 and 2014 is around 7 mm/year while the calculated rate of settlement is approximately 11 mm/year when calculating with creep and 6 mm/year when calculating without creep.

Figure 6.12 illustrates the calculated excess pore water pressure in section 1/085. The excess pore water pressure at year 1967 is highest at a depth of approximately 28 m which is at the same depth as the toe of the piles. At year 2050, the excess pore water pressure has not dissipated.

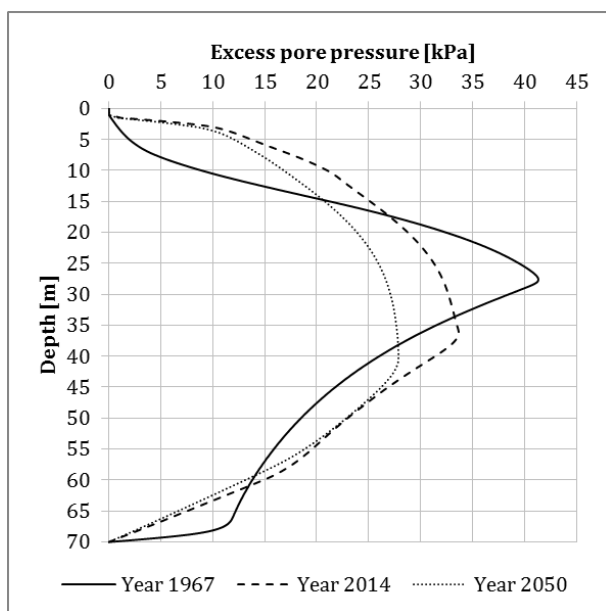


Figure 6.12. Calculated excess pore water pressure plotted against depth at the year 1967, 2014 and 2050 in section 1/085.

Figure 6.13 shows the calculated effective stresses in section 1/085. The effective stresses are exceeding the preconsolidation pressure down to a depth of about 7 m. The effective stresses do not reach the preconsolidation pressure during the calculation period below this depth. However, the effective stresses are close to the preconsolidation pressure down to a depth of approximately 25 m.

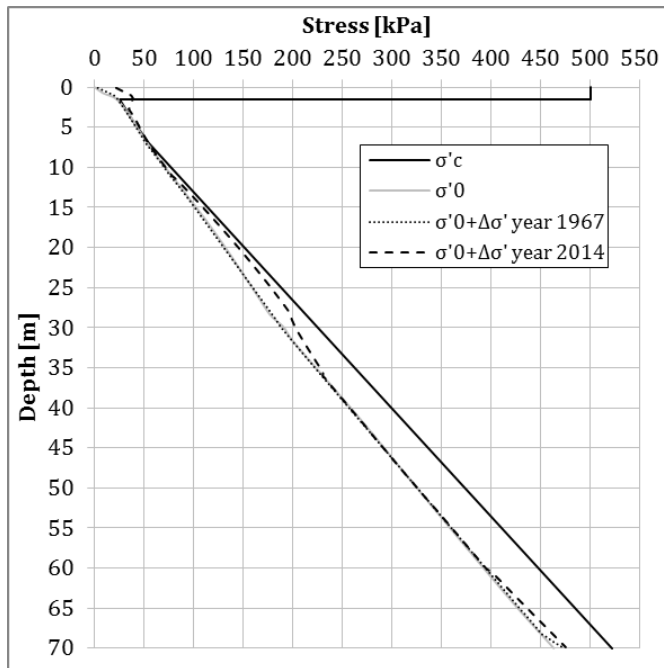


Figure 6.13. Preconsolidation pressure and calculated effective stresses in 1967 and 2014 in section 1/085 plotted against depth.

Figure 6.14 presents the calculated strain in section 1/085. As can be seen, the largest strains can be found in the upper part of the profile, with the largest value around a depth of 1 m.

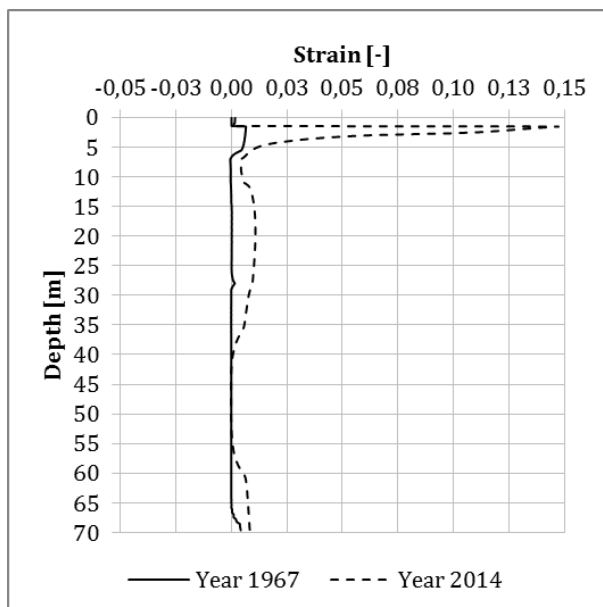


Figure 6.14. Calculated strain plotted against depth in year 1967 and 2014 in section 1/085.

## 6.4 Discussion of the results

The calculated settlements from GS Settlement in section 1/000, see Figure 6.1, differs from the measured settlement the section. However, the result shows that the rate of settlement between year 1985 and 2014 is captured in the calculations when creep effects are included. The calculation without creep effects gives a lower rate of

settlement compared to the measured. Even though there is a small difference in the results between calculations performed with and without creep effects, the rate of settlement indicates that the calculations with creep effects, captures the measured settlement better. The calculated settlements in section 1/045 differ a lot, both regarding the rate of settlement and the magnitude of settlements, compared to the measured. In section 1/085 the magnitude of settlements differs from the measured. However, the rate of settlement between year 1985 and 2014 is rather similar to the measured. A possible reason for the large difference between the calculated and measured settlements in section 1/045 and 1/085 could be found in how the load distribution from the piles is modelled. There are also uncertainties regarding the measured settlements; since the measured settlements are only measured from year 1980 and the designed geometry of the embankment is used in the calculations, the total settlement is uncertain.

By comparing the hand calculations with the calculated results from GS Settlement, shown in Figure 6.2, it can be seen that the calculations in GS Settlement gives reasonable results.

In all the studied sections, there is still excess pore water pressure at the end of the calculation period. This shows that the consolidation is still ongoing at the year of 2050. Therefore, it can be assumed that the dissipation of excess pore water pressure have a large impact on the resulting settlements. The excess pore water pressures in section 1/000 (see Figure 6.3 and Figure 6.4), shows that the additional load due to the added asphalt have a significant impact on the consolidation process. In the calculations where no asphalt is added after the construction of the embankment, there is less excess pore water pressure in year 2014 and 2050 compared to the calculations where additional asphalt is added to the embankment. The development of excess pore water pressure in all studied sections seems to be reasonable. As can be predicted, the initial excess pore water pressures distribution follows the stress distribution caused by the applied loads. It can be expected that the excess pore water pressure redistributes so that the pressure in the soil profile evens out. It is therefore realistic that the excess pore water pressures increases in the parts of the profile where initial excess pore water pressure is low and decreases in the parts where the initial pressure is high.

The calculated effective stresses in section 1/000 presented in Figure 6.5 shows that the preconsolidation pressure is only exceeded in the first 7 m of the profile. The calculated effective stress is lower compared to the total stresses shown in the stress chart (see Figure 5.7) since there is still excess pore water pressure in the profile and that the consolidation is not completed in year 2014. In section 1/045 and 1/085, the calculated effective stresses do not exceed the preconsolidation pressure in year 2014 since the consolidation process is slow. In the stress charts in section 5.3 it can be seen that after the consolidation process is completed, the preconsolidation pressure will be exceeded.

The initial permeability and the water content are higher in the upper 10 to 15 m of the soil profile compared to greater depths (see Appendix 2.1 and Appendix 2.3), it can therefore be expected that larger strains will occur in the upper part of the soil profile compared the rest. High water content indicates high permeability which gives a high rate of consolidation. The strains in all sections seem to be reasonable. It can be

seen that strains have occurred in the soil profile where additional stresses are applied. In section 1/000, most of the strains occur in the upper part of the soil profile since loads are modelled as surface loads and due to the high permeability. In section 1/045 and 1/085, strains can also be seen in deeper part of the soil profile due to the load distributed by the piles. The strains in the bottom of the profiles can be expected due to the drained boundary condition in the model at a depth of 70 m. A small negative strain (heave) can be seen in the graphs in all the studied sections. This can be explained due to the increased excess pore water pressures which lead to decreased effective stresses in some parts of the profile.

## 7 Sensitivity analysis

A sensitivity analysis has been carried out in order to evaluate how different input parameters affect the results of the calculations. This chapter contains a sensitivity analysis of some of the chosen soil parameters and the function of the foundation. Furthermore, an alternative calculation has been performed where ongoing settlements have been taken into account.

### 7.1 Initial permeability

Settlement calculations for section 1/000 and 1/085 have been performed with varying initial permeability. The results indicate that the consolidation process is still ongoing at the end of year 2050. Therefore, the initial permeability was chosen to be analysed since it is an important parameter in the consolidation process. The analysis was carried out by increasing the original initial permeability 2, 3 and 5 times. These values are reasonable since they are within the normal range of permeability for clay.

Figure 7.1 shows the results from the settlement calculations for section 1/000 with the different initial permeability together with the measured settlement. It can be seen that the changes in permeability have an impact on the results, where an initial permeability 3 times higher than the original would fit the measured settlements the best.

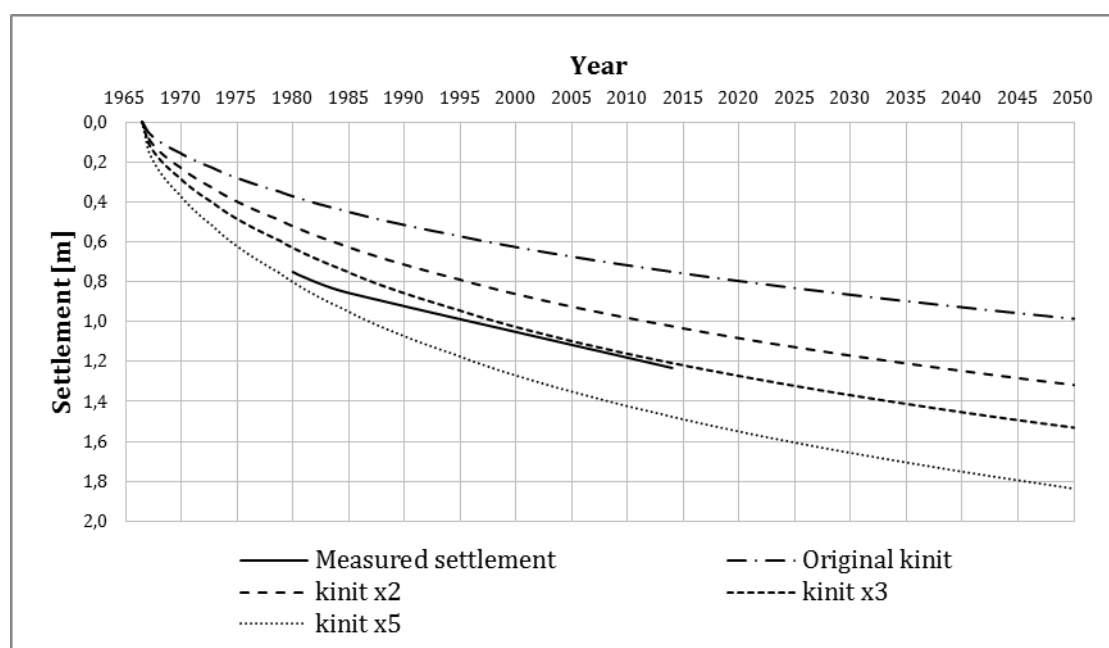


Figure 7.1. Results from settlement calculations for section 1/000 performed with different initial permeability. The measured settlements are also plotted in the graph. Section 1/000 is not founded on piles.

In Figure 7.2, the results from the settlement calculations carried out with different initial permeability in section 1/085 is shown. As can be seen, the calculated settlements are influenced by the change in initial permeability. However, the measured settlements are still larger compared to the calculated.

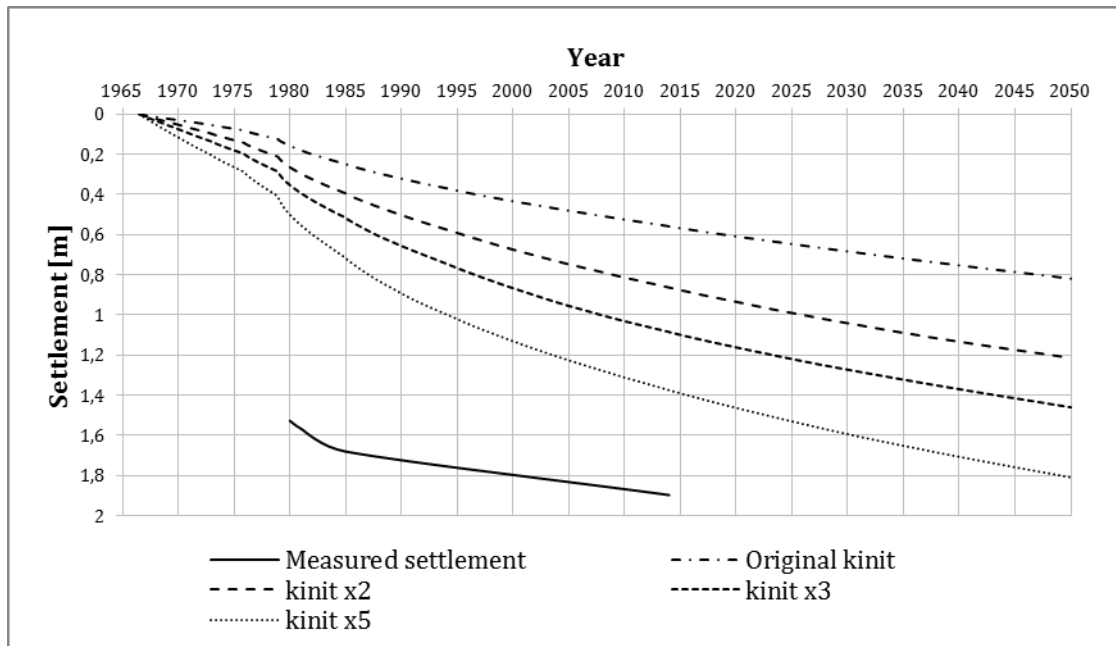


Figure 7.2. Results from settlement calculations for the piled section 1/085 performed with different initial permeability. The measured settlement is also plotted in the graph.

The calculated excess pore water pressures for year 2014 in the soil profile are plotted in Figure 7.3 for section 1/000 and in Figure 7.4 for section 1/085. As can be seen there is a significant difference in remaining excess pore water pressures between the different calculations in both sections. Calculations performed with a higher initial permeability give a lower excess pore water pressure at year 2014.

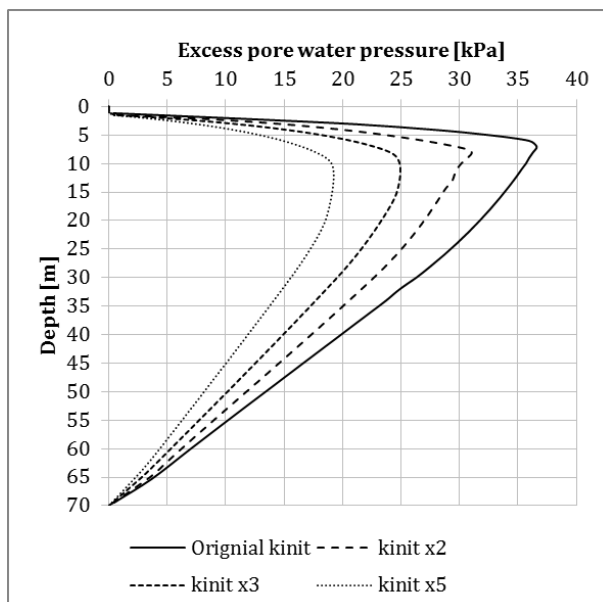


Figure 7.3. Calculated excess pore water pressure in year 2014 at section 1/000 from calculations with different initial permeability.

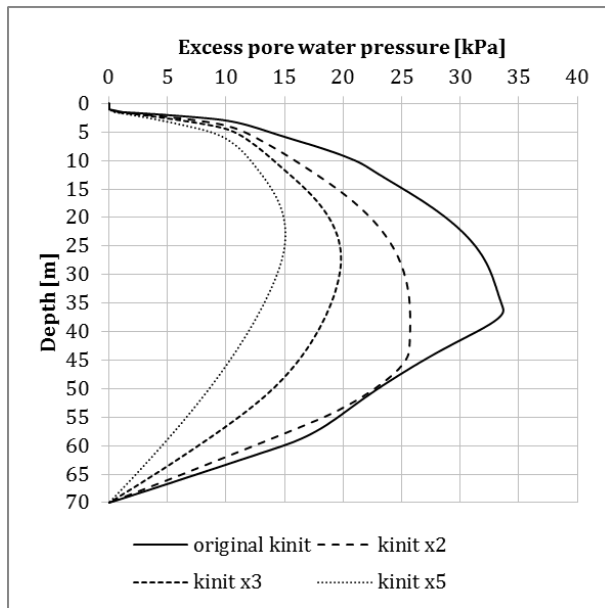


Figure 7.4. Calculated excess pore water pressure in year 2014 at section 1/085 from calculations with different initial permeability.

## 7.2 Time resistance numbers – $r_0$ and $r_1$

The influence of the time resistance numbers on the calculation results are analysed for one section without piles (section 1/000) and for one section with piles (section 1/085). It is interesting to carry out a sensitivity analysis for the initial time resistance number  $r_0$  since this parameter is difficult to evaluate from the available field investigations in the studied area. Calculations were performed with  $r_0=500$  and  $r_0=8000$  since these values represents a very low and a very high initial time resistance number according to (Olsson, 2010). The original calculations were performed with  $r_0=1500$ . Figure 7.5 shows the settlements in section 1/000 calculated with  $r_0=500$ ,  $r_0=8000$  and  $r_0=1500$ , plotted together with the measured settlement.

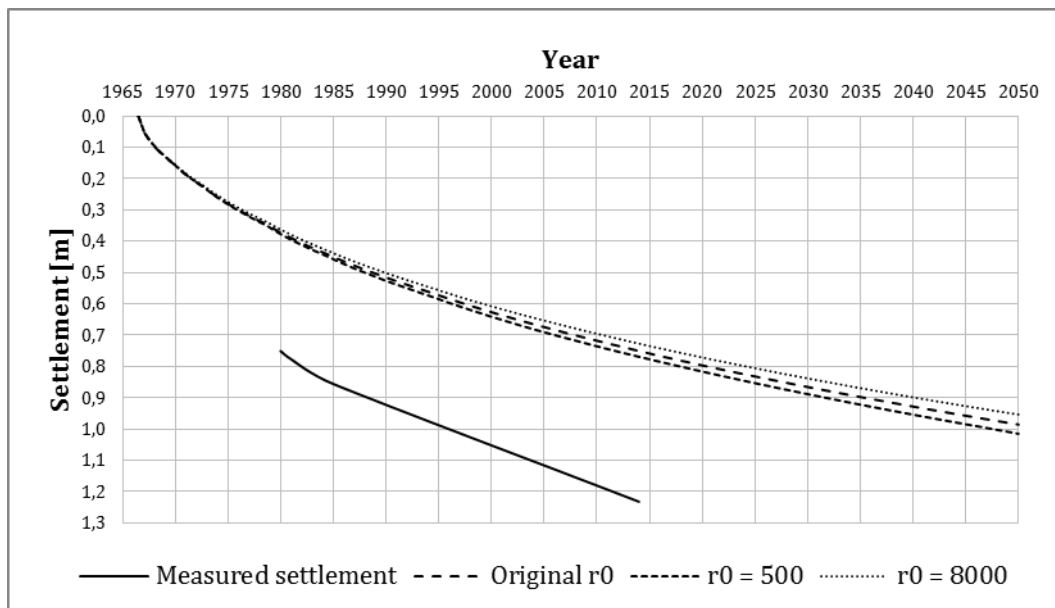


Figure 7.5. Results from settlement calculations for section 1/000 performed with different  $r_0$ . The measured settlement is also plotted in the graph.

It can be seen that  $r_0$  has a small influence on the calculated settlements in section 1/000. The settlements in section 1/085 calculated with different  $r_0$  can be seen in Figure 7.6. The value of  $r_0$  has a slightly larger influence on the calculated settlements in section 1/085 than in section 1/000.

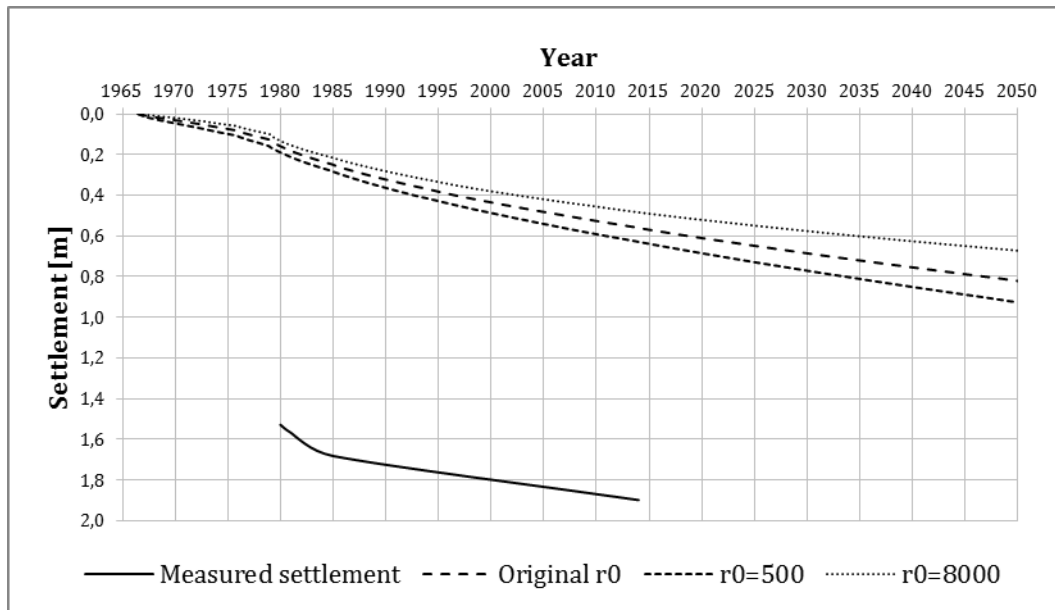


Figure 7.6. Results from settlement calculations for section 1/085 performed with different  $r_0$ . The measured settlement is also plotted in the graph.

The strains in section 1/000 calculated with different initial time resistance numbers are plotted against depth in Figure 7.7. The strain at the depth 65 m to 70 m are influenced by the changed initial time resistance number. In the rest of the profile, there is no significant difference between the calculations.

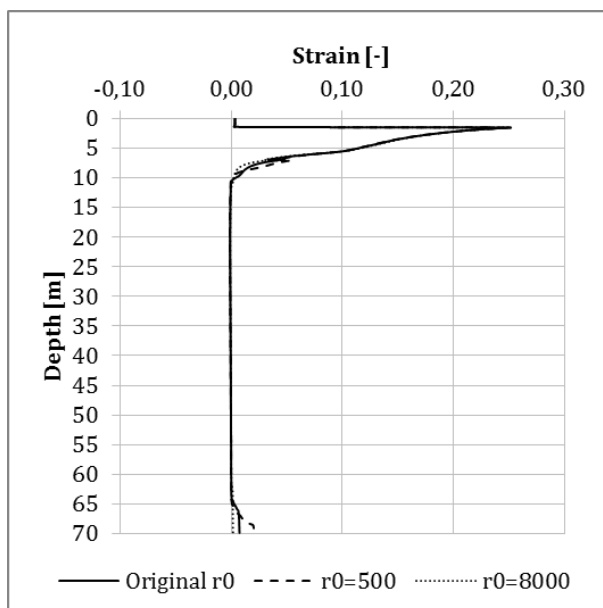


Figure 7.7. Strain in year 2014 at section 1/000 calculated with different  $r_0$  plotted against depth.

Figure 7.8 shows the strains in section 1/085 calculated with different  $r_0$  values. It can be seen that a changed  $r_0$  has the largest effect on the strain in the bottom of the soil profile and at a depth of around 15 m to 30 m.

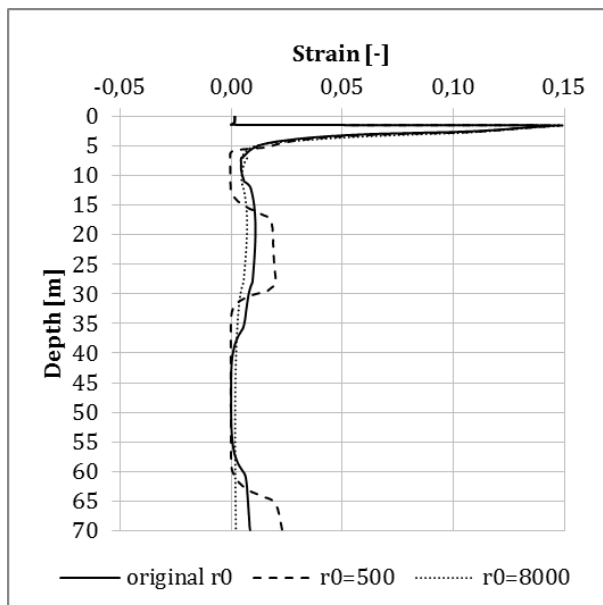


Figure 7.8. Strain in year 2014 at section 1/085 calculated with different  $r_0$  against depth.

The time resistance number  $r_1$  is evaluated empirically from the natural water content. A variation of  $\pm 20\%$  for  $r_1$  is chosen for the sensitivity analysis since it corresponds to reasonable values of the natural water content. It was found that changing the  $r_1$  with  $\pm 20\%$  have a small effect on the calculation results both for section 1/000 and for section 1/085. The settlements in section 1/000 calculated with the different  $r_1$  values are shown in Figure 7.9. Figure 7.10 shows the settlements calculated with different values of  $r_1$  in section 1/085.

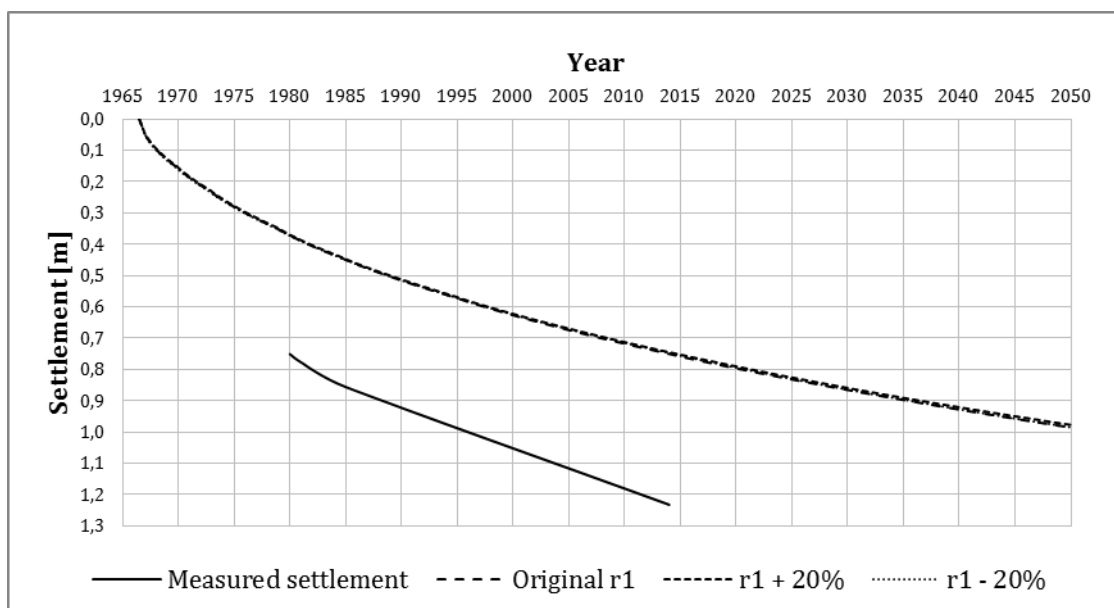


Figure 7.9. Results from settlement calculations for section 1/000 performed with different  $r_1$ . The measured settlement is also plotted in the graph.

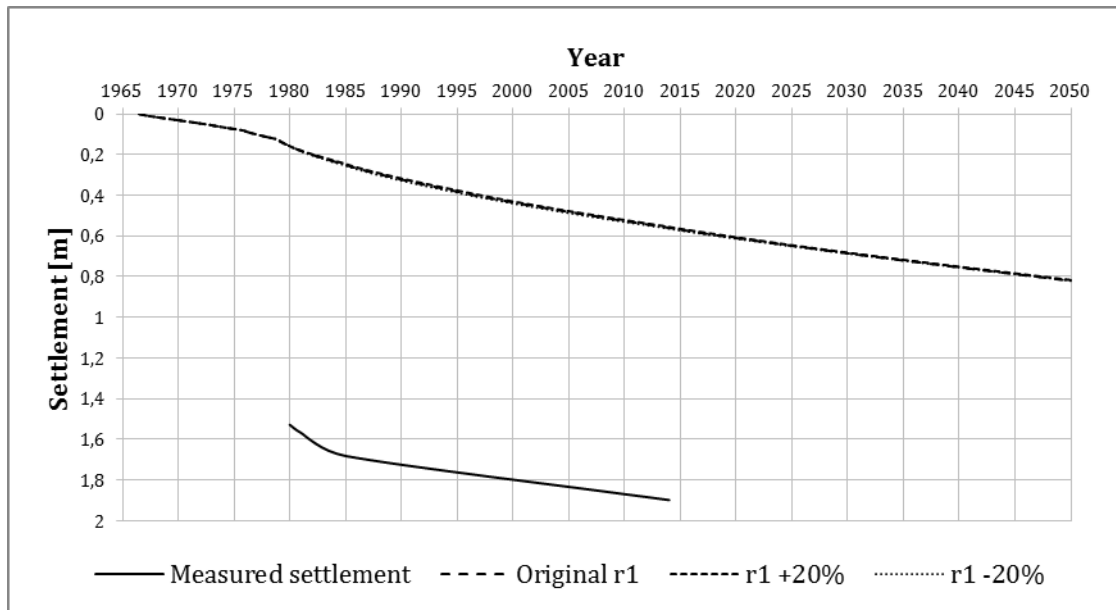


Figure 7.10. Results from settlement calculations for section 1/085 performed with different  $r_1$ . The measured settlement is also plotted in the graph.

The strain calculated with different  $r_1$  values are shown in Figure 7.11 and Figure 7.12 for section 1/000 and 1/085 respectively. As can be seen, there is no significant difference between the calculations.

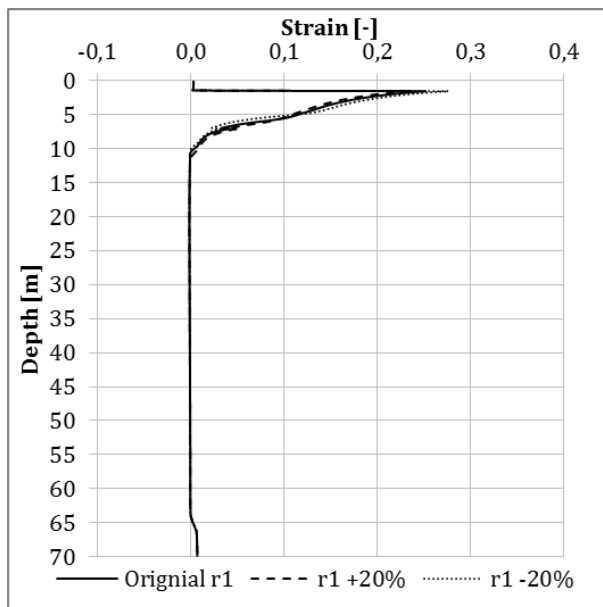


Figure 7.11. Strain in year 2014 at section 1/000 from calculations with  $r_1$  plotted against depth.

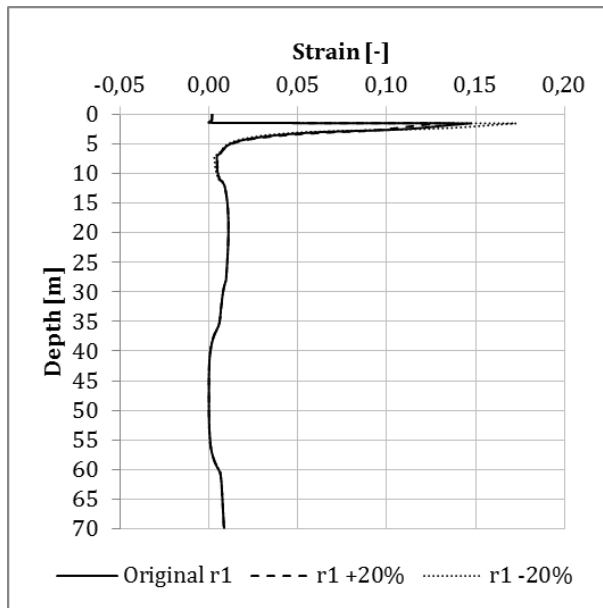


Figure 7.12. Strain in year 2014 at section 1/085 from calculations with  $r_1$  plotted against depth.

### 7.3 Preconsolidation pressure

The preconsolidation pressure is an important parameter affecting the development of settlement in the soil as described in section 2.1.1. Therefore, a sensitivity analysis for the preconsolidation pressure has been carried out. By studying Figure 4.6, it was decided to vary the preconsolidation pressure with  $\pm 5\%$  from the original preconsolidation pressure. However, the preconsolidation pressure is not changed in the analysis in the first 7 m due to the normally consolidated conditions described in section 4.2.2.

Figure 7.13 shows settlements calculated with different preconsolidation pressures in section 1/000. As can be seen, the calculated settlement does not change significantly with a higher or lower preconsolidation pressure. The measured settlement in section 1/000 still differs from the calculated settlement.

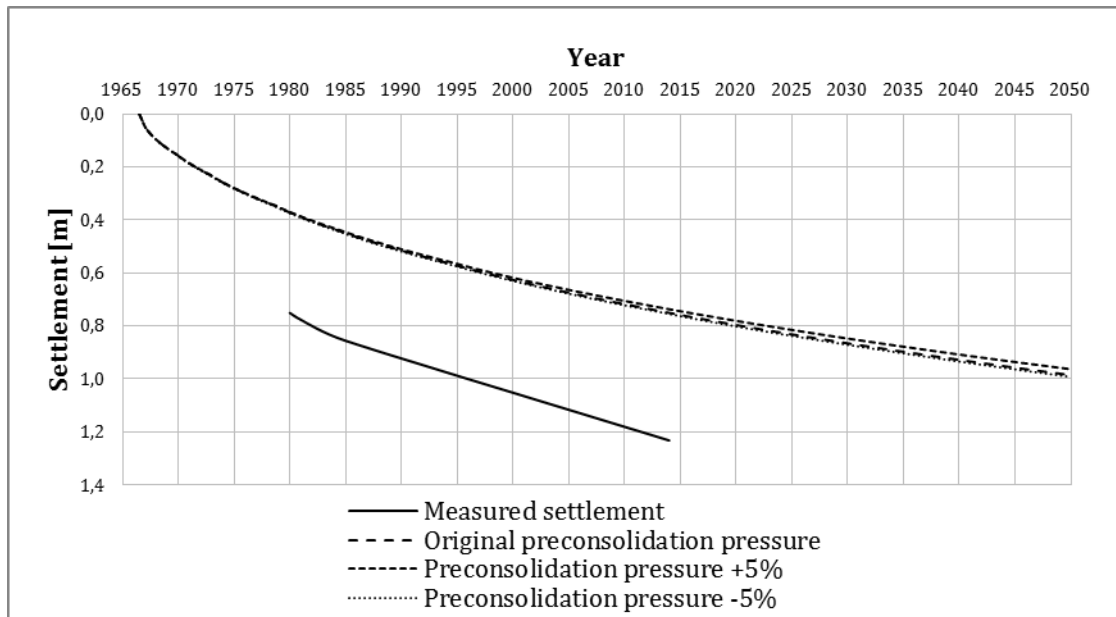


Figure 7.13. Calculated settlement in section 1/000 with varying preconsolidation pressures. The measured settlement is also shown in the graph.

In Figure 7.14 the calculated effective stress in year 2014 is plotted with the different preconsolidation pressures in section 1/000 in the first 40 m. When studying the chart, it can be seen that the calculated effective stresses is equal or above the preconsolidation pressure in the first 10 m of the soil profile. Below a depth of 10 m, the preconsolidation pressure is higher than the calculated effective stresses.

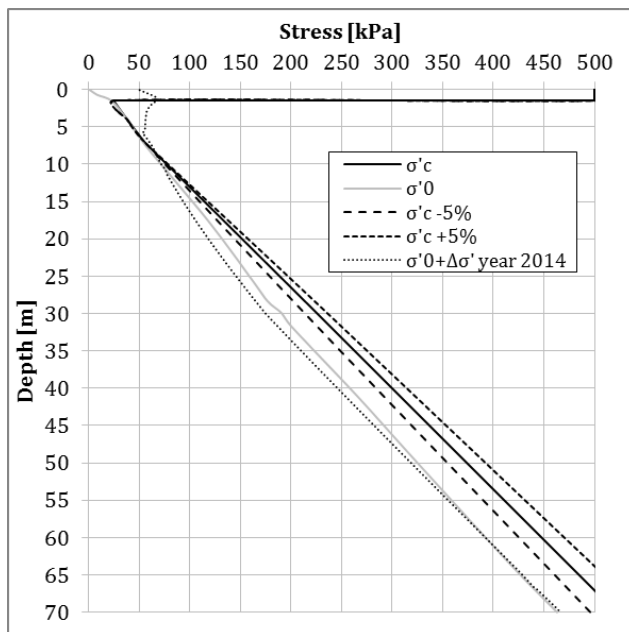


Figure 7.14. Different preconsolidation pressure plotted against depth in section 1/000. The calculated effective stress in year 2014 is also plotted in the graph.

Figure 7.15 illustrates the calculated settlements with varying preconsolidation pressures in section 1/085. The calculated settlement does not change much when varying the preconsolidation pressure. As can be seen, the measured settlement in the section is still greater compared to the calculated settlements.

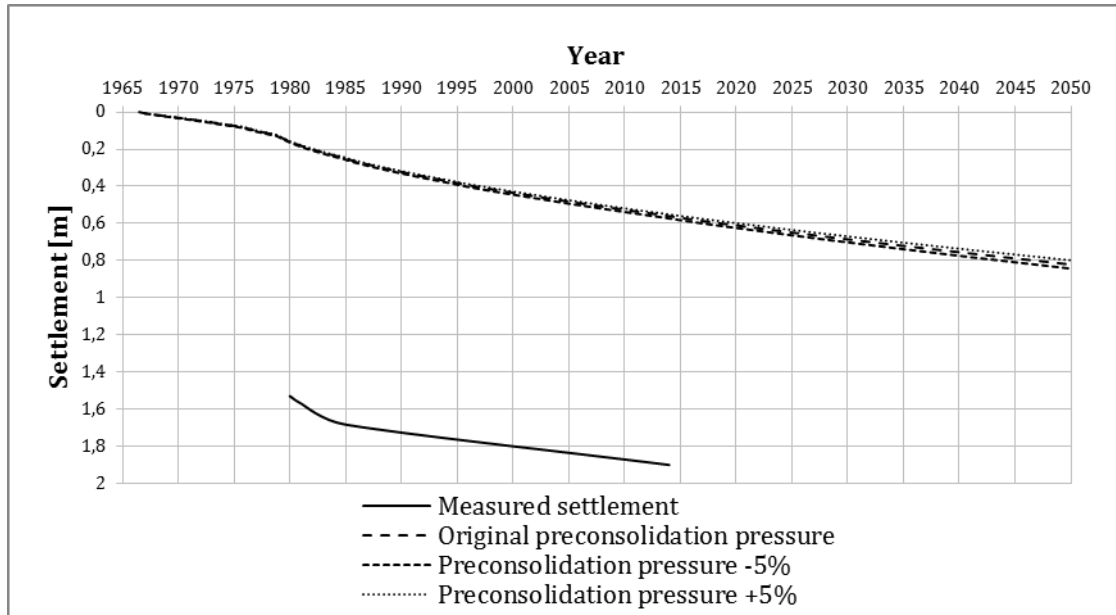


Figure 7.15. Settlements calculated with varying preconsolidation pressure in section 1/085. The measured settlement is also shown in the graph.

The effective stresses calculated with varying preconsolidation pressure in section 1/085 can be seen in Figure 7.16. The calculated effective stresses are above or close to the preconsolidation pressure in the upper 15 m of the soil profile. Below this depth, the calculated effective stresses are not exceeding the preconsolidation pressure.

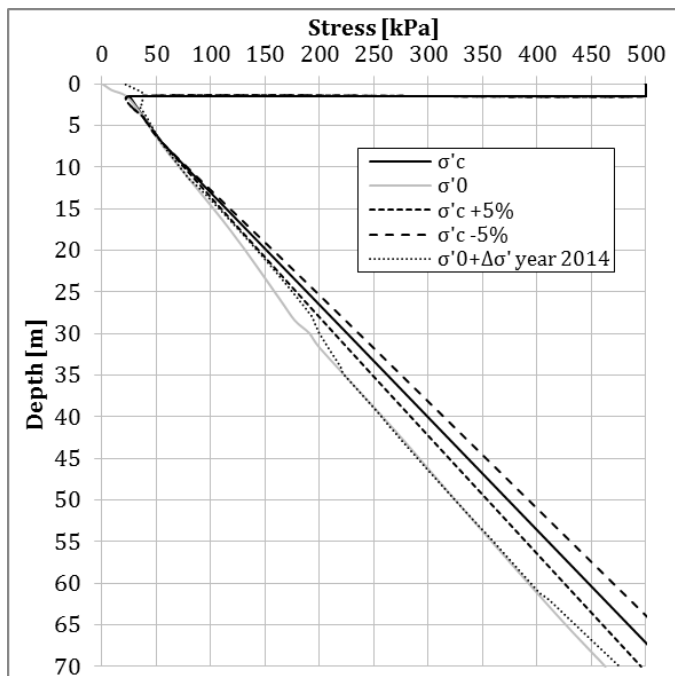


Figure 7.16. Different preconsolidation pressure plotted against depth in the piled section 1/085. The calculated effective stresses in year 2014 is also plotted in the graph.

## 7.4 Geotechnical bearing capacity of piles

The calculations of the geotechnical bearing capacity of the piles are uncertain. The adhesion between piles and soil and the shear strength of the soil might be overestimated. Therefore, a sensitivity analysis was carried out by reducing the calculated geotechnical bearing capacity with 20%.

In Figure 7.17, the additional stresses calculated with reduced geotechnical bearing capacity of the piles implemented in GS Settlement are shown. The stress distribution was calculated as described in section 5.2. As can be seen, the additional stresses are higher in the upper part of the soil profile compared to when the geotechnical bearing capacity is not reduced (see Figure 5.6). By reducing the geotechnical bearing capacity of the piles, more load will be applied on the ground surface. Therefore, the additional stresses will become higher compared to the original calculations. However, the stresses at greater depth are lower compared to the original calculations.

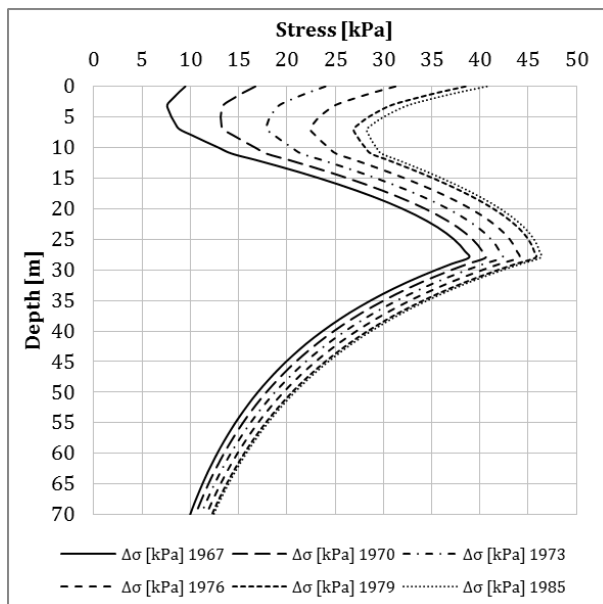


Figure 7.17. Additional stresses in section 1/085 plotted against depth. The geotechnical bearing capacity of the piles is reduced with 20%.

Figure 7.18 shows the calculated settlement in section 1/085 with and without reduced geotechnical bearing capacity. As can be seen, the settlement increases with a reduced geotechnical bearing capacity with approximately 0,2 m, however, the rate of settlement is similar to the original calculations.

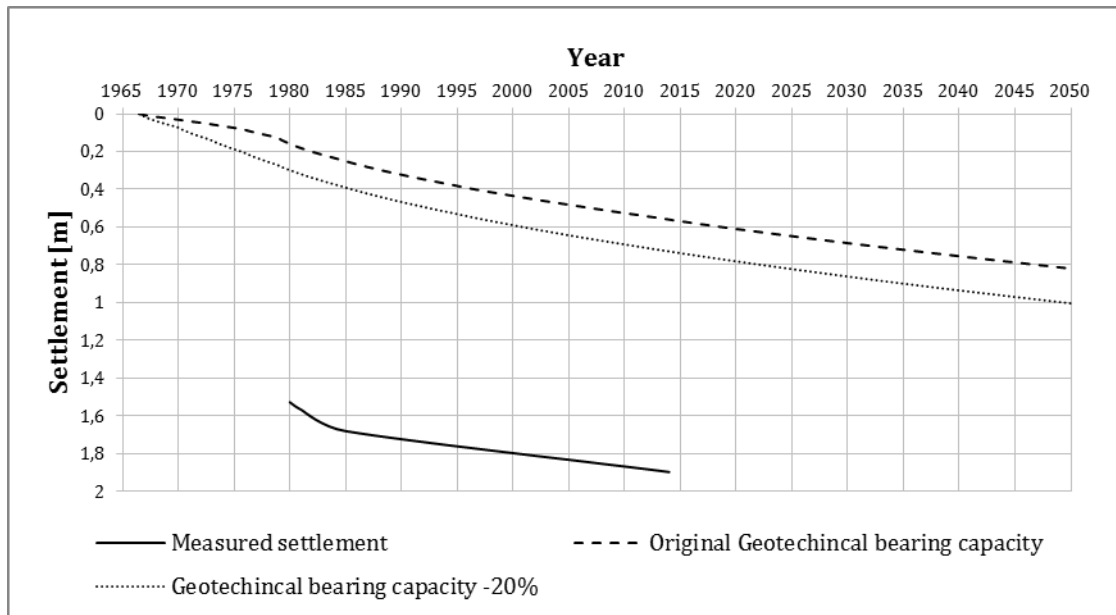


Figure 7.18. Settlements in section 1/085 calculated with and without reduced geotechnical bearing capacity of the embankment piles. The measured settlement is also shown in the graph.

In Figure 7.19 the calculated effective stresses with and without reduced geotechnical bearing capacity of the piles are plotted against depth in the upper 40 m. In the first 5 m of the profile the effective stresses are higher in the case when the geotechnical bearing capacity of the piles are reduced. However, deeper in the profile, the calculated effective stresses becomes smaller compared to the original calculated effective stresses.

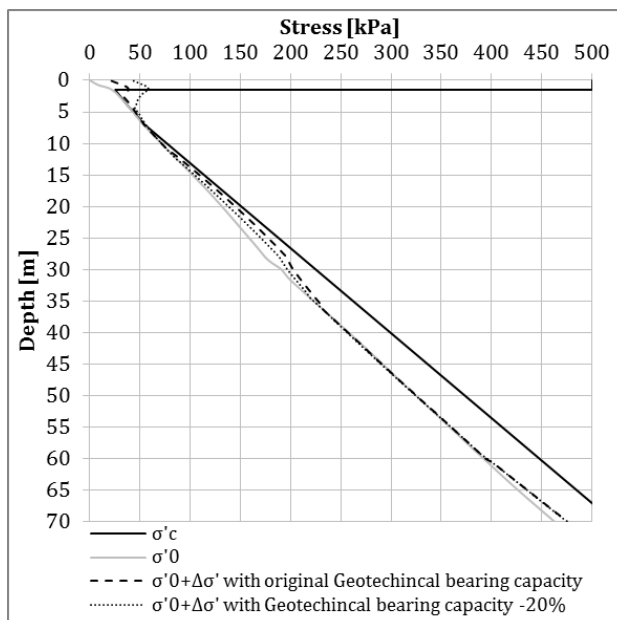


Figure 7.19. Effective stresses in year 2014 calculated with the geotechnical bearing capacity of the embankment piles reduced with 20% plotted against depth together with the original calculated effective stresses in section 1/085.

The strain in the soil profile calculated with and without reduced geotechnical bearing capacity of the piles in section 1/085 can be seen in Figure 7.20. As can be seen, the

strain in the upper part of the profile increases with a reduced geotechnical bearing capacity compared to the original. However, at a greater depth, the strain is lower compared to the original.

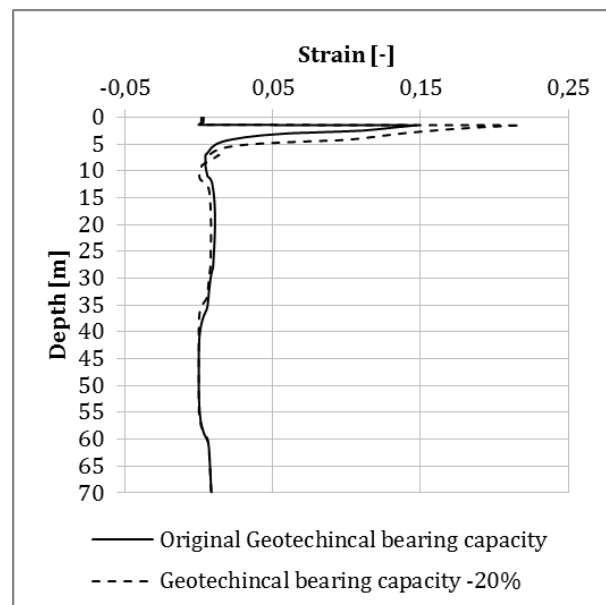


Figure 7.20. Strains in section 1/085 plotted against depth calculated with different geotechnical bearing capacity of the piles.

## 7.5 An alternative approach of modelling including ongoing settlements

The settlement calculations described in chapter 5 starts in year 1950, 17 years before the road embankment is built. A small surface load of 2 kPa is applied in year 1950 in order to start the calculation process in the program. This means that ongoing settlements caused by loads applied earlier are not included in the model. In order to see how the calculation results would differ if the ongoing settlements were included, an alternative calculation is carried out for section 1/000. As described in chapter 4.1, Marieholm started to develop as an industrial area around year 1900. It can therefore be assumed that the existing filling material was added around this time. In the alternative calculation the layer of filling material is removed and a load corresponding to the weight of the fill is applied in the beginning of the calculation. The rest of the loads are applied at the same times as in the original calculation according to chapter 5.2.1. The calculation period is from year 1900 to year 2050. The resulting settlements from the alternative calculation can be seen in Figure 7.21. The rate of settlement between year 1954 and 1964, just before the construction of the embankment is around 7 mm/year.

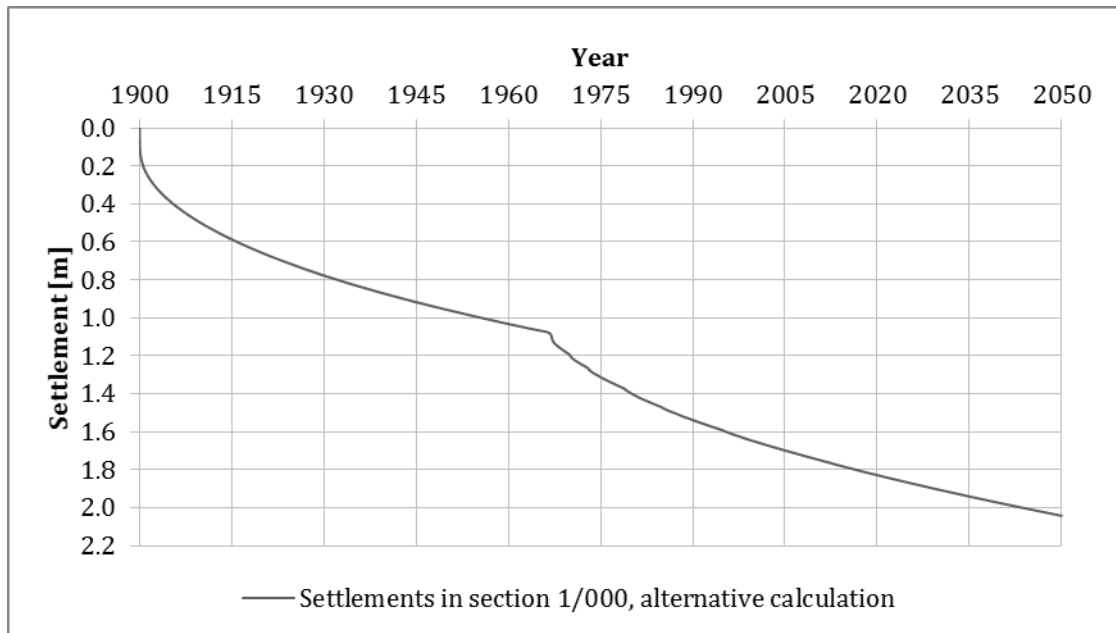


Figure 7.21. Resulting settlements in section 1/000 calculated with an alternative model starting in year 1900.

Figure 7.22 illustrates the calculated remaining excess pore water pressure at year 1905 and 1966. There is still a significant amount of excess pore water pressure in the soil profile in year 1966 due to the load applied in year 1900.

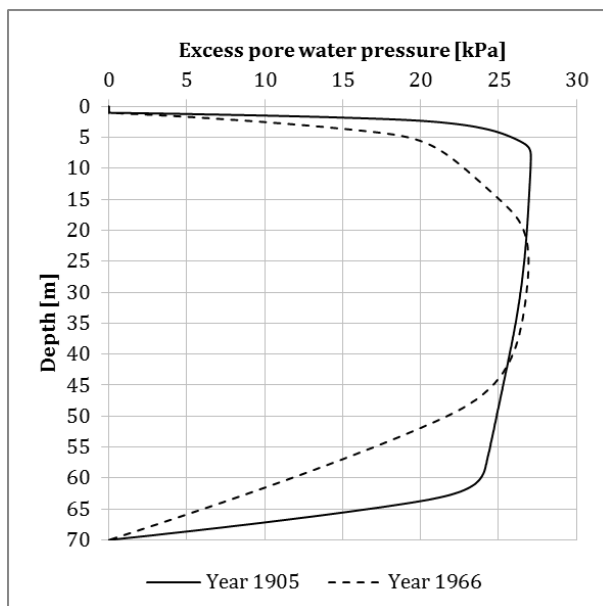


Figure 7.22. Calculated excess pore water pressure in section 1/000 at the year 1905 and 1966 before the construction of the embankment. The excess pore water pressure is due to the filling material modelled as a surface load in year 1900.

In Figure 7.23, the calculated settlement from the original calculation is plotted together with the resulting settlements from the alternative calculation and the measured settlement in section 1/000. The calculated settlement from the alternative model is plotted from year 1967 when the road embankment was built. The calculated settlement development from year 1967 is similar in both calculations. As can be seen

the alternative calculation gives slightly smaller settlements compared to the original model, the difference is however not significant.

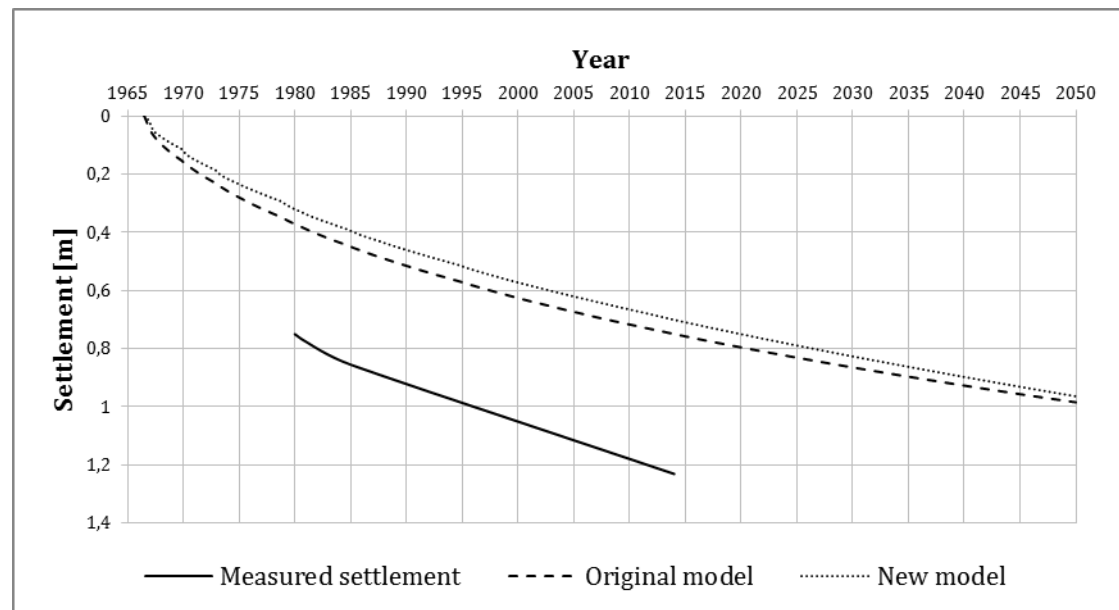


Figure 7.23. Resulting settlements in section 1/000 calculated with the original model and with the alternative model including ongoing settlements, plotted together with the measured settlements.

## 7.6 Discussion of results from sensitivity analysis

This section contains a discussion regarding the results from the performed sensitivity analysis.

### 7.6.1 Initial permeability

The permeability is one of the most important parameters for the consolidation process, since it is governing how fast the excess pore water pressure can dissipate. It is therefore reasonable that a change in initial permeability has a big influence on the calculated settlements.

### 7.6.2 Time resistance numbers

As shown in section 3.1, the initial time resistance number  $r_0$  is governing the creep strain rate when  $\sigma'_v \leq b_0 \sigma'_c$ . In the calculations for section 1/000 almost all settlements occur in the upper 10 m of the soil profile where the effective stresses exceeds the preconsolidation pressure early in the consolidation process. It is therefore reasonable that the  $r_0$  value has a small effect on the calculated settlements. As can be seen in Figure 7.7 it is only the strain in the deepest 5 m that is affected by the changed  $r_0$ , which is reasonable since the effective stresses at this depth is below the preconsolidation pressure. In section 1/085 most strains occur in the upper parts of the soil profile due to the surface loads and at a depth of about 10-30 m due to the loads transferred by the piles. As can be seen in Figure 6.13 the calculated effective stresses are during the calculation slightly lower than the preconsolidation pressure at 10-30 m depth. It is therefore realistic that the  $r_0$  value has a rather large influence on the strain at these depths, as shown in Figure 7.8. The strain in the upper parts of the soil profile is not affected by the  $r_0$  value since the calculated effective stresses are exceeding the preconsolidation pressure.

Changing the  $r_1$  value with 20% had almost no effect at all on the calculation results. This might be due to that it is a rather small change, and because consolidation is the dominating process in the development of the settlements. It can be seen in Figure 7.11 and Figure 7.12 that it is only the strain in the upper parts of the soil profile that is affected by the changed  $r_1$ . This is reasonable since the effective stresses are exceeding the preconsolidation pressure in this part of the profile and since  $r_1$  is governing the creep strain rate for a stress situation where  $\sigma'_v \geq b_1 \sigma'_c$ .

### 7.6.3 Preconsolidation pressure

Varying the preconsolidation pressure with  $\pm 5\%$  does not have a significant impact on the settlement in the studied sections. In section 1/000, the embankment is modelled as a surface load, therefore, the largest stresses is to be found in the upper part of the profile. By studying Figure 7.14, it can be seen that by having the original preconsolidation pressure, the calculated effective stresses exceed the preconsolidation pressure in the first 7 m. When lowering the preconsolidation pressure with 5%, the effective stresses exceed the preconsolidation pressure to a depth of 10 m. It is therefore reasonable that varying the preconsolidation pressure in section 1/000 does not affect the calculated settlements significantly.

In section 1/085 the embankment is piled, therefore, the load is distributed to a greater depth compared to in section 1/000. As can be seen in Figure 7.16, the calculated stresses are only exceeding the original preconsolidation pressure in the first 5 m. By decreasing the preconsolidation pressure with 5%, the effective stresses are close to the preconsolidation pressure at a depth from 5 m to 25 m. However, since the calculated effective stresses do not exceed the preconsolidation pressure, it is realistic that the calculated settlements do not increase significantly by decreasing the preconsolidation pressure with 5%.

As expected, increasing the preconsolidation pressure in section 1/000 and 1/085 does not affect the calculated resulting settlements. Since the calculated stresses in all the studied sections are only slightly over or close to the original preconsolidation pressure, the increase of preconsolidation pressure should not have a big impact on the calculated settlements.

### 7.6.4 Geotechnical bearing capacity

By reducing the geotechnical bearing capacity of the piles, the neutral plane will probably move up and a larger percentage of the load will be distributed from the surface. It is therefore reasonable that the additional stress increases in the upper part and decreases in the lower part of the profile.

The calculated settlement increases with approximately 0,2 m when the geotechnical bearing capacity of the piles decreases. This can probably be explained due to the increased calculated effective stresses in the upper part of the soil profile as can be seen in Figure 7.19.

When studying the strain in the profile in Figure 7.20, it can be seen that the strain increases in the upper part of the profile and decreases in the middle of the profile when comparing the calculations with and without a decreased geotechnical bearing capacity of the piles. Since the effective stresses increases in the upper part of the

profile and decreases at a greater depth, it is reasonable that the strain change in the same way.

### **7.6.5 Alternative approach of modelling including ongoing settlements**

The results from the sensitivity analysis indicate that including the ongoing settlements in the model does not have a big impact on the calculated settlements after construction of the embankment. It is reasonable that the alternative calculation model gives smaller settlements after 1967 than the original calculation method since the same initial permeability was used in both methods. Due to the decreasing permeability during consolidation, the permeability is lower in year 1967 in the alternative model than in the original. The creep strain rate at year 1967 will probably be lower in the calculation starting in year 1900 compared to the original calculation. This could also explain the smaller settlements in the alternative model.

The analysis shows that at year 1966, there is still excess pore water pressure in the soil profile. It can also be seen in Figure 7.21 that the development of settlement has not stagnated before the construction of the embankment in 1967. This gives an indication of ongoing consolidation settlements at the time for the construction of the embankment. The calculated rate of settlement before the construction of the embankment was about 7 mm/year, which close to the rate of settlement measured between year 2003 and year 2008 (which was 6 mm/year) at borehole 21015 as described in section 4.4. However, it is a higher rate of settlement compared to 0,5-2mm/year as reported by (Hallingberg, et al., 1996).

## **8 Other factors causing embankment settlement**

The calculations performed and described earlier in this report have been carried out in order to investigate settlements in the soil below the road embankment. It is however possible that some of the measured settlements are caused by compression of the embankment itself. In addition there are many things that may have gone wrong during the construction of the embankment in 1967; failure of piles and or pile caps, the shape of the piles might not be equal to the drawings and the adhesion between piles and soil might be overestimated. This chapter discusses some possible factors that may have contributed to the measured settlements.

### **8.1 Properties of the embankment material**

A possible cause of immediate settlements in the embankment is bad quality of the material used, and/or insufficient compaction of the material during construction. Insufficient compaction during construction might cause compaction of the embankment material after the road has been put into use (Holtz & Kovacs, 1981).

Bad quality of the embankment material could also cause problems with the development of the soil arching mechanism in the piled sections of the embankment, described in section 2.3.3. The internal friction angle is an important parameter that affects the efficacy of load transfer by soil arching (Chevalier, et al., 2007). A high internal friction angle gives a better load transfer than a low internal friction angle. Since the properties of the material used when constructing the studied embankment in Marieholm is uncertain, it is difficult to estimate how well the soil arching has developed.

### **8.2 Pile and pile cap design**

In year 1974 guidelines were established regarding the design of embankment piles and pile caps by Statens Vägverk (Statens vägverk, 1974). Since the guidelines were published 1974, one can assume that similar design criteria was used when designing the road embankment in Marieholm in 1967.

According to Statens Vägverk (1974), the dimensions of embankment piles should be designed with regard to stability analysis of the embankment. Load transferring between piles and the surrounding soil were in most cases not a major concern. It is therefore possible that the embankment piles are not designed in an optimal way in order to prevent settlements.

The pile caps were in 1974 designed in order to carry the load from the weight of the embankment and traffic load (Statens vägverk, 1974). The pile cap area should also be large enough to prevent embankment material to distribute load to the soil between the pile caps. However, the guidelines of 1974 are not as detailed as the design criteria for piled embankment today.

The required pile spacing was calculated according to recommendations from (Trafikverket, 2011) as described in section 2.3.3. Based on characteristic values of geotechnical bearing capacity of the piles, the spacing should be 1,9 m in section

1/045 and 1,8 m in section 1/085. However, the spacing according to construction drawings (see Appendix 3.1) is 2,15 m and 1,9 m respectively.

Swedish practice recommends having an area covering ratio of the pile caps larger than 40 % (Trafikverket, 2011). When calculating the area covering ratio in section 1/045 and 1/085 it can be stated that the area covering ratio is 18 % respectively 22 %. It is clear that the design of the pile spacing and pile cap size does not comply with the current recommendations.

According to a study performed by (Bergdahl, et al., 1979), a road embankment can settle even though the piles do not settle below the embankment. It was stated that having a high piled embankment with small pile caps, settlements in the ground surface below the pile caps can lead to even settlements along the road surface. Based on this study, there is a possibility that the embankment in Marieholm have settled more than the installed piles.

### 8.3 Lateral displacement

The measured settlement of the studied road embankment in Marieholm could be explained partly due to lateral displacement of the embankment. There are three different possible failure modes of the embankment that could contribute to the measured settlement; internal stability, foundation stability and global stability (Almedia & Soares Marques, 2013).

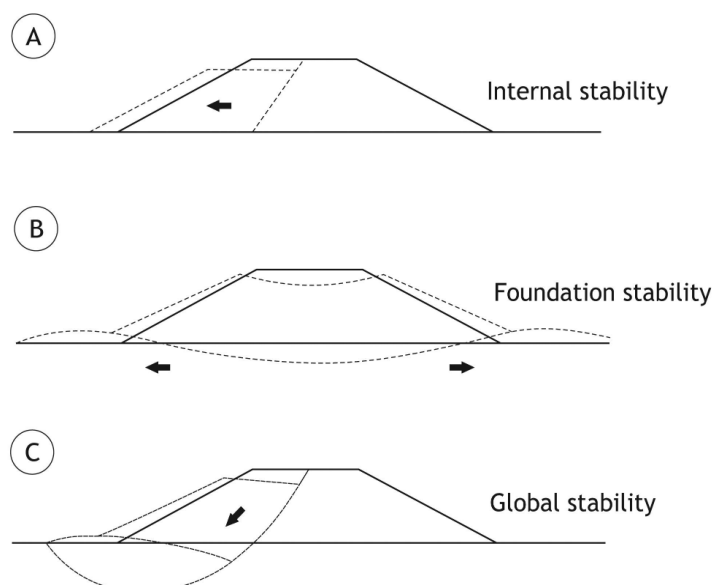


Figure 8.1. Different failure modes of embankment; (A) internal stability, lateral sliding of the embankment, (B) foundation stability, failure in the foundation, (C) global stability, failure in both embankment and foundation (Almedia & Soares Marques, 2013).

In Figure 8.1 the three different failure modes are illustrated. When the ground surface under the embankment is intact and the body of the embankment is failing, it is called internal stability failure. This can lead to settlement of the road surface by lateral displacement of the embankment without displacement of the ground surface. Foundation stability failure is caused by exceeding the bearing capacity of the ground

surface under the embankment. Global stability failure is a global foundation failure of both the embankment and ground surface.

## **8.4 Construction defects**

The input data to the calculations performed in this report are based on construction drawings. It is however possible that the actual construction of the embankment and the embankment piles differs from what is stated in the drawings. There is a possibility that settlements in the piled sections of the studied embankment in Marieholm are partly caused by construction defects. A case study performed by (Alenius, et al., 1979) describes a piled road embankment in Stockholm where large settlements occurred. The foundation of the embankment in Stockholm was similar to the foundation of the embankment in Marieholm studied in this report. In the case study of the embankment in Stockholm it was found that the reason for the large settlements was a number of missing pile caps and one missing pile. A number of other construction defects were also found, such as eccentric pile caps and pile caps with insufficient reinforcement. It is possible that similar construction defects are present in the studied embankment in Marieholm.

## 9 Conclusions

The aim of this thesis was to analyse the settlements of the embankments connected to Slakthusbron Bridge constructed in year 1967. Analysis was only performed on the southern embankment since it was assumed that the conditions are similar for both embankments.

The analysis was performed by comparing measured settlements between year 1980 and 2014 with calculated settlements in GS Settlement. Since no settlements have been measured during the period between the construction of the embankment and year 1980, it is hard to evaluate the settlement between these years. However, it can be concluded that large settlement has occurred in the first 13 years after the construction of the embankment.

The settlements were analysed in three different sections of the embankment; 1/000, 1/045 and 1/085. The embankment in section 1/000 is founded without piles and section 1/045 and 1/085 with piles. The large settlements that occurred before year 1980 have not been obtained in the calculations. Nevertheless, the development and rate of settlements after year 1980 have been captured in the calculations rather good in section 1/000 and 1/085. Figure 9.1 illustrates the calculated settlements with creep and measured settlements in all studied sections of the embankment between year 1980 and 2014. The results from the calculations indicate that the settlements will continue in the future with the same rate as in year 2014 in section 1/000.

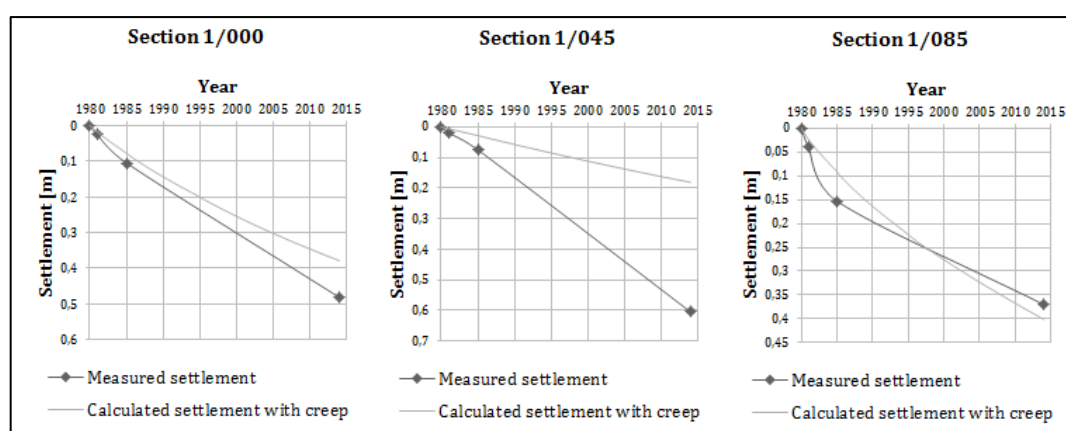


Figure 9.1. Calculated settlements with creep plotted with measured settlements in all studied sections of the road embankment. The data plotted in the graphs is the previously presented results (in chapter 6), however, the settlements are set to 0 at year 1980.

It is concluded that the models representing the piled sections (section 1/045 and 1/085) of the embankment does not comply with the reality since there are uncertainties regarding the modelling of the embankment piles. The effect of the embankment piles have probably not been captured in the model. The calculated total settlements from year 1967 differs more from the measured settlements in the piled sections compared to section 1/000. The model of section 1/000 is therefore considered to be a more realistic model.

According to the calculations, the additional stresses in the soil are close to or have exceeded the preconsolidation pressure in all studied sections. This is considered to be one of the main reasons for the measured settlements. The additional asphalt added to the embankment after the construction has increased the additional stresses in the soil. Without the addition of asphalt, the settlements would have been smaller.

The results from the calculations indicate that the consolidation process is slow due to the thick layers of clay under the embankment. According to the calculations, the consolidation process is still ongoing at year 2050 in all studied sections.

It is shown in the sensitivity analysis, that the permeability of the clay and the geotechnical bearing capacity of the piles have a large impact on the calculated results. The results are not sensitive to changes of the creep parameters.

It can be concluded that the large measured settlements have not been obtained in the calculations. The measured settlements are probably not only caused by the consolidation of the clay. It is likely that other factors such as compression of embankment material or construction defects have contributed to the measured settlements.

## **10 Recommendation for further investigations**

This thesis only analyse the settlement in 1D, therefore, a 3D-analysis should be performed in order to include the effects from the surrounding area and possible lateral displacement of the embankment.

There are several uncertainties regarding the properties of the embankment and the material why more investigation regarding the material of the embankment should be performed in order to verify assumptions in this thesis.

In the studied piled sections, the function of the piles is uncertain. Therefore an investigation of the function of the piles and pile caps including eventual construction failures is suggested.

The function of a piled embankment and the interaction between piles and soil is difficult to analyse. Therefore, further research regarding modelling of piled embankments is needed.

In order to make a better prediction of the settlements and to follow up this study, the settlements should be measured continuously in the future.

## 11 References

- Alén, C., 2012. *Pile Foundations - Short handbook*, Göteborg: Educational material at Chalmers university of technology.
- Alenius, U., Hellgren, A. & Rinkert, A., 1979. *Sättningar i pålad väg- och tunnelbanebank i Rågsved, Stockholm*. Esbo, NGM.
- Almedia, M. d. S. S. & Soares Marques, M. E., 2013. *Design and Performance of Embankments on Very Soft Soils*. Leiden: CRC Press.
- Bergdahl, U., Lingfors, R. & Nordstrand, P., 1979. *Bankpålningars verkningssätt - en studie med modellförsök*. Esbo, NGM.
- Chevalier, B., Gaël, C. & Pascal, V., 2007. *Load transfers and arching effects in granular soil layer*. Grenoble, Laboratoire 3S-R : Sols, Solides Structures et Risques.
- Claesson, P., 2003. *Long term settlements in soft clay*, Gothenburg: Chalmers University of Technology.
- Eriksson, P., Jendeby, L., Olsson, T. & Svensson, T., 2004. *Kohesionspålår*, Linköping: Commission on Pile research.
- Fellenius, B. H., 2004. *Unified Design of piled foundations with emphasis of settlement calculations*, Los Angeles: Geo-Institute Geo-TRANS conference.
- Google, n.d. *Google maps*. [Online] Available at: <https://maps.google.se/maps?output=classic&dg=brw> [Accessed 5 February 2014].
- Göteborgs Stadsbyggnadskontors Arkiv, 2015. *Historiska kartor*. [Online] Available at: [www.goteborg.se](http://www.goteborg.se) [Accessed 06 02 2015].
- Hallingberg, A., Olsson, T. & Svensk, I., 1996. *Marieholmsbron över Göta älv*. Reykjavik, NGM.
- Hallingberg, A., Olsson, T. & Svensk, I., 1996. *Marieholmsbron över Göta älv*. Reykjavik, NGM.
- Holtz, R. D. & Kovacs, W. D., 1981. *An Introduction to Geotechnical Engineering*. New Jersey: Prentice Hall.
- Jendeby, L., 1986. *Friction piled foundations in soft clay, A study of load transfer and settlements*, Göteborg: Chalmers University of Technology.
- Knappett, J. A. & Craig, R. F., 2012. *Craig's Soil Mechanics*. Oxon: Spon Press.

Lantmäteriet, 2013. *Kartsök och ortnamn.* [Online] Available at: <http://kso2.lantmateriet.se/#> [Accessed 10 April 2015].

Larsson, R., 2008. *Jords egenskaper*, Linköping: Swedish geotechnical institute.

Larsson, R., Bengtsson, P.-E. & Eriksson, L., 1997. *Prediction of settlements of embankments on soft, fine-grained soils*, Linköping: Swedish Geotechnical Institute.

Larsson, R. et al., 2007. *SGI Information 3 Skjuvhållfasthet - Utvärdering i kohesionsjord*, Linköping: SGI.

Lönnroth, G., 2000. *Kulturhistoriskt värdefull bebyggelse i Göteborg - Ett program för bevarande Del II*, Göteborg: Stadsbyggnadskontoret.

Olsson, C. & Holm, G., 1993. *Pålgrundläggning*. Solna: AB Svensk Byggtjänst.

Olsson, M., 2010. *Calculating long-term settlement in soft clays - with special focus on the Gothenburg region*, Linköping: Swedish Geotechnical Institute.

Satibi, S., Raymond, v. d. M. & Martino, L., 2007. *Piled Embankments: Literature review and required further research using numerical analysis*, Stuttgart: University of Stuttgart.

Statens vägverk, 1974. *Bankålning*, s.l.: Statens vägverk.

Sällfors, G., 2001. *Geoteknik: jordmateriallära, jordmekanik*. 3rd ed. Göteborg: s.n.

Trafikverket, 2011. *TK Geo 11, Trafikverkets tekniska krav för geokonstruktioner*, Borlänge: Trafikverket.

Trafikverket, 2013b. *E6/E45/E20, Marieholmsförbindelsen (ED1) - 7.1 Markteknisk undersökningsrapport MUR, Geoteknik*, Göteborg: Trafikverket.

Trafikverket, 2013. *Förstudie E45 Slakthusmotet*, Göteborg: Trafikverket.

Trafikverket, 2014. *Marieholmsförbindelsen (ED2) - 7.1 Markteknisk undersökningsrapport MUR, Geoteknik*, Göteborg: Trafikverket.

Vianova GeoSuite AB, 2013. *GS Settlement Help*. Solna: Vianova GeoSuite AB.

Vianova Systems AS, n.d. *Novapiont GS Settlement Product Sheet*. Sandvika: Vianova Systems AS.

ÅF Infrastructure AB, 2013. *E45 Slakthusmotet PM Geoteknik*, Göteborg: ÅF Infrastructure AB.

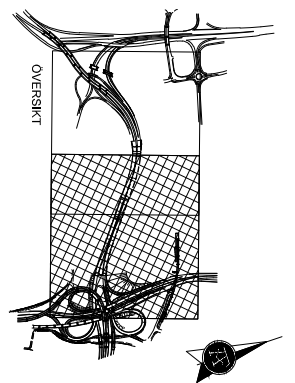
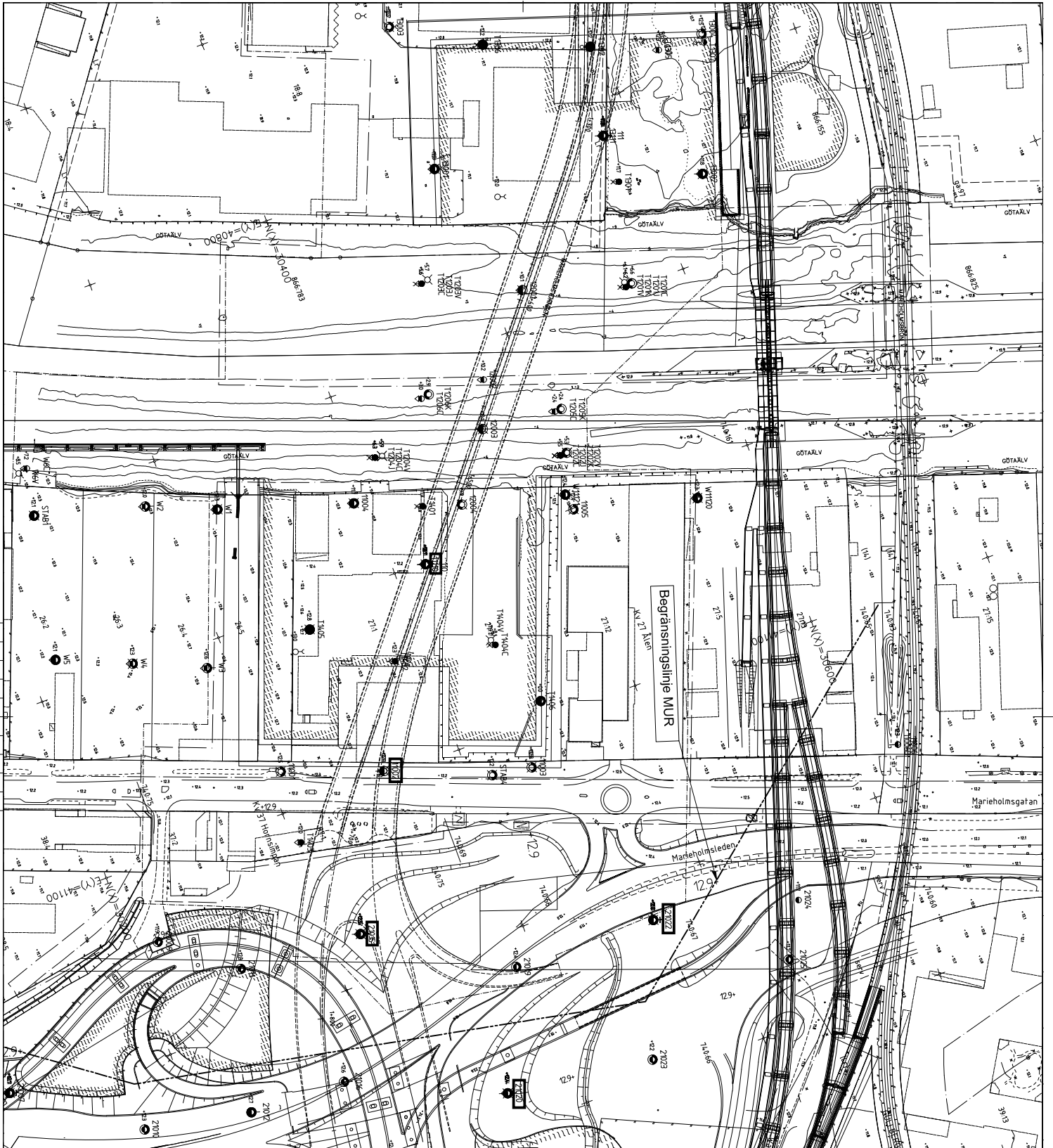
ÅF Infrastructure AB, 2015. *Sammanställning av sättningsmätningar för E45 Slakthusmotet [Internal report]*, Göteborg: ÅF Infrastructure AB.









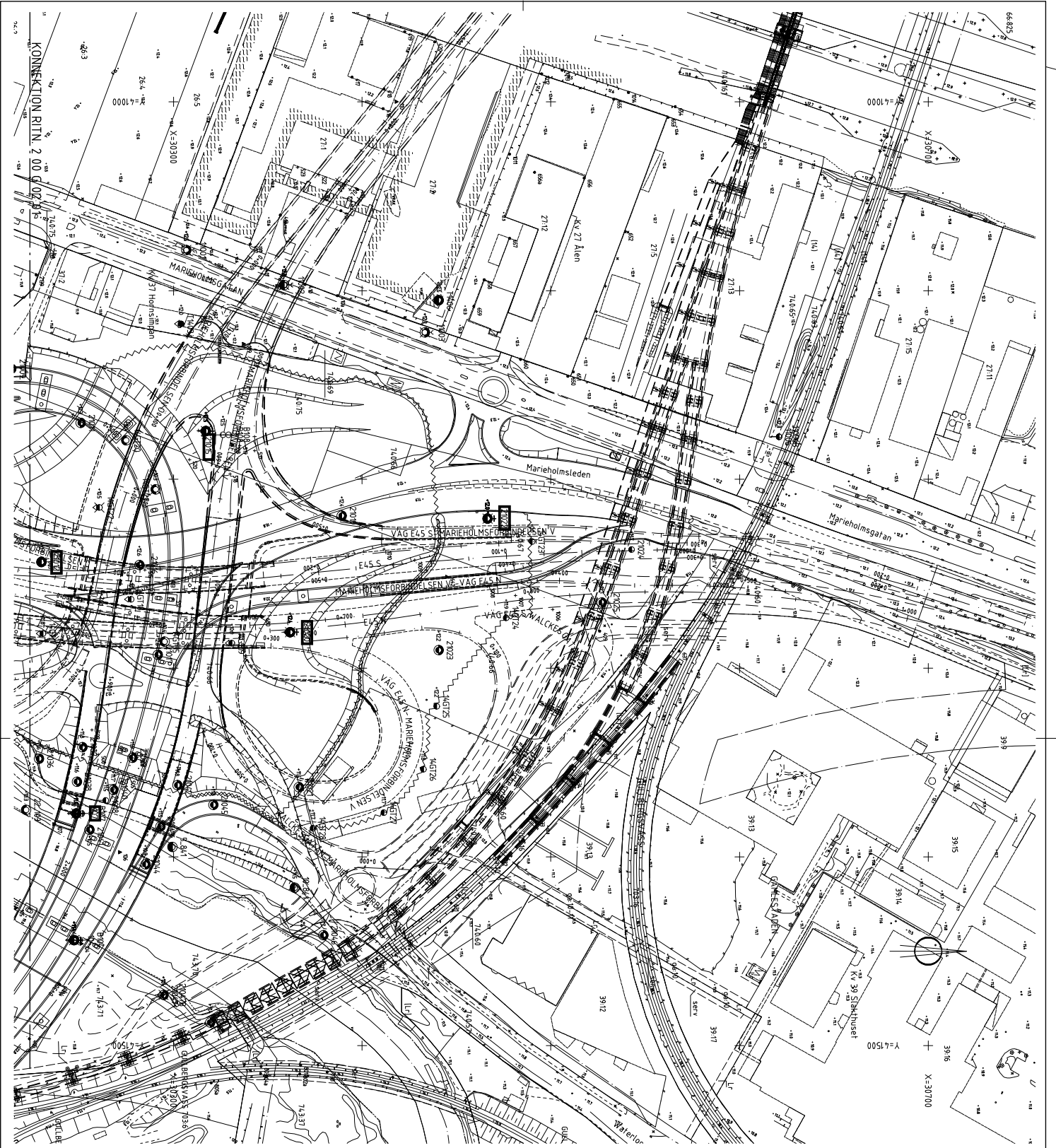


### FÖRKLARINGAR

- XXX-210 Sondringpunkt från Geoteknisk inventering Marieholm-Ringområdet, planerad tunnel under Göta älv, Sammanställning av utförda geotekniska undersökningar daterad 2003-04-17
- STAB X Sondringpunkt utförd av Skanska teknik AB, Projekt Marieholmströmen daterad 1998-02-09
- XXXX Sondringpunkt utförd av WSP samhallbyggnad, Projekt Marieholmströmen daterad 2004-10-07
- W XXX Sondringpunkt utförd av Geotekniska 2009 på uppdrag av WSP samhallbyggnad Under projektet Marieholmstunneln
- TXXXX Sondringpunkt utförd av Geotekniska 2009 Projekt Marieholmstunneln

PROJEKT	TRAFIKVERKET	TRAFIKVERKET
UNDERSÖKNING	GEOTEKNISK UNDERSÖKNING	GEOTEKNISK UNDERSÖKNING
PL AN	PL AN	PL AN
SKALA	SKALA	SKALA
1:1000	1:1000	1:1000
PROJEKTANT	R. ÖSKARSSON	R. ÖSKARSSON
REVISOR	R. ÖSKARSSON	R. ÖSKARSSON
UTGIVNINGSDATUM	2013-05-15	2013-05-15
PROJEKTNUMMER	85 4 2 36 12 4 00 G 11 02	85 4 2 36 12 4 00 G 11 02
PROJEKT	85 4 2 36 12 4 00 G 11 02	85 4 2 36 12 4 00 G 11 02





**ANNÄRKNING**  
 KOORDINATSYSTEMET I PLAN: LOKAL ANPASSNING AV  
 GÖTEBORGS STADS KOORDINATSYSTEM  
 KOORDINATSYSTEM HÖJD: GÖTEBORGS STADS GH-88

**BETECKNINGAR**

SVENSKA  
 BETECKNINGSSYSTEM: SGR/BGS  
 HEMSIDA: WWW.SGR.NET/BETSYSTEM VERSION 2001:2

ENSKELSKA  
 TRAFIKVERKET'S ÖVERSÄTTNINGSGRÄNSEL FRÅN  
 SGR:s BETECKNINGSSYSTEM TILL BETECKNINGAR  
 ENLÖT SS-EN 14:688-1

RITNINGEN AVSER ENDAST  
 REDOVISNING AV  
 GEOTEKNISK UNDERSÖKNING

BORRHÅL MED ID NR:  
 10-585 - 11-585, 26-585, 30-585 - 32-585 (VIKVI)  
 0156-240, 0160-240 (MSP)  
 AR ENDAST REDOVISADE I PLAN

BORRHÅL, REDOVISAS MED SVENSKA JORDARTS-FÖRKORTNINGAR

xxx HJUGUBAR  
 xxx FÖLAR  
 xxx SPK ASFALT  
 o BALSSÅNG

0 20 40 80  
 METER

BYGGHANDLING  
 ABBETSHANDLING

PROJEKTANT	GEOTEKNISKA AB	BE	2014-06-09
PROJEKTANT	GEOTEKNISKA AB	BRH	2013-12-19
BYGGHANDLING	M/S SVENSSON	BYGGHANDLING	2012-10-31
BYGGHANDLING	BRITTI-FABRIK HENNINGSSON	BYGGHANDLING	2012-10-31

TRAFIKVERKET  
 MARIEHOLMSTUNNELN  
 ED2 ANSLUTNINGAR MARIEHOLM  
 GEMENSAM ANLÄGGNINGSDEL

PLAN  
 GEOTEKNISK UNDERSÖKNING

GEOTEKNIK PLAN

SKALA 1:1000

85 42 36 12 20060202

B

## Appendix 2.1 – Water content and liquid limit

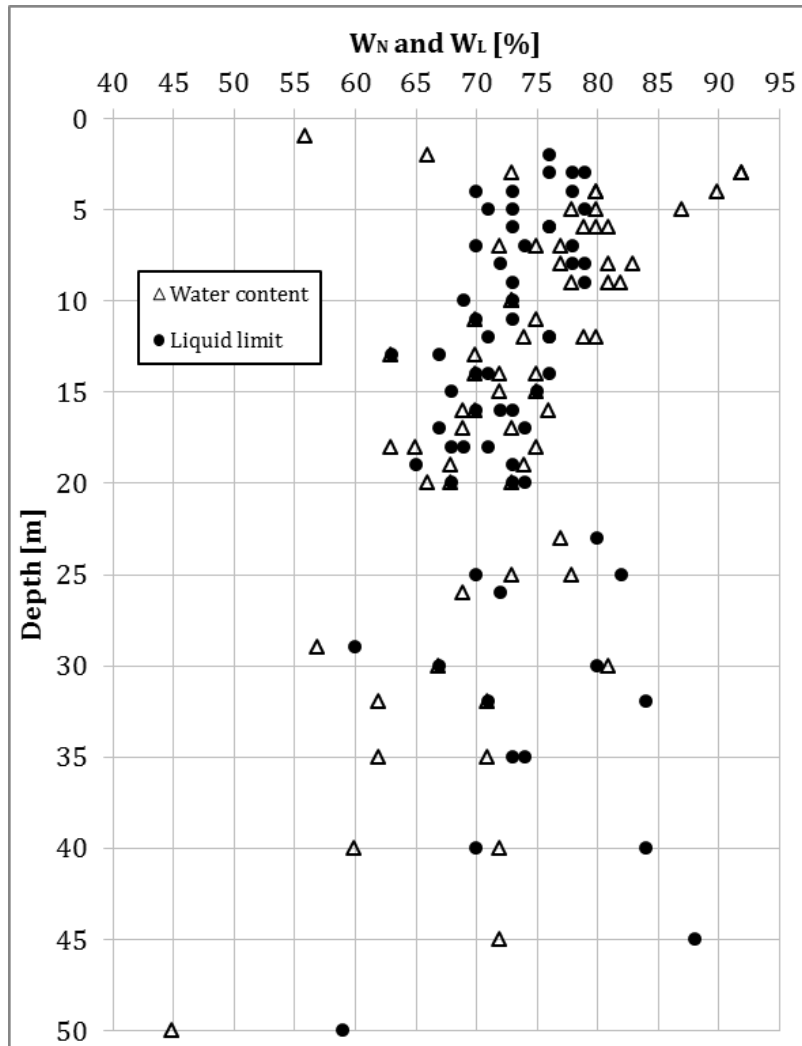


Figure 1. Water content and liquid limit evaluated from boreholes S84-SGI, 81-16 and 81-21, plotted against depth.

## Appendix 2.2 – Pore pressure

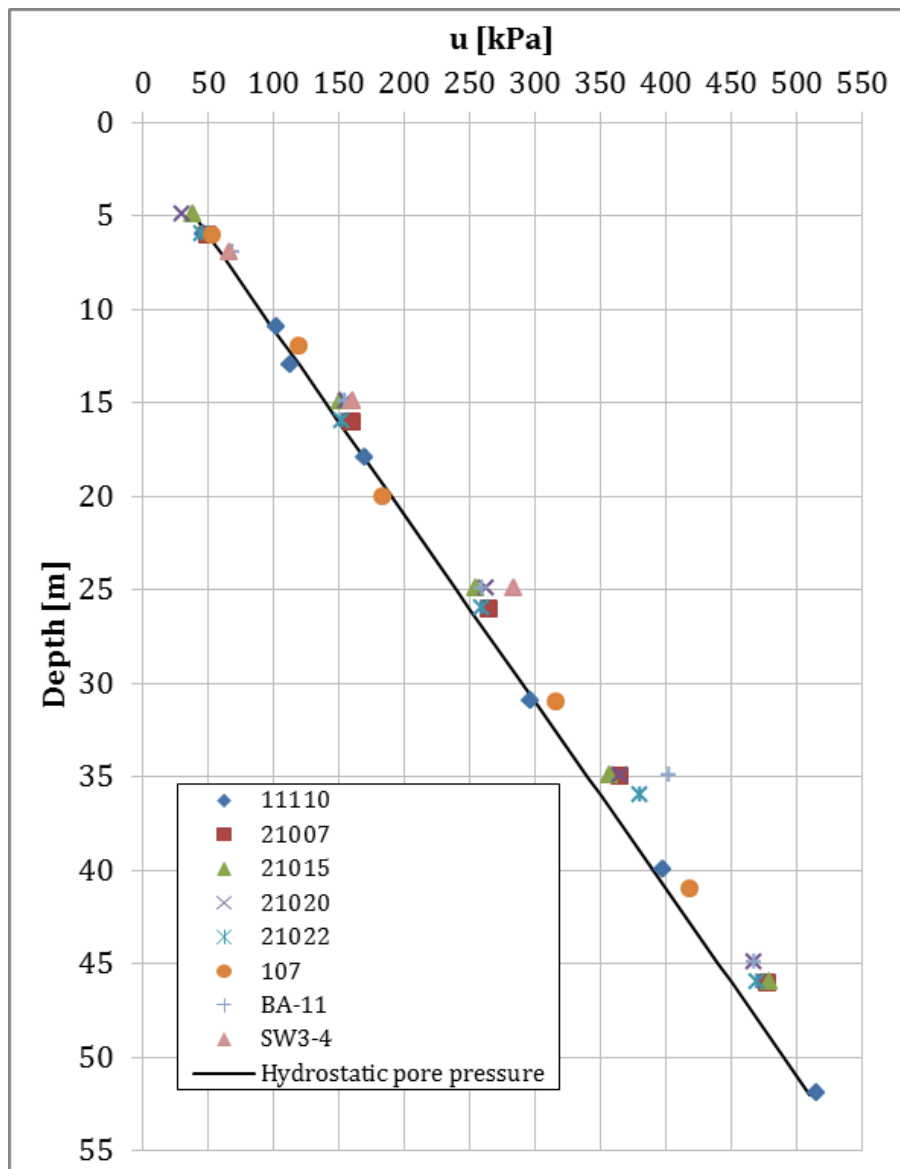


Figure 1. Measured pore pressures plotted against depth together with the hydrostatic pore pressure.

**Appendix 2.3 – Initial permeability and permeability reduction coefficient**

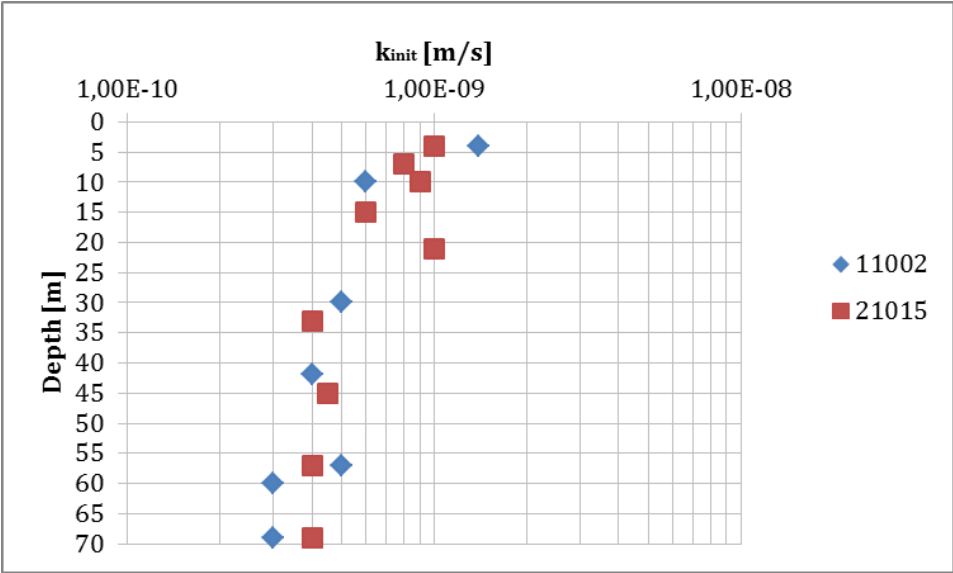


Figure 1. Initial permeability plotted against depth. The initial permeability is evaluated from CRS-tests.

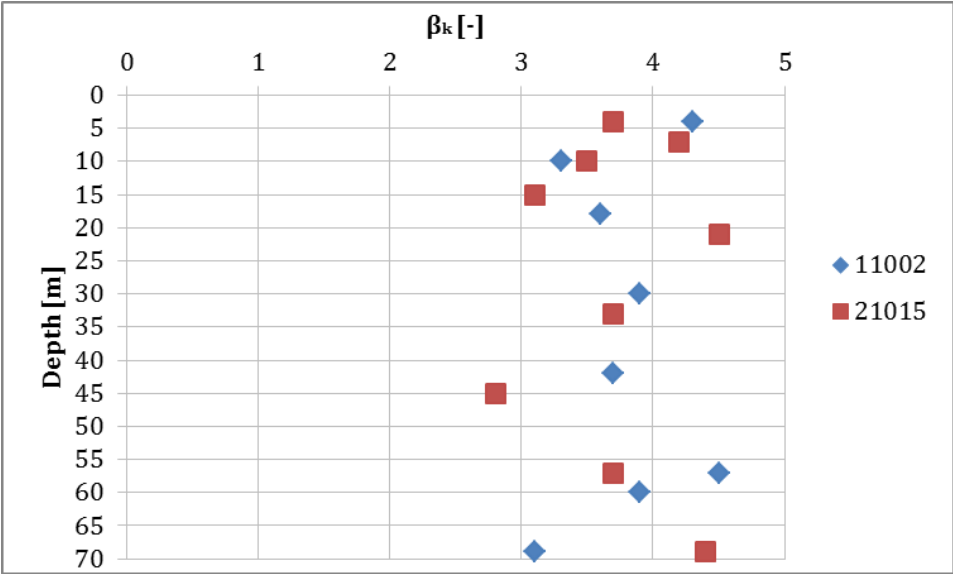


Figure 2. Permeability reduction coefficient plotted against depth. The permeability reduction coefficient is evaluated from CRS-tests.

## Appendix 2.4 – $\sigma'_L$

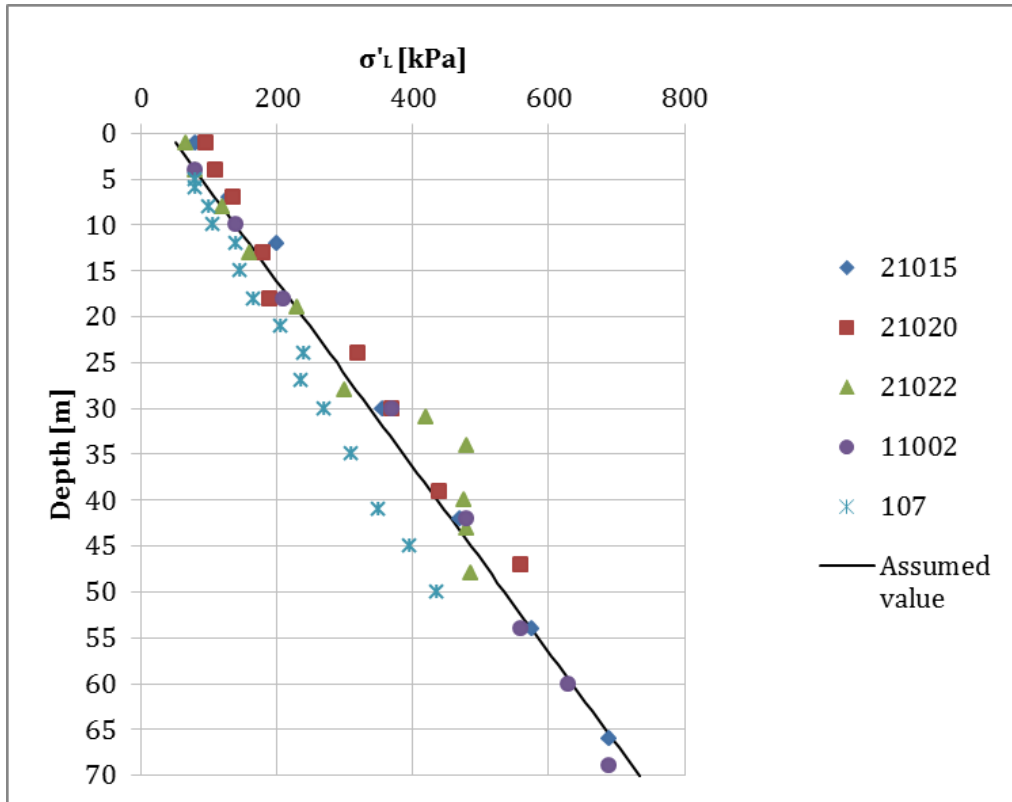


Figure 1. Evaluated values from CRS-tests for  $\sigma'_L$  plotted against depth together with the assumed values used for the calculations.

## Appendix 2.5 - $M'$

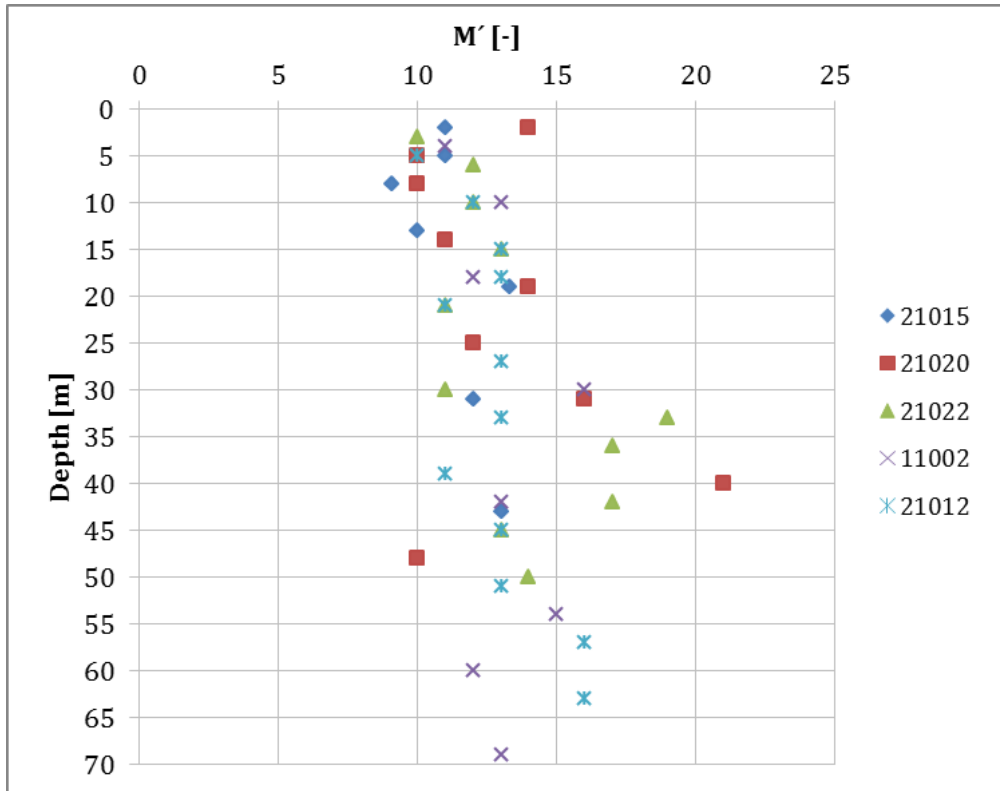


Figure 1. Evaluated values from CRS-tests for  $M'$  plotted against depth.

## Appendix 2.6 - $a_0$ and $a_1$

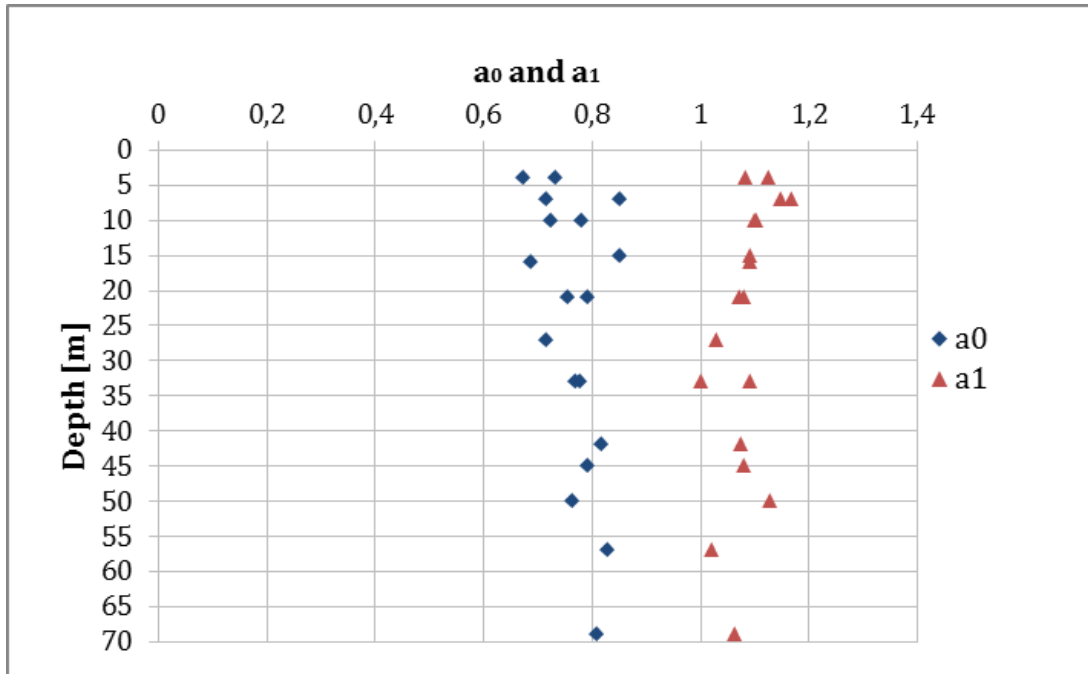


Figure 1. Evaluated values for  $a_0$  and  $a_1$  plotted against depth. The values are evaluated from CRS tests performed on undisturbed samples from borehole 20015 and 21020.

## Appendix 2.7 - Time resistance number $r_1$

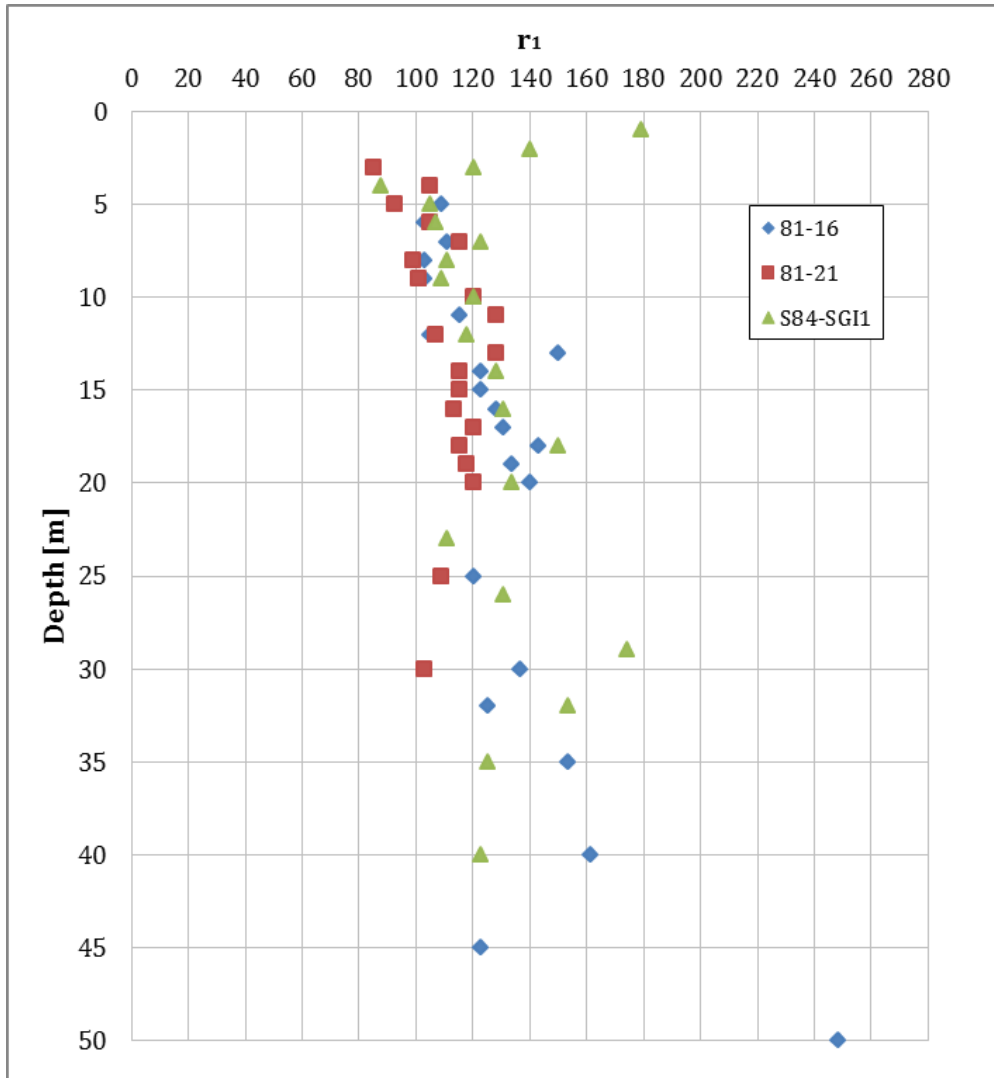


Figure 1. Evaluated  $r_1$  values plotted against depth.





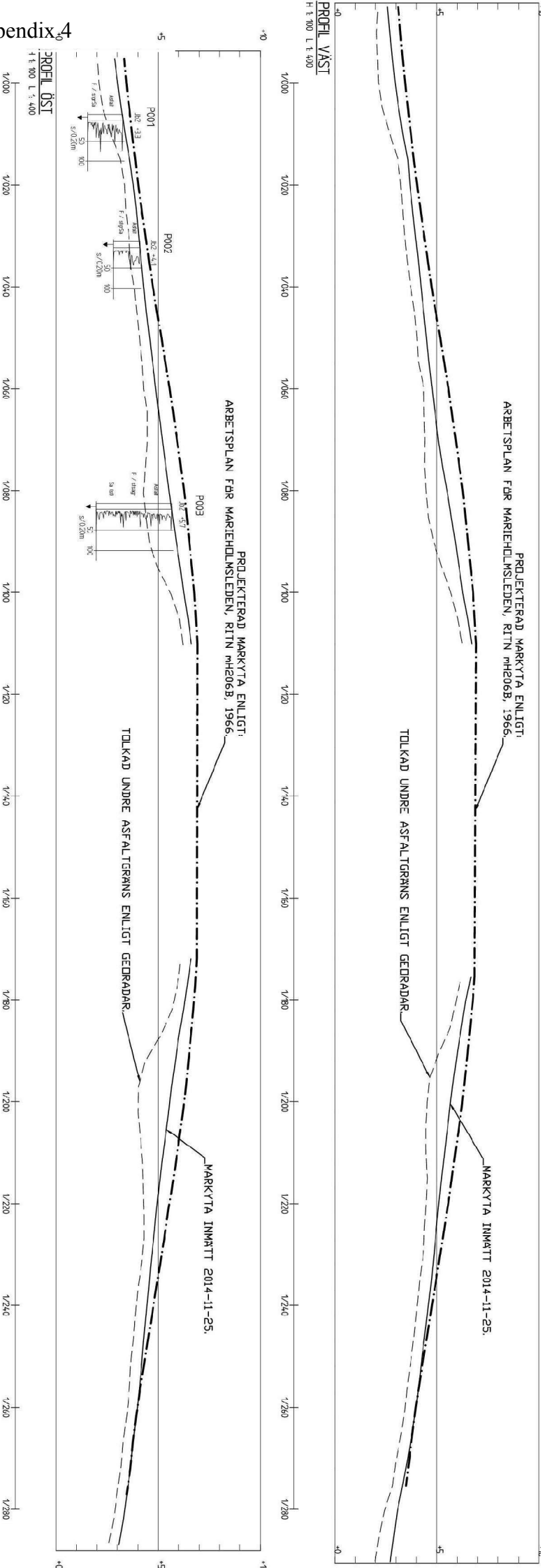


Figure 1. Profile views of the eastern and western side of the road embankments connected to Slakthusbron Bridge. The road surface level and the asphalt thickness measured in year 2014 is shown together with the designed road surface level in year 1967, modified from (ÅF Infrastructure AB, 2015).

## Appendix 5 – Hand calculations

<b>Input data:</b>			
$\gamma_{\text{soil}}$	16 kN/m <sup>3</sup>		
Groundwater level:	1 m		
$u$	10 kPa higher than hydrostatic		
$M_0$	3150+450(z-4)		
$M_L$	229+30z		
$\sigma'_c$	1,87+7,44z		
<b>Weight of embankment:</b>	31,65 kPa		

Layer	Thickness	z (middle)	$\sigma$	$u$	$\sigma'_0$	$\Delta\sigma'$	$\sigma'_0 + \Delta\sigma'$	$\sigma'_c$	$M_0$	$M_L$	$\Delta\delta$
		0	0	0	0	31,7	31,7				
		1	16	0	16	30,1	46,1				
1 - 4 m	3	2,5	40	16	24	28,0	52,0	20,47	2475	304	0,272
4-8 m	4	6	96	51	45	24,1	69,1	46,51	4050	409	0,237
8 - 12 m	4	10	160	91	69	20,7	89,7	76,27	5850	529	0,162
12 - 20 m	8	16	256	152	104	17,2	121,2	120,91	8550	709	0,016
20 - 30 m	10	25	400	244	156	13,7	169,7	187,87	12600	979	0,011
30 - 40 m	10	35	560	343	217	11,1	228,1	262,27	17100	1279	0,007
40 - 50 m	10	45	720	446	274	9,4	283,4	336,67	21600	1579	0,004
50 - 60 m	10	55	880	549	331	8,1	339,1	411,07	26100	1879	0,003
60 - 70 m	10	65	1040	650	390	7,2	397,2	485,47	30600	2179	0,002
										$\delta_{tot} [m]$	0,713

Time dependency	Year	1967	1970	1973	1979	1985	2014	2050	
	Time [yr]	0	3	6	12	18	47	83	
$C_v$ [m <sup>2</sup> /s]	0,0000003	Time [s]	0	94608000	189216000	378432000	567648000	1482192000	2617488000
$h$ [m]	35	$T_v$		0,023	0,046	0,093	0,139	0,363	0,641
		$u$ [%]	0	0,18	0,25	0,33	0,4	0,67	0,82
		$\delta$ [m]	0	0,13	0,18	0,24	0,29	0,48	0,59

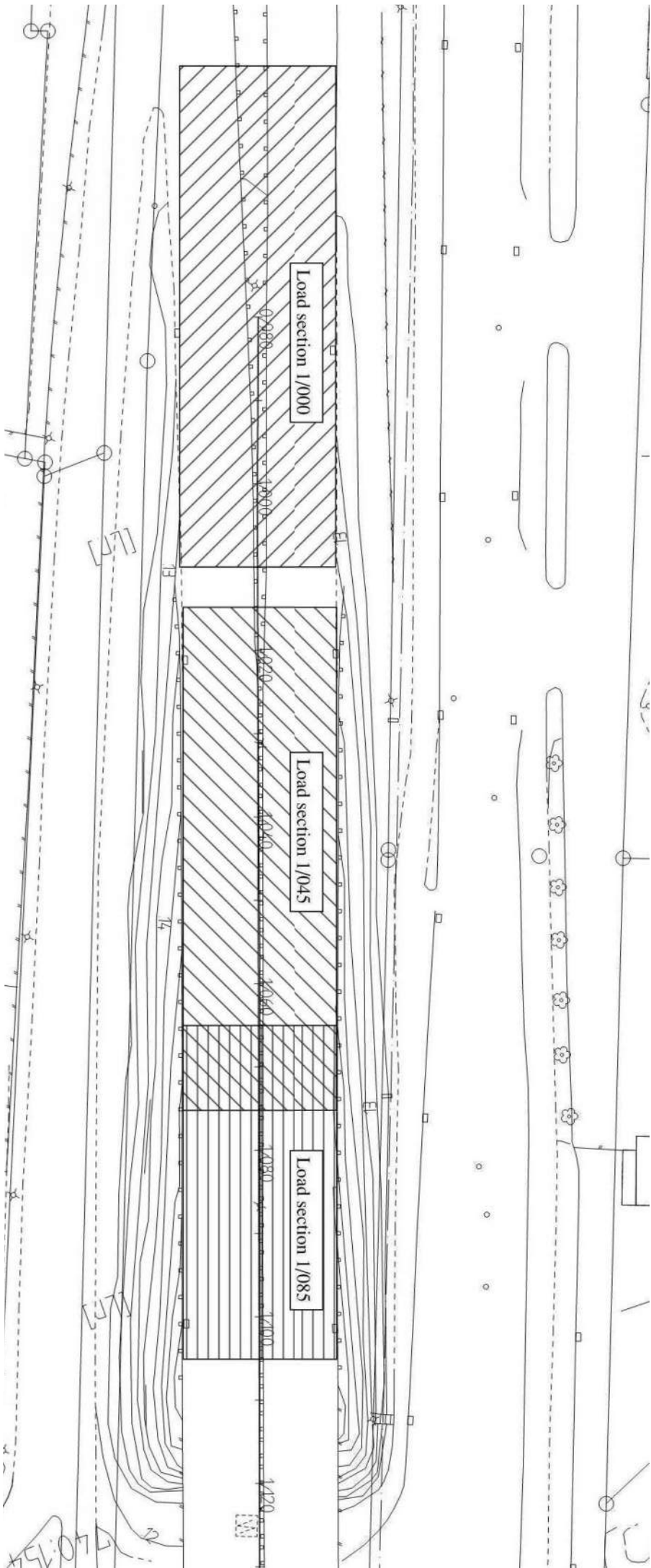


Figure 1. Assumed load distribution areas in the calculations in different sections, modified from (ÅF Infrastructure AB, 2015).

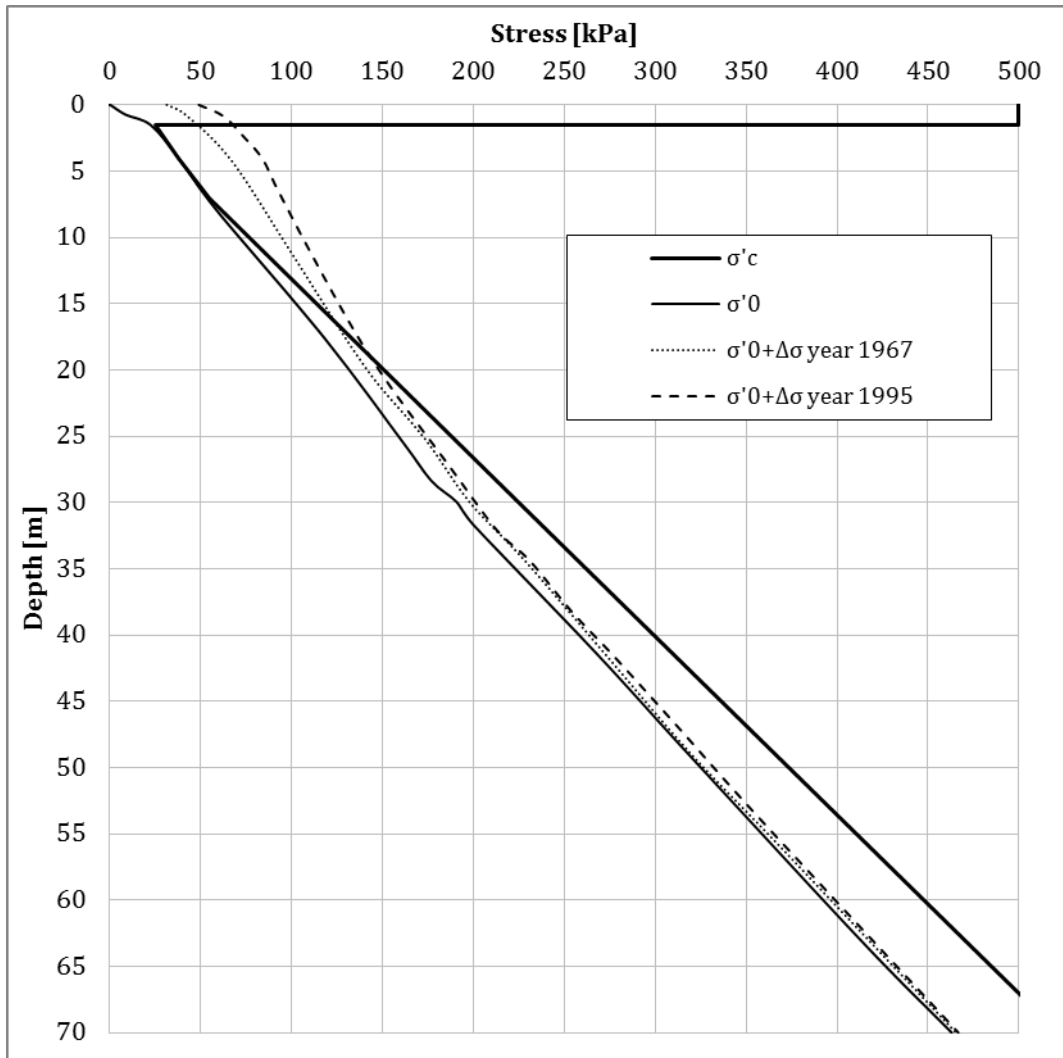
Depth [m]	Pile type TT1			Pile type TT2			Geotechnical bearing capacity per meter (average) [kN]	
	$\theta$ [m]	cu [kPa]	$\alpha$	Geotechnical bearing capacity per meter [kN]	$\theta$ [m]	cu [kPa]		$\alpha$
0	0.72	12.6	0.45					
1	0.76	12.6	0.45					
2	0.80	12.6	0.45					
3	0.84	12.6	0.45	3.33				3.40
4	0.88	12.6	0.45	3.49				3.65
5	0.88	14.4	1.08	9.57				10.00
6	0.86	16.2	1.08	10.47				10.93
7	0.83	18	1.08	11.31				11.79
8	0.81	19.8	1.08	12.08				12.58
9	0.78	21.6	1.08	12.79				13.30
10	0.76	23.4	1.08	13.43				13.95
11	0.74	25.2	1.08	14.00				14.53
12	0.71	27	1.08	14.51				15.03
13	0.69	28.8	1.08	14.96				15.47
14	0.66	30.6	1.08	15.34				15.84
15	0.64	32.4	1.08	15.65				16.13
16	0.61	34.2	1.08	15.90				16.36
17	0.59	36	1.08	16.08				16.51
18	0.57	37.8	1.08	16.20				16.59
19	0.54	39.6	1.08	16.25				16.61
20	0.52	41.4	1.08	16.24				16.55
21	0.49	43.2	1.08	16.16				16.42
22	0.47	45	1.08	16.02				16.22
23	0.45	46.8	1.08	15.81				15.95
24	0.42	48.6	1.08	15.53				15.61
25	0.40	50.4	1.08	15.19				15.19

Figure 1. Geotechnical bearing capacity calculated for each meter along piles of type TT1 and TT2.

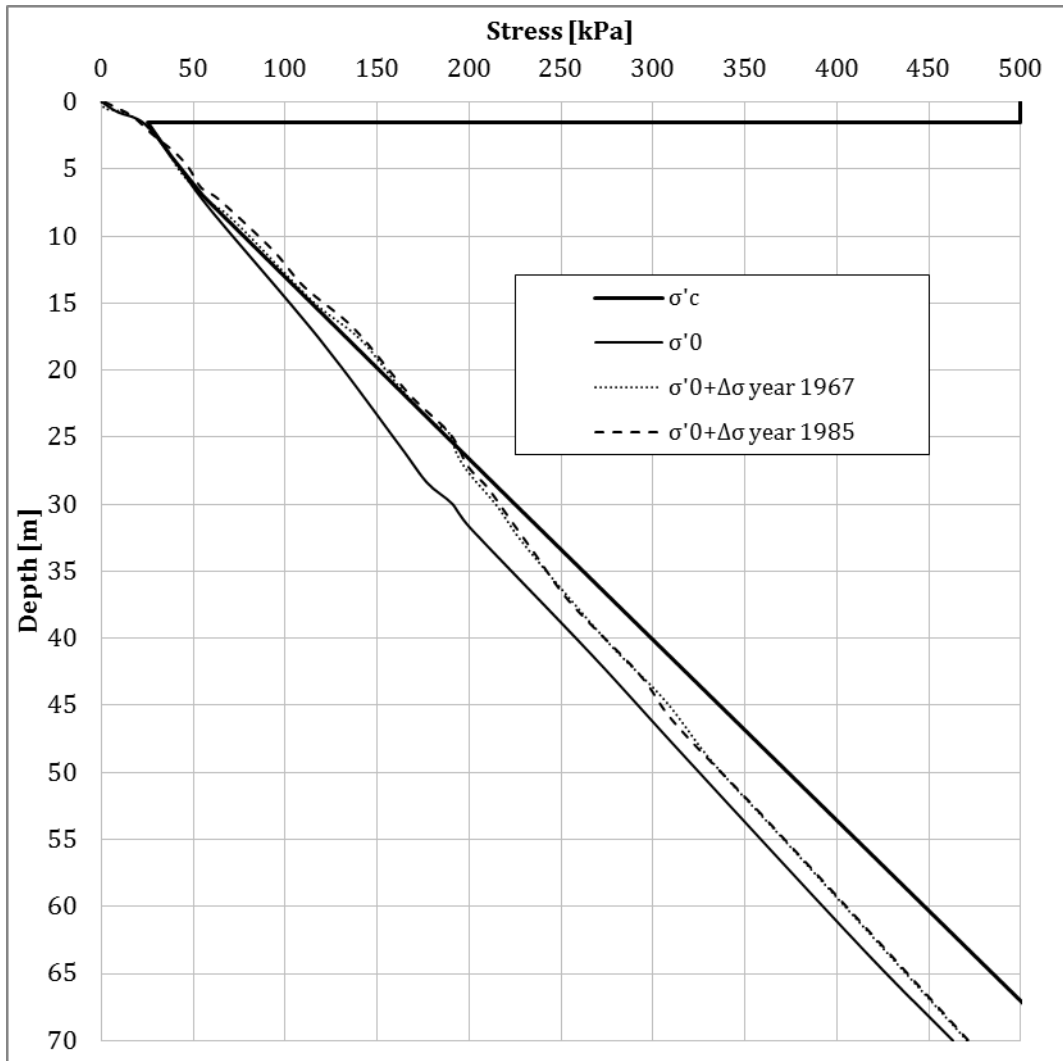
Depth [m]	Pile type TT4				Pile type TT5				Geotechnical bearing capacity per meter (average) [kN]
	$\theta$ [m]	cu [kPa]	$\alpha$	Geotechnical bearing capacity per meter [kN]	$\theta$ [m]	cu [kPa]	$\alpha$	Geotechnical bearing capacity per meter [kN]	
0	0.72	12.6	0.45						
1	0.76	12.6	0.45		0.63	12.6	0.45		
2	0.79	12.6	0.45		0.67	12.6	0.45		
3	0.82	12.6	0.45	3.27	0.70	12.6	0.45		
4	0.86	12.6	0.45	3.40	0.74	12.6	0.45	2.93	3.10
5	0.89	14.4	0.45	4.04	0.78	12.6	0.45	3.08	3.24
6	0.92	16.2	0.45	4.72	0.81	14.4	0.45	3.69	3.86
7	0.96	18	0.45	5.43	0.85	16.2	0.45	4.34	4.53
8	0.96	19.8	1.08	14.34	0.89	18	0.45	5.03	5.23
9	0.93	21.6	1.08	15.18	0.92	19.8	0.45	5.77	10.05
10	0.9	23.4	1.08	15.95	0.96	21.6	0.45	6.55	10.86
11	0.87	25.2	1.08	16.65	1.00	23.4	0.45	7.36	11.66
12	0.85	27	1.08	17.27	1.04	25.2	0.45	8.23	12.44
13	0.82	28.8	1.08	17.81	1.04	27	1.08	21.15	19.21
14	0.79	30.6	1.08	18.28	1.00	28.8	1.08	21.69	19.75
15	0.76	32.4	1.08	18.67	0.96	30.6	1.08	22.13	20.20
16	0.73	34.2	1.08	18.98	0.92	32.4	1.08	22.45	20.56
17	0.71	36	1.08	19.22	0.88	34.2	1.08	22.67	20.83
18	0.68	37.8	1.08	19.38	0.84	36	1.08	22.78	21.00
19	0.65	39.6	1.08	19.47	0.80	37.8	1.08	22.78	21.08
20	0.62	41.4	1.08	19.48	0.76	39.6	1.08	22.67	21.07
21	0.59	43.2	1.08	19.41	0.72	41.4	1.08	22.46	21.07
22	0.57	45	1.08	19.27	0.68	43.2	1.08	22.13	20.97
23	0.54	46.8	1.08	19.05	0.64	45	1.08	21.70	20.77
24	0.51	48.6	1.08	18.76	0.60	46.8	1.08	21.16	20.48
25	0.48	50.4	1.08	18.39	0.56	48.6	1.08	20.51	20.10
26	0.45	52.2	1.08	17.94	0.52	50.4	1.08	19.75	19.63
27	0.43	54	1.08	17.42	0.48	52.2	1.08	18.88	19.07
28	0.40	55.8	1.08	16.82	0.44	54	1.08	17.91	18.41
					0.40	55.8	1.08	16.82	17.66
									16.82

Figure 1. Geotechnical bearing capacity calculated for each meter along piles of type TT4 and TT5.

### Appendix 8.1 – Stress chart for section 1/000



## Appendix 8.2 – Stress chart for section 1/045



### Appendix 8.3 – Stress chart for section 1/085

